Analysis of a Divergent Pumping Well Tracer Test in an Unconfined and Anisotropic Aquifer

by

David A. Chace

submitted in partial fulfillment of the requirements

for the degree of

Master of Science in Hydrology

New Mexico Institute of Mining and Technology

Summer 1993

DEDICATION

To graduate students everywhere, if only the rest of the population could experience the joy!

We congregate at an institution of higher education with glorious dreams
of contributing to the vastness of human knowledge.
We spend a significant portion of our lives in attaining goals
not our own, but those of others who can see the bigger picture.
Our trials and tribulation seem to go unnoticed by our advisors
and only the other graduate students sympathize with the problems.
But worry not you graduate students that are only beginning
the time passes and obstacles are overcome.
The original goals may not be met, but you will complete your self-imposed sentence.
One can only contribute what they are able, the rest should not cause sleepless nights.

-- D. A. Chace

ACKNOWLEDGEMENTS

I would like to extend a special thanks to my advisor, Chia-Shyun Chen for his patience and support during my time here at New Mexico Tech. The work and results that are reported here were supported financially by USGS(14-08-001-G1744) and WRRI(1423640 and 4-23652). Thanks is also extended to Ted Stans of the U. S. Fish and Wildlife Service for his permission and assistance in using the Sevilleta National Wildlife Refuge for the research site. I would also like to extend personal thanks to the other graduate students that were crucial to the completion of this project, including Chris Holmes, Jingfang He, and Jinzhong Liu. Thanks is also extended to Irl Downes, the driller, who's help and consultation were invaluable to the timely completion of the project and to Miles Olinger, who's expertise in getting the data-logger up and running is much appreciated.

TABLE OF CONTENTS

LIST OF FIGURES

LIST OF TABLES

ABSTRACT

A radially divergent pumping well tracer test was conducted in an unconfined, anisotropic alluvial aquifer at a field site north of Socorro, New Mexico during the summer of 1992. Groundwater samples were obtained from observation wells with teflon bailers and bromide (groundwater tracer) concentration breakthrough curves plotted. The anisotropic aquifer under study has an anisotropy eccentricity of 1.13 and principal directions of N 58° E (major semi-axis) and N 32° W (minor semi-axis). A two-dimensional dispersion model was developed to analyze the observed bromide breakthrough curves. The model assumes that the solute is transported horizontally through the saturated flow regime by advection and dispersion and vertically by one-dimensional diffusion from the saturated flow regime into the overlying unsaturated zone. The groundwater flow field in this model is steady-state and under the appropriate anisotropic conditions. Both the resident and flux-concentration solutions are obtained for this model. It is found that neglecting the aquifer anisotropy in the analysis of pumping well tracer tests in an anisotropic aquifer can cause significant errors in the determination of the fitted parameters (i.e. longitudinal dispersivity and molecular diffusion) in the saturated flow regime. It is also found that the flux-concentration solution produces a better match to the observed data when the aquifer anisotropy is taken into account and, thus, is considered to be the more correct method of analysis (the resident-concentration solution more closely approximates the observed data when the anisotropy is neglected and is, therefore, considered to be an artifact). The magnitude of the longitudinal dispersivity, assumed to be of the non-tensor form and used as a fitting parameter, was found to be directionally dependent with the lowest values occurring in the SE direction and highest values occurring in the NE

direction. The magnitude of the vertical diffusion, also a fitting parameter, was found to mimic the trend of the longitudinal dispersivity.

INTRODUCTION

In the summer of 1992 a radially divergent pumping well tracer test was conducted in an anisotropic, unconfined alluvial aquifer at a field site near Socorro, New Mexico as shown in Figure 1. The research site where the pumping well tracer test was conducted is located on the flood plain of the Rio Salado within the boundaries of the Sevilleta National Wildlife Refuge approximately 32 kilometers north of Socorro, New Mexico as shown in Figure 1a. In the region of the research site the Rio Salado, an ephemeral tributary of the Rio Grande, is a dry channel on the average of 320 days per year. The Sevilleta aquifer is unconfined and anisotropic with a shallow water table of approximately 3.05 meters below the ground surface and split-spoon soil samples obtained during the coarse of this research suggest that the aquifer is relatively homogeneous. The aquifer consists of Holocene Rio Salado alluvium overlying Pleistocene axial stream deposits of the Sierra Ladrones formation. The Rio Salado alluvium consists of interbedded sand, gravel, and silt. The axial stream deposits also consist of interbedded sand and silt with occasional gravel and clay layers. Although the exact thickness of the aquifer is unknown, the drilling experiences suggest that the thickness is more than 24.38 meters.

A total of two 15.24 centimeter wells, three multilevel samplers/piezometers (MLSP), and ten 5.08 centimeter observation wells exist at the research site. The locations and configuration of these wells are shown in Figure 1b. Well B, approximately 60 meters southeast of Well A, was primarily used for water supply. Both Well A and Well B are constructed from 15.24 centimeter PVC pipe. Well A is cased from the ground surface to 6.1 meters below the ground surface with solid 15.24 centimeter PVC pipe and screened from 6.1 to 25.91 meters below the

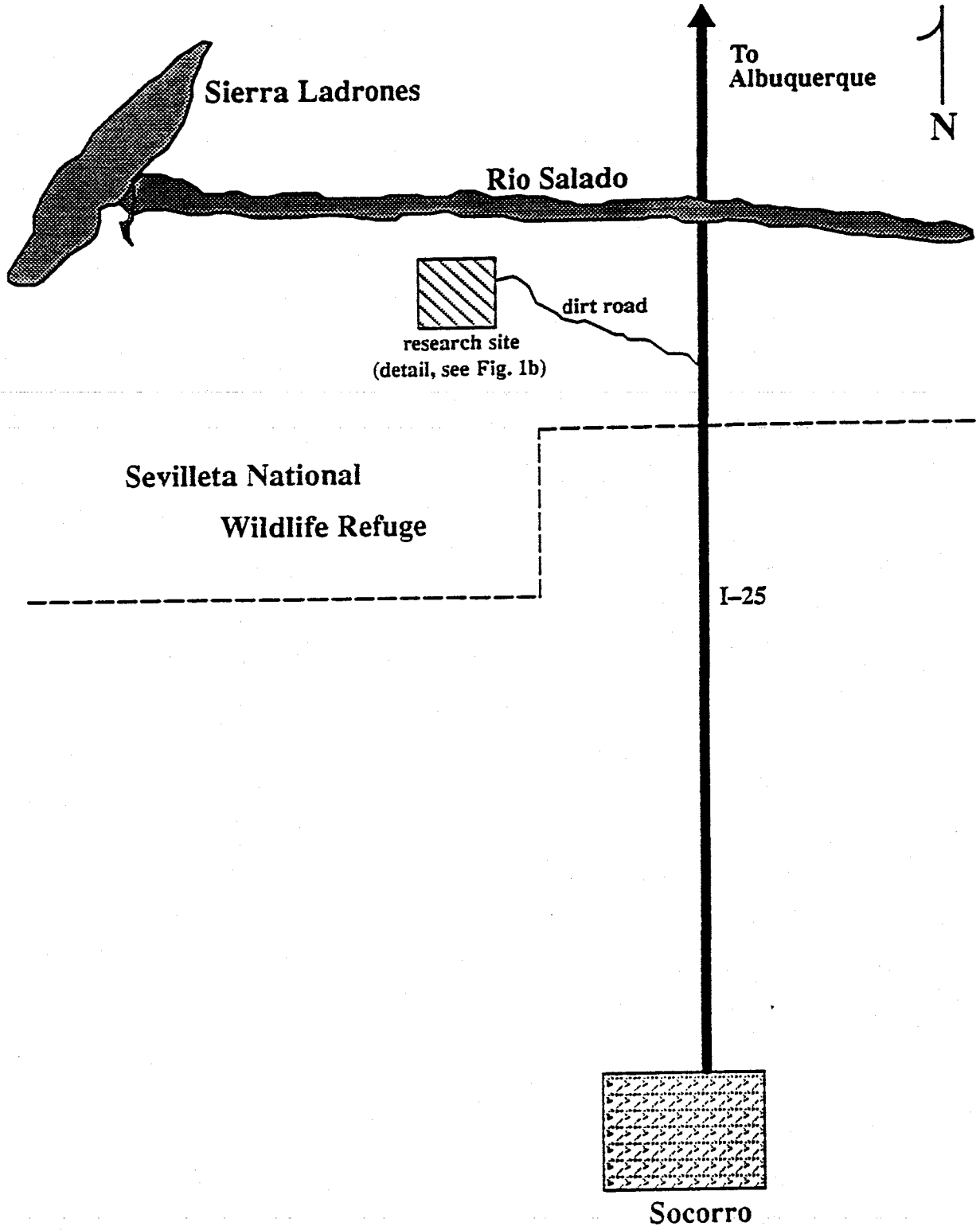

Figure 1a. Research site inside the Sevilleta National Wildlife Refuge north of Socorro, New Mexico.

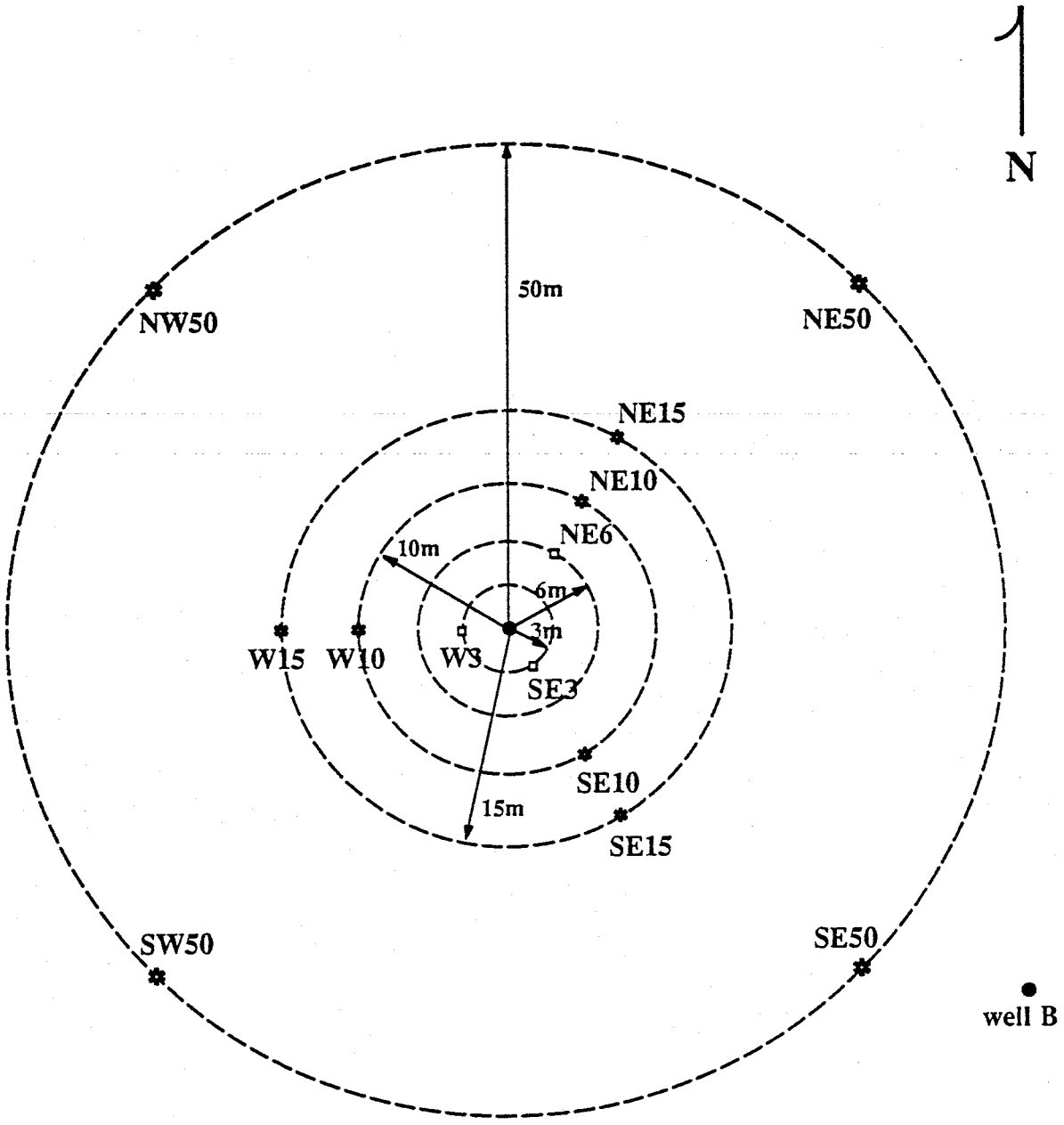

● – 15.24 cm Well A, approximately 60 meters from 15.24 cm Well B

✱ – 5.08 cm observation well

▫ – functional multilevel samplers/piezometers (MLSP)

Figure 1b. Locations of observation wells and MLSP's at the Sevilleta research site.

ground surface with 15.24 centimeter, machine slotted PVC pipe. The machine cut slots are approximately 0.8 millimeters wide. Well B is of similar design but extends to only 12.19 meters below the ground surface. Well A is at the center of the well field to be used for field experiments. There are MLSP's and observation wells installed on three rays in the directions of west (W), northeast (NE), and southeast (SE) on four concentric circles which surround Well A with radii of 3, 6, 10, and 15 meters. The ten observation wells are constructed of 5.08 centimeter PVC pipe. Due to problems encountered during the installation of these observation wells, the depths and screened intervals vary from one to the next. Figure 2 indicates the completion depths and screened intervals of each of the observation wells. It should be noted that the well screen in each of these wells is 5.08 centimeter, machine slotted PVC pipe with 0.8 millimeter slots. Also, the MLSP's can offer depth-specific groundwater samples for three-dimensional analysis, but this is not addressed here and the reader is referred to Chen et al. [1993] for further information. Each of the observation wells is designated by its direction and distance measured with respect to Well A. For example, SE10 represents the observation well located 10 meters from Well A in the SE direction. Observation wells NW50, NE50, SE50, and SW50 do not coincide with the three rays on which the other MLSP's and observation wells fall, as shown in Figure 1b. These four observation wells were used, primarily, to monitor the regional groundwater flow field. The regional groundwater movement, as monitored by these four observation wells, was relatively uniform from NW to SE, in general, with a small hydraulic gradient of approximately 10^{-3} m/m, provided no significant rainfall events occur. Due to the relatively small pumping rates (no more than 6.3×10^{-3} m^3/s or 100 gpm) used in the tracer tests, the flow domain remained unchanged in the vicinity of these wells.

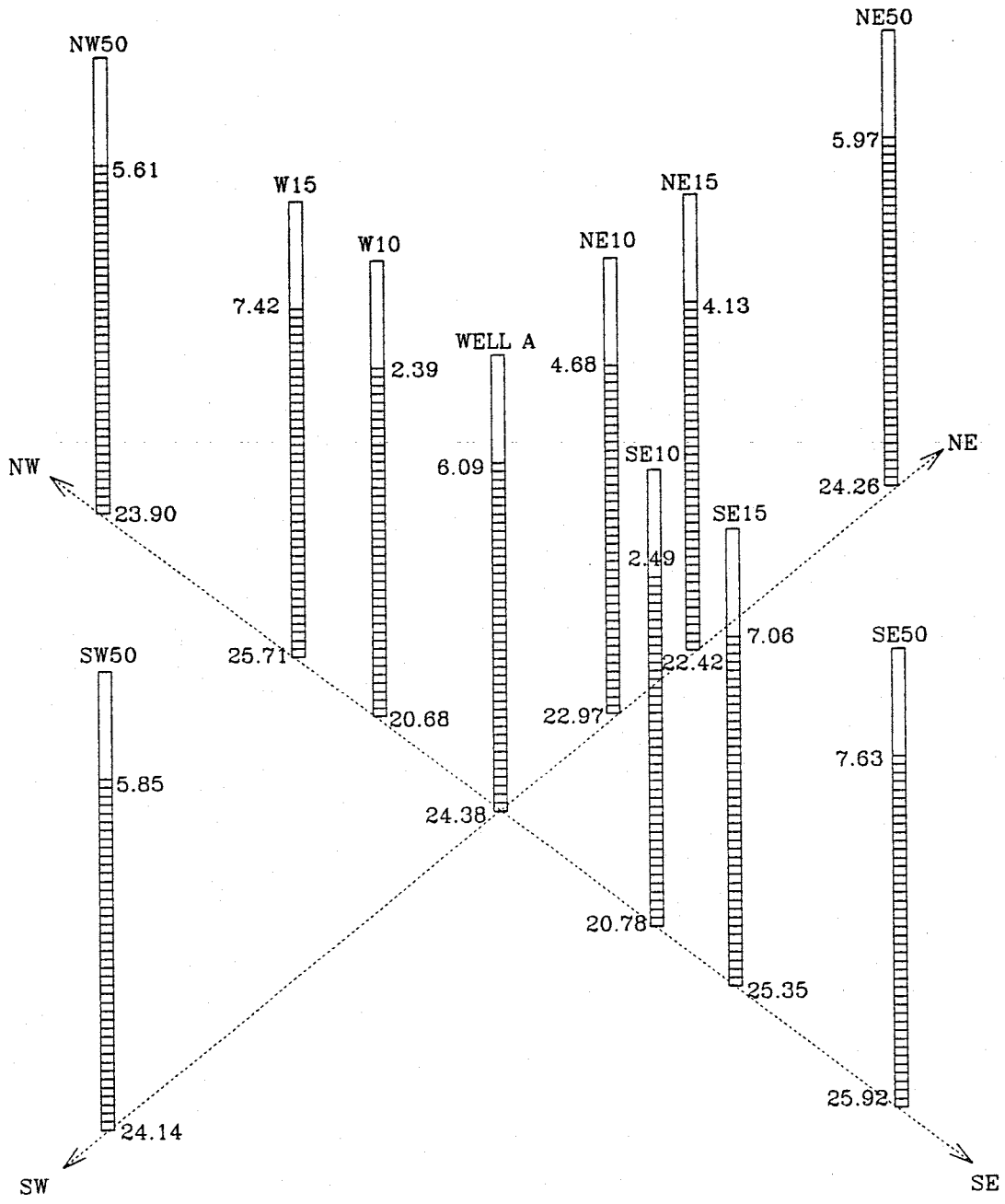

Figure 2. Depths of well screens measured with respect to the top of Well A.

Preliminary pumping tests and soil sample analysis suggested that the hydrogeological conditions surrounding Well A are rather complex. Drawdown data collected from these tests showed two interesting conditions:

(1) Without packers set in Well A, drawdown distributions measured at depths above 14 meters were noticeably less than those measured below 14 meters. This indicated that the hydraulic conductivities of the saturated thickness above 14 meters were larger than those below 14 meters. When packers were placed inside Well A at about 13 to 14 meters, drawdown distributions measured at depths below 14 meters were negligibly small relative to those measured above 14 meters, provided that the pumping took place from above the packers. If pumping took place from below the packers placed at this depth inside Well A, drawdown distributions measured at depths above 14 meters were negligibly small relative to those measured below 14 meters. This observation suggests that a low-permeability layer exists at approximately 13 to 14 meters below the ground surface in the vicinity of Well A. The existence and thickness of this low-permeability layer were not discernable from the soil samples, possibly due to the fact that the soil sampling missed the layer.

(2) An anomalous drawdown pattern was noticed in the vertically-averaged drawdown data obtained from the 5.08 centimeter observation wells. When water was pumped from below the packers placed at any depth inside Well A, the drawdown at the more distant wells W15 and SE15 was greater than the drawdown at the closer wells W10 and SE10, respectively. This anomaly also existed during pumping tests in which no packers were used in Well A. However, the anomaly disappeared when water was pumped from above the packers wherever they were placed inside Well A. As shown in Figure 2, W15, SE15, and Well A are all deeper than 24

meters while W10, SE10, NE10, and NE15 are all shallower than 24 meters. Therefore, a possible explanation for the anomalous drawdown distribution is that a high-permeability zone exists below 24 meters in the vicinity of Well A. When water was pumped from Well A from below or without the packers, this high-permeability zone transmitted most of the water to Well A and hence, more drawdown occurred in W15 and SE15 which both penetrate into this zone. When water was pumped from above the packers inside Well A, the flow regime above this possible high-permeability zone was the primary contributor to the yield of Well A and, therefore, it had little impact on the drawdown in W15 and SE15.

In order to simplify the groundwater flow field in the vicinity of Well A it was decided that a set of inflatable packers be placed in Well A between 12.19 and 14.63 meters below the ground surface during the conduction of any pumping well tracer tests. Therefore, the Sevilleta aquifer is effectively separated into an upper and lower stratum by a proposed low permeability layer located in between 12 and 14 meters below the ground surface. In so doing, the injection of water into Well A, above the packers, has a minimal influence on the lower stratum and the investigation can be focussed on the upper stratum only. Packers were not placed in any of the observation wells and, therefore, the upper and lower strata were not isolated from one another in the observation wells. However, in collecting the groundwater samples from these wells, the bailers were not lowered past 12 meters below the ground surface. By adopting this procedure, any influence from the lower stratum was minimized. Figure 3 shows the physical conceptualization of the field conditions and transport mechanisms that are perceived to exist at the Sevilleta research site.

The current study applies the resident and flux-concentration solutions to concentration data

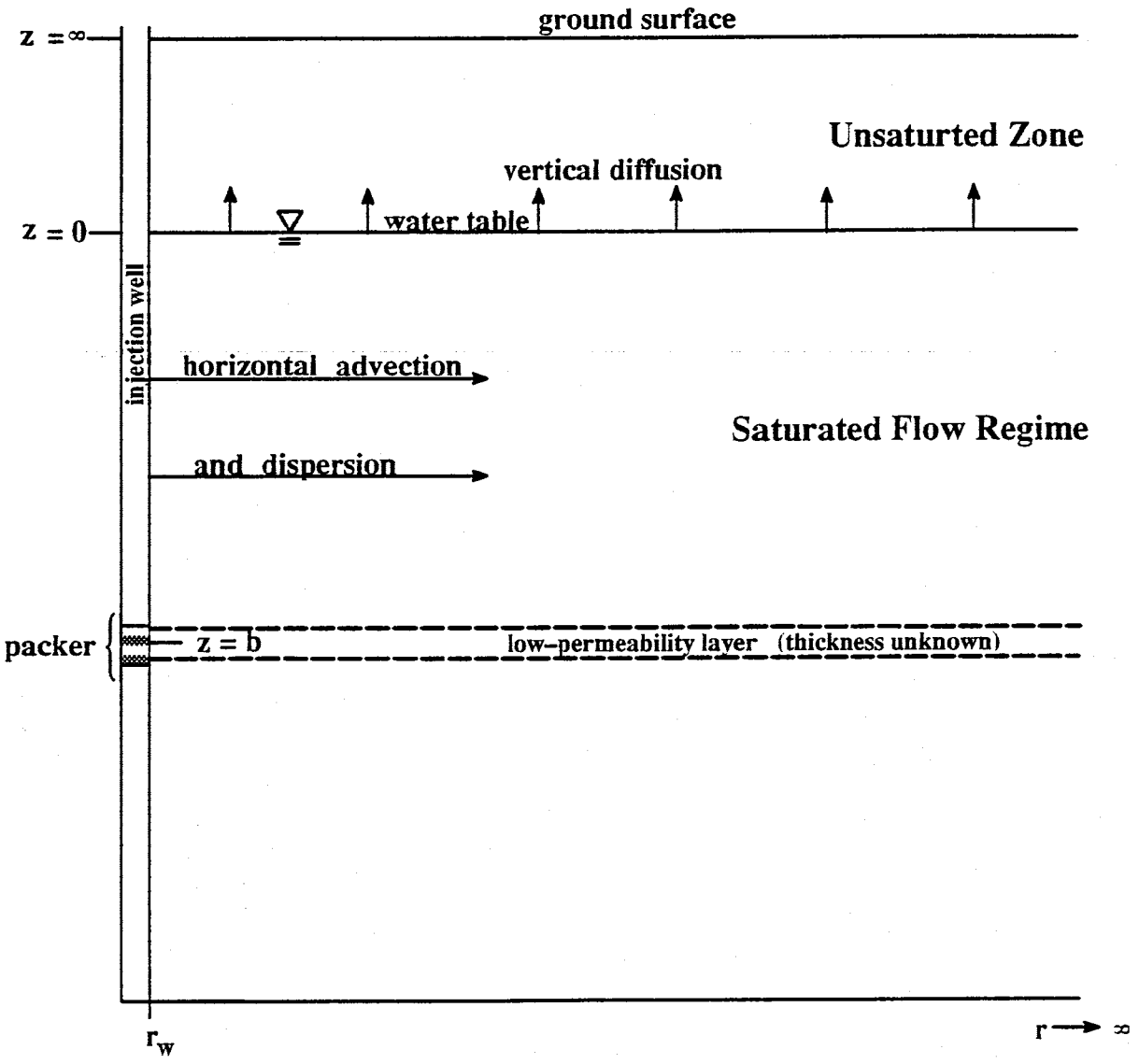

Figure 3. Conceptualization of the solute transport mechanisms at the Sevilleta research site.

obtained from an anisotropic, unconfined alluvial aquifer. The model that was employed was based on the two-dimensional radial dispersion solution with a Cauchy (third-type) boundary condition at the injection well as in Chen [1987] but was modified in order to incorporate a vertical diffusion parameter into the solution as given by Chen [1985]. The vertical diffusion parameter was implemented to account for possible tracer mass moving from the saturated flow regime into the overlying unsaturated zone during the test. Upon obtaining a best fit to the field data from two different observation wells by adjusting the longitudinal dispersivity, a_L, and the vertical diffusion parameter, α, it was found that the flux-concentration solution does, indeed, produce better fits than the resident-concentration solution. This result may be a reflection of the fact that the concentrations were obtained from an observation well which is considered to be a large-scale measuring device.

The study focusses on a two-dimensional, radially divergent pumping well tracer test. The Sevilleta aquifer anisotropy and other hydraulic parameters were characterized by Chen et al. [1993]. The results of the aquifer characterization were $K_x = 1.62 \times 10^{-3}$ m/s in the direction of N 58° E and $K_y = 1.27 \times 10^{-3}$ m/s in the direction of N 32° W as shown in Figure 4. Groundwater from a water supply well (Well B) located approximately 60 meters from the injection well (Well A) was used to establish the steady-state flow domain prior to the introduction of the groundwater tracer. Bromide was selected as the groundwater tracer because of its conservative nature and because background bromide concentrations were minimal in the native groundwater.

The field configuration of the pumping well tracer test is shown in Figure 5. As stated previously, the divergent groundwater flow field was established by pumping water from Well

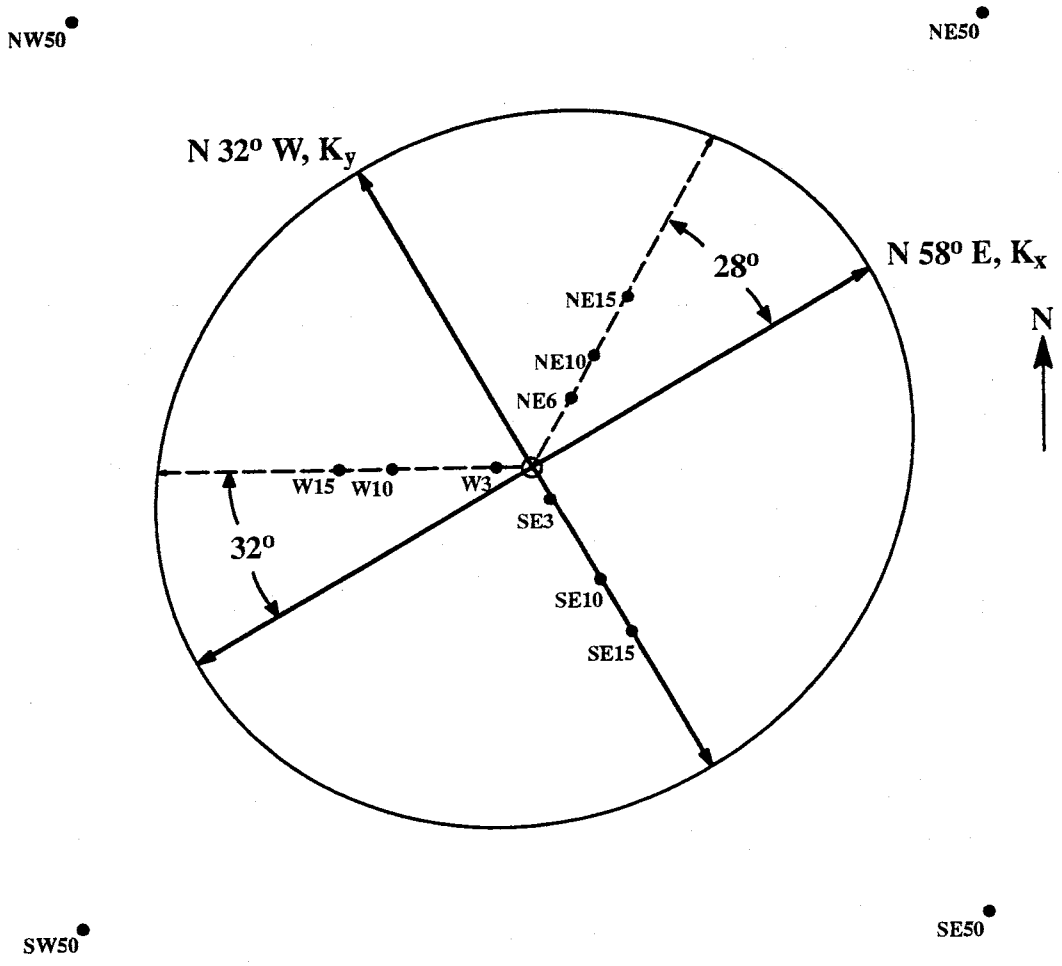

$K_x = 1.62 \times 10^{-3}$ m/s
$K_y = 1.27 \times 10^{-3}$ m/s

Figure 4. The planar anisotropy ellipse estimated from large–time drawdown data.

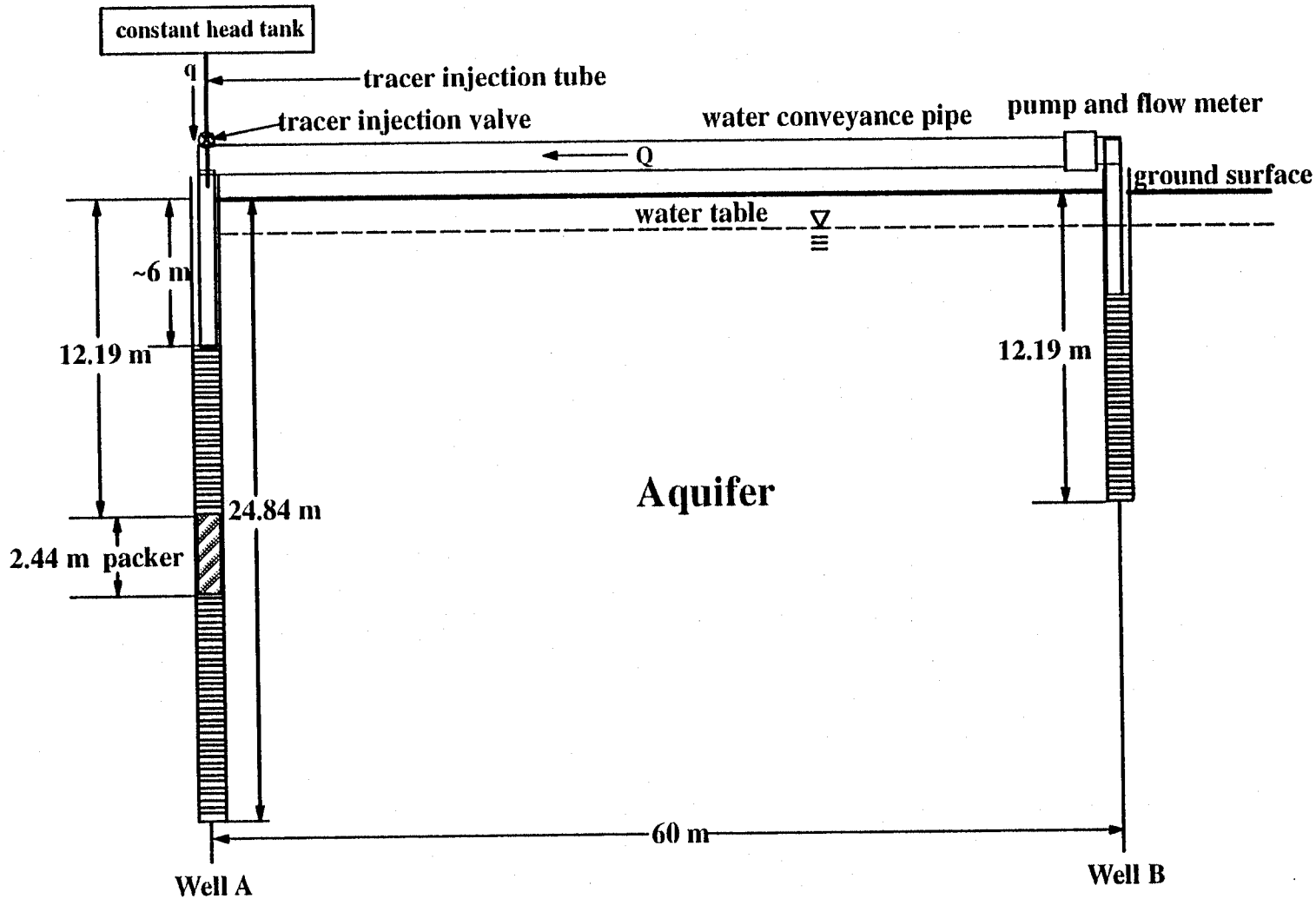

Figure 5. Field setup of the pumping well tracer test.

B and injecting it into Well A. Three hundred liters of tracer solution at a concentration of 268,000 mg/l bromide was introduced into the flow stream of Q = 13.4 m^3/hr, prior to entering Well A, for a duration of 1.38 hours. The tracer solution was stored in the constant head tank as shown in Figure 5. The introduction of the bromide solution was initiated approximately 13 hours after the injection of water was started by opening the tracer injection valve which allowed the tracer solution to enter the flow stream in the water conveyance pipe. To ensure that the bromide was fairly well mixed inside the well bore of Well A, samples were collected and analyzed from three different depths within Well A. The results of this analysis are given in Figure 6 and show that the tracer was very uniformly distributed over the length of the injection well at an average concentration of 4338 mg/l while the tracer injection was taking place (83 minutes). However, after the tracer injection was complete, there is a notable vertical concentration distribution within the well bore of Well A. Groundwater samples taken from 9.14 meters show the fastest decrease in concentration and samples taken 12.19 meters show the slowest decrease in concentration. This phenomenon could be attributed to density differences between the tracer solution and the native aquifer water which would cause the tracer solution to sink to the lower portion of Well A. Another explanation would be that the trajectory of the injection water forced the residual tracer solution into the lower portion of Well A. A constant value of 4338 mg/l was used as the injection concentration, C_0. Both vertically-averaged and depth-specific groundwater samples were collected during the test, however, analysis of these depth-specific samples was carried out by Chen et al. [1993] and is not discussed here. Vertically-averaged groundwater samples were collected at W10, NE10, SE10, W15, NE15, and SE15 using teflon bailers. Upon collection, the groundwater samples were put into containers

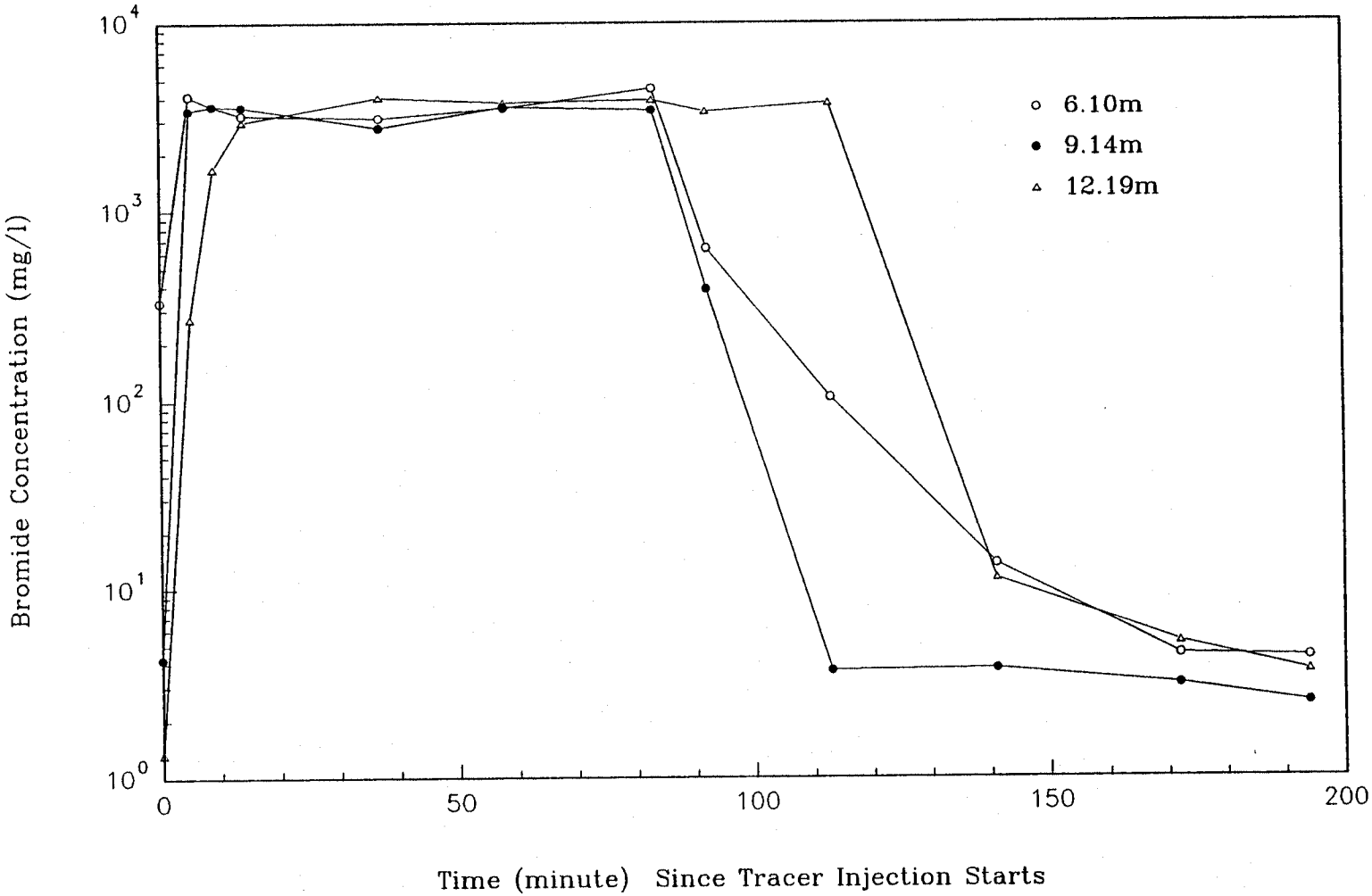

Figure 6. Bromide concentrations measured at Well A.

and transported to a laboratory for analysis by high performance liquid chromatography (HPLC). A total of 1573 vertically-averaged and depth-specific groundwater samples were collected during this tracer test.

The HPLC analysis of the groundwater samples collected from observation wells SE10, SE15, W10, W15, NE10, and NE15 yielded the bromide breakthrough curves as shown in Figures 7 and 8. However, because the bromide concentrations in wells W10, W15, SE15, and NE15 are negligibly small or show no apparent peak concentration, they were not used for further analysis. Only the breakthrough curves from observation wells NE10 and SE10 were used for curve matching analysis.

Radial dispersion solutions suitable for solute transport in pumping well tracer tests have been given by many investigators (e.g., Ogata, 1958; Raimondi et al., 1959; Hoopes and Harleman, 1967a,b; Gelhar and Collins, 1971; Tang and Babu, 1979; Sauty, 1980; Chen, 1985, 1986, 1987; Chen and Woodside, 1988; Hseih, 1986; Güven et al., 1985; Guvanasen and Guvanasen, 1987; Yates, 1988; Novakowski, 1992). All of these solutions assume that the aquifer is isotropic and, therefore, are not applicable for this research.

There has been much research conducted concerning the advection-dispersion equation as it applies to solute movement through porous media as well as applications of the resident and flux-concentrations (Kreft and Zuber, 1978, 1986; Maloszewski and Zuber, 1982; Parker and van Genuchten, 1984; Chen, 1985, 1986, 1987; and Novakowski, 1992). Kreft and Zuber [1978] defined two types of solute concentrations. Resident concentration was so defined as the mass of solute per elementary volume of the porous medium at a given time and flux-concentration was defined as the mass of solute crossing a unit area per element of time. Here,

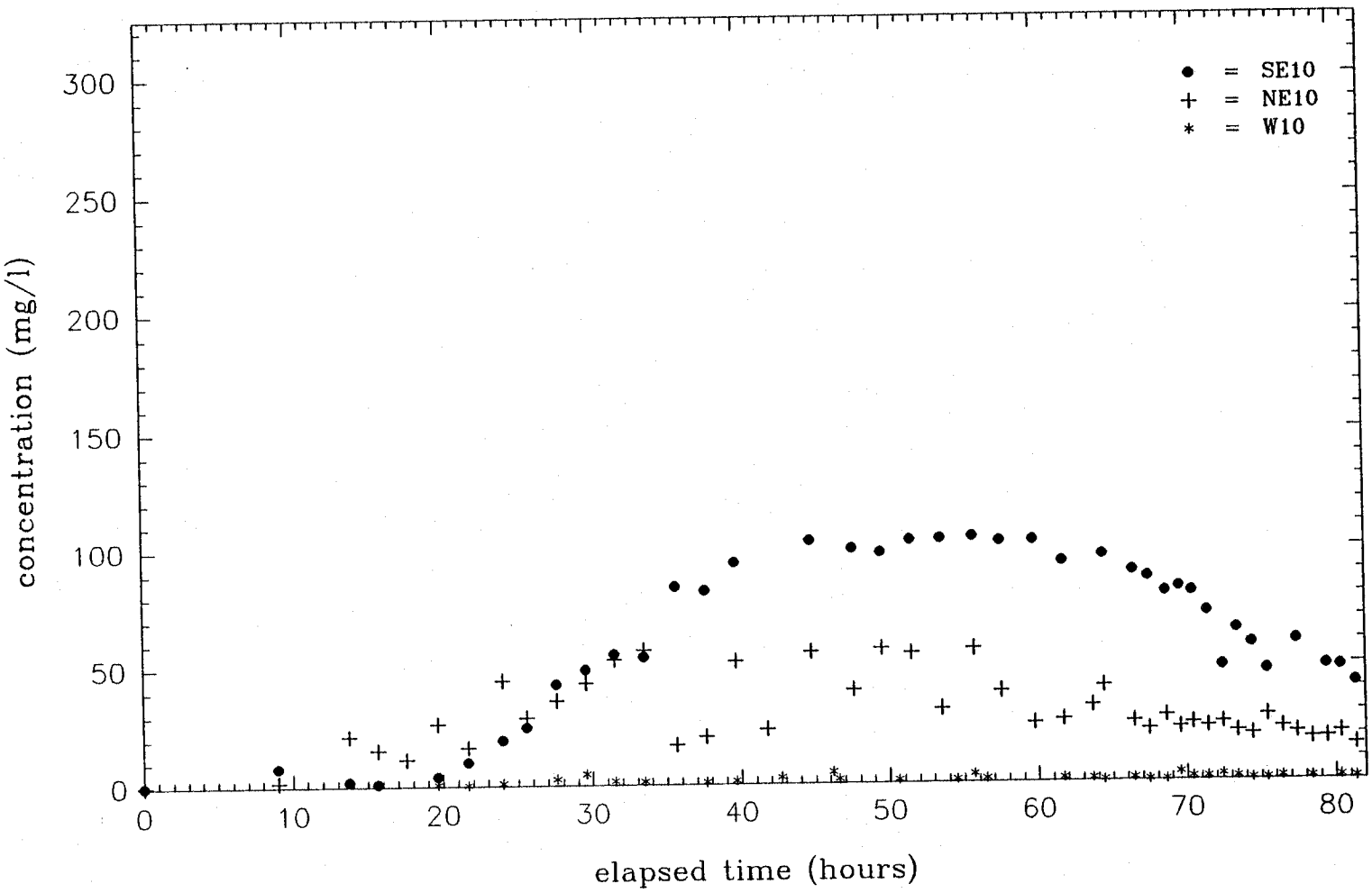

Figure 7. Bromide concentrations measured at observation wells SE10, W10, and NE10.

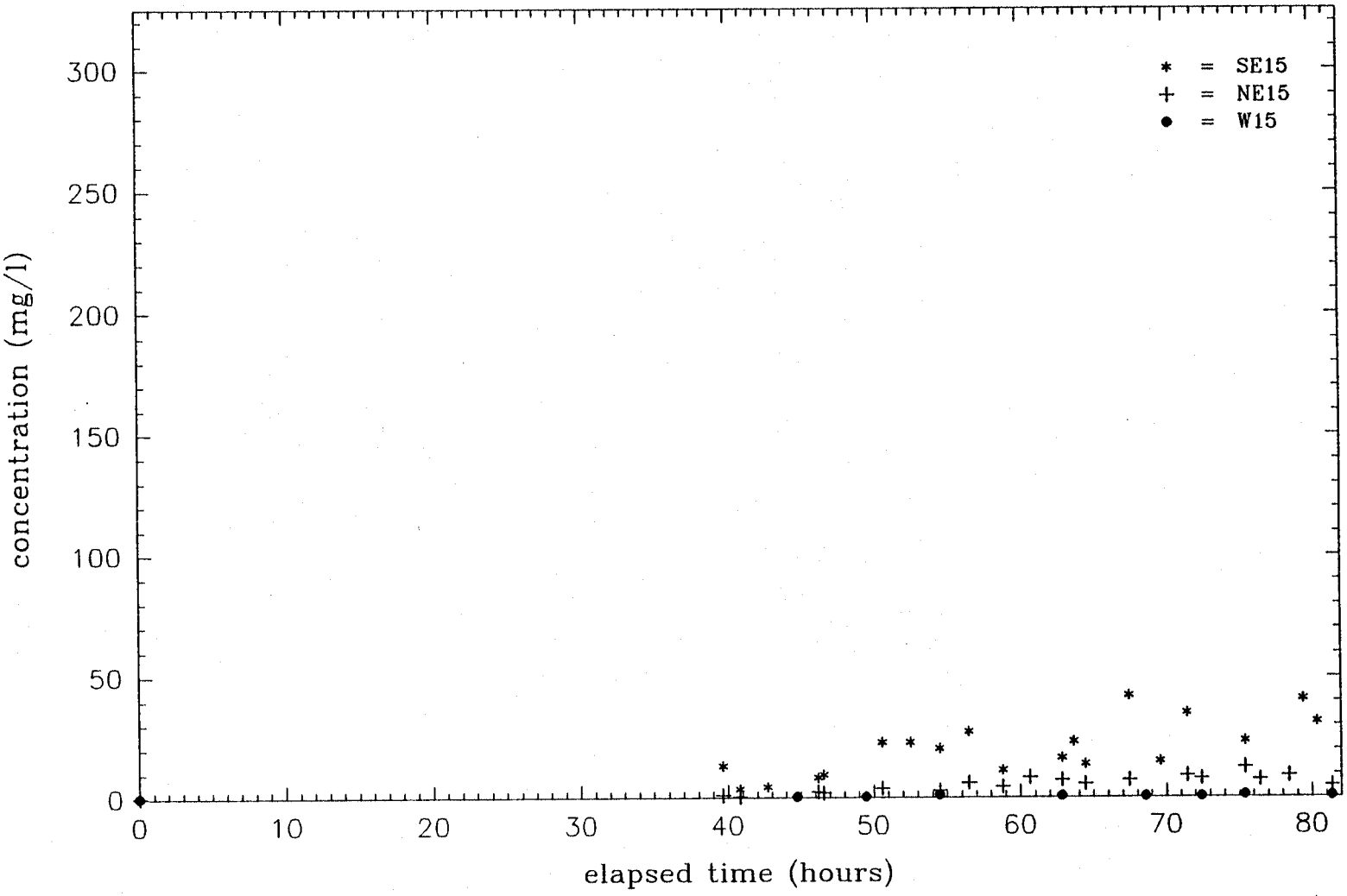

Figure 8. Bromide concentrations measured at observation wells SE15, W15, and NE15.

a model was developed which provides both resident and flux-concentrations in order to evaluate both solutions under the conditions of the pumping well tracer test. Kreft and Zuber [1978] and Parker and van Genuchten [1984] suggest that solute concentrations obtained from large-scale measuring devices such as sampling wells or pan lysimeters represent flux rather than resident-concentration values. In this study, the results of the two solutions are evaluated with regard to this theory. Novakowski [1992] conducted a radially divergent pumping well tracer test in a fractured shale using a sampling device which eliminates the mixing volume in the sampling well. He stated that samples obtained in such a manner can be interpreted with equal success using the solution in Chen [1987] which applies a Cauchy (third-type) boundary at the injection well or his Equation (24).

As stated by Sposito et al. [1986], that the present body of data is neither extensive nor highly precise, and the detailed solute movement mechanisms through natural porous media are not understood well. Therefore, the purposes of this paper are **(1)** to investigate the influence of aquifer anisotropy in solute transport problems and **(2)** to investigate the differences between the resident-concentration and flux-concentration solutions when applied to groundwater samples obtained from observation wells in an unconfined alluvial aquifer.

FIELD SITE DESCRIPTION

The field site, which contains the three multilevel samplers/piezometers (MLSP), ten fully-screened monitoring wells, and the two 15.24 centimeter water supply wells, is located approximately 32 kilometers north-northwest of Socorro, New Mexico within the boundaries of the Sevilleta National Wildlife Refuge. The field site exists on an old flood plain of the Rio Salado, an ephemeral tributary of the Rio Grande River, which is a dry channel on the average of 320 days per year. Soil horizons have not yet formed to any significant extent. The land surface is sparsely vegetated with four-wing salt bush (atriplex canescens) and a few grasses as described by Stephens and Knowlton [1986].

The aquifer in which the piezometers, sampling tubes, monitoring wells, and water supply wells are installed consists of Holocene Rio Salado alluvium overlying Pleistocene axial stream deposits of the Sierra Ladrones formation. The Rio Salado alluvium consists of interbedded sand, gravel, and silt and the axial stream deposits also consist of interbedded sand and silt with occasional gravel and clay layers (Fort, 1992). Split spoon samples taken from boreholes NW50, SE15, and SE50 show the contact between the Rio Salado formation and the axial stream deposits to be located between 13.72 and 19.81 meters below the present ground surface (BGS). The increasing depth of the contact from the north to the south direction indicates that the original Rio Salado stream channel was located farther to the south than the present channel. It was originally thought that the Rio Salado aquifer was limited to the Rio Salado alluvium (Zody, 1988). However, later seismological studies conducted in the vicinity of the field site along with the information gathered from the drilling procedures indicate that the aquifer extends into the Sierra Ladrones formation (Fort, 1992). The total thickness of the aquifer is unknown,

but it is assumed to be greater than 100 meters. Approximately 400 meters to the east of the field site, the normal Loma Blanca fault cuts across the aquifer running in an almost due north-south direction. Zody (1988) found that there was a significant steepening of the hydraulic gradient from the fault back for approximately 300 meters. It is unknown whether the effects of this fault extend into the vicinity of the area of study, however, there is little or no tilting of outcropping beds of the Sierra Ladrones formation in the vicinity of the field site.

EQUIPMENT DESIGN AND INSTALLATION

Design of Fully-Screened Observation Wells

The ten fully-screened observation wells that were installed at the field site were constructed of 5.08 centimeter PVC pipe that is capped on the bottom. The lower 18.29 meters of each of the ten observation wells is screened with 0.8 millimeter, machine cut slots and the uppermost portion of each of the observation wells is solid. Each of the slots has a circumferential length of 3.18 centimeters. There are three columns of slots around the circumference of the pipe. Each column contains 40 slots per 30.5 centimeters of PVC pipe, and thus a total of 120 slots were machine cut per 30.5 centimeters of PVC pipe. These slots represent an open surface area to closed surface area ratio of approximately 6.5 percent. It should be noted that due to unanticipated problems associated with the installation of the fully-screened observation wells, there is a variation in depth among the ten individual observation wells. The design and vertical variation of the fully-screened observation wells are shown in Figures 9 and 2, respectively.

Design of Multilevel Samplers/Piezometers

The purpose of the multilevel sampler/piezometer clusters is to allow depth specific groundwater samples and water level measurements to be taken at a single borehole. The traditional method of "nesting" several boreholes, each completed to a different depth, is costly and increases the potential of disturbing the natural flow field. An MLSP, installed in a single borehole, reduces the amount of drilling that is required and hence the cost and disruption of the aquifer are also reduced. In addition, the groundwater sampling intakes and piezometer intakes can be treated as single points in the horizontal plane.

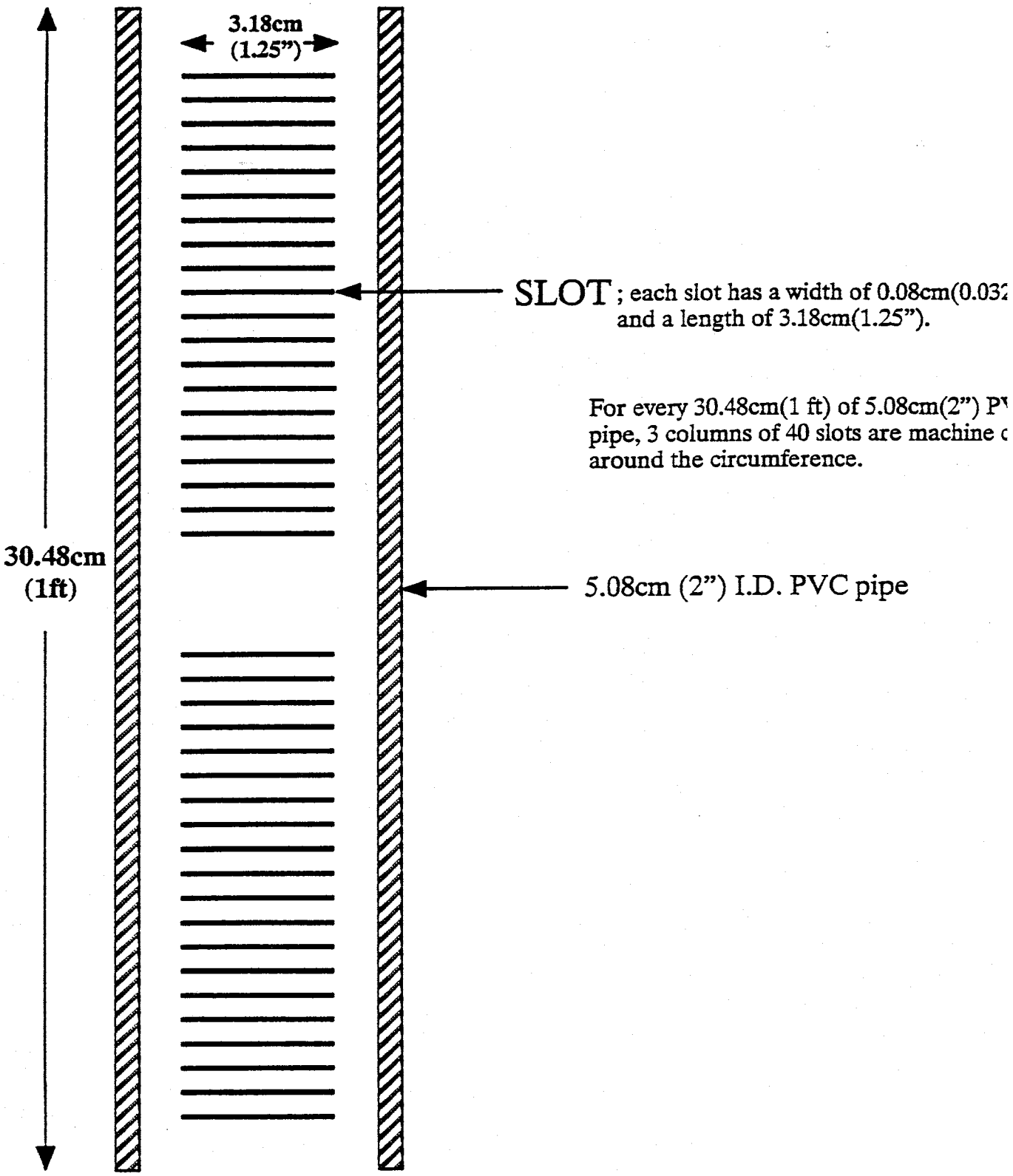

Figure 9. Design of the fully–screened observation wells.

The key issue in designing the MLSP's are that the screened intervals must remain isolated from one another and the screened interval must exist in good hydraulic connection with the aquifer. In a single partially penetrating piezometer or sampling tube, the annulus around the device intake is generally gravel packed in order to ensure that a good hydraulic connection exists between the device intake and the aquifer and the annulus above device intake is filled with bentonite and/or is grouted in order to ensure that the device intake remains isolated from the rest of the aquifer. Due to the fact that the intake sections of these samplers/piezometers are so small and in such close proximity to one another, it was deemed too difficult to accurately place the gravel packs. A slight misalignment of a gravel pack would have meant disastrous consequences. For this reason, it was decided that the annulus in each of the boreholes would be backfilled with native drill cuttings in order to make the hydraulic conductivity in the annulus approximately the same as the hydraulic conductivity of the aquifer.

The original design of the samplers/piezometers was based on the use of a 15.24 centimeter PVC casing to accommodate the sampling tubes and the piezometers. Before the installation of this casing, 19.1 millimeter ports (openings) are cut into the wall of the casing at various depths. On the inside of the casing these ports are connected to 9.6 millimeter inside diameter tubing that is long enough to extend from the depth of the port to 6.1 meters BGS. In the top 6.1 meter section of the casing a 19.1 millimeter PVC pipe is installed for every port. This sampler/piezometer cluster can be installed by first drilling a 18.7 centimeter borehole. The 15.24 centimeter casing is then installed in 6.1 meter sections. Before a new section is added to the portion that is already in the borehole, all of the tubes from the lower sections are threaded through it. Upon reaching the top 6.1 meter section of casing, each tube is connected

to a 19.1 millimeter inside diameter PVC pipe and the entire string is lowered into the borehole until the top of the casing is near the ground surface. The 19.1 millimeter PVC pipe was included in the apparatus design in order to allow water level measurements to be made using a sounding device or a steel tape as long as the water levels do not decline past 6.1 meters BGS; which is the case, even during pumping, at this field site.

One sampler/piezometer of this design was fabricated but was never installed due to the change of drilling rigs that took place as discussed in the section on drilling history. In order to facilitate installation using a 8.26 centimeter hollow stem auger, the 15.24 centimeter PVC casing had to be eliminated from the design. The new design, like the original, has 9.6 millimeter flexible tubing that runs from the device intake to 6.1 meters BGS where it is connected to a section of rigid PVC pipe. In the new design, however, the flexible tubing and rigid PVC pipe are not contained within a casing but are tied together into bundles. In order to accommodate a greater number of piezometers to be installed in a single borehole, the diameter of the upper section of rigid PVC pipe was reduced from 19.1 to 12.7 millimeters inside diameter. This specification allowed seven piezometers as well as eleven 3.18 millimeter inside diameter sampling tubes to run from various depths to the ground surface. These 3.18 millimeter tubes will allow the collection of depth specific groundwater samples to be readily obtained.

This MLSP design is installed by drilling a borehole using a 8.26 centimeter hollow stem auger. With the auger still in the borehole acting to keep the borehole free of debris, the bundled flexible tubing with a weight attached is lowered into the hollow portion of the auger. When the entire length. including the upper standpipe section, has been lowered into the augers

the augers are simply pulled out from around the MLSP, leaving the bundle in place. In order to keep the MLSP straight, a nylon rope running the entire length of the bundle is kept tight as the augers are pulled out from around the MLSP. The design of the multilevel samplers/piezometers is shown in Figure 10.

Overall, this design is less expensive and easier to install than the original design and its advantages include the following:

1. The 15.24 centimeter casing is not needed.
2. Field fabrication is not required.
3. Drilling with augers is much simpler than a rotary rig that uses drilling fluid.
4. More sampling points can be incorporated into the well field.

Drilling History

The original project design called for a 15.24 centimeter center well surrounded by nine multilevel samplers and 24 piezometers. Having recognized the difficulties associated with drilling in unconsolidated, sandy materials, it was decided to reduce the number of boreholes by adopting a multilevel sampler/piezometer design. The design that was adopted is depicted in Figure 10 and each of the newly designed multilevel samplers/piezometers can produce depth specific drawdown data as well as depth specific groundwater samples. Depth specific drawdown data can be obtained from seven individual vertical location within each borehole while depth specific groundwater samples can be obtained from eleven individual vertical locations within each borehole. The drawdown data can be collected from 6.10, 9.14, 12.19, 15.24, 18.29, 21.34, and 24.38 meters BGS and the groundwater samples can be collected from

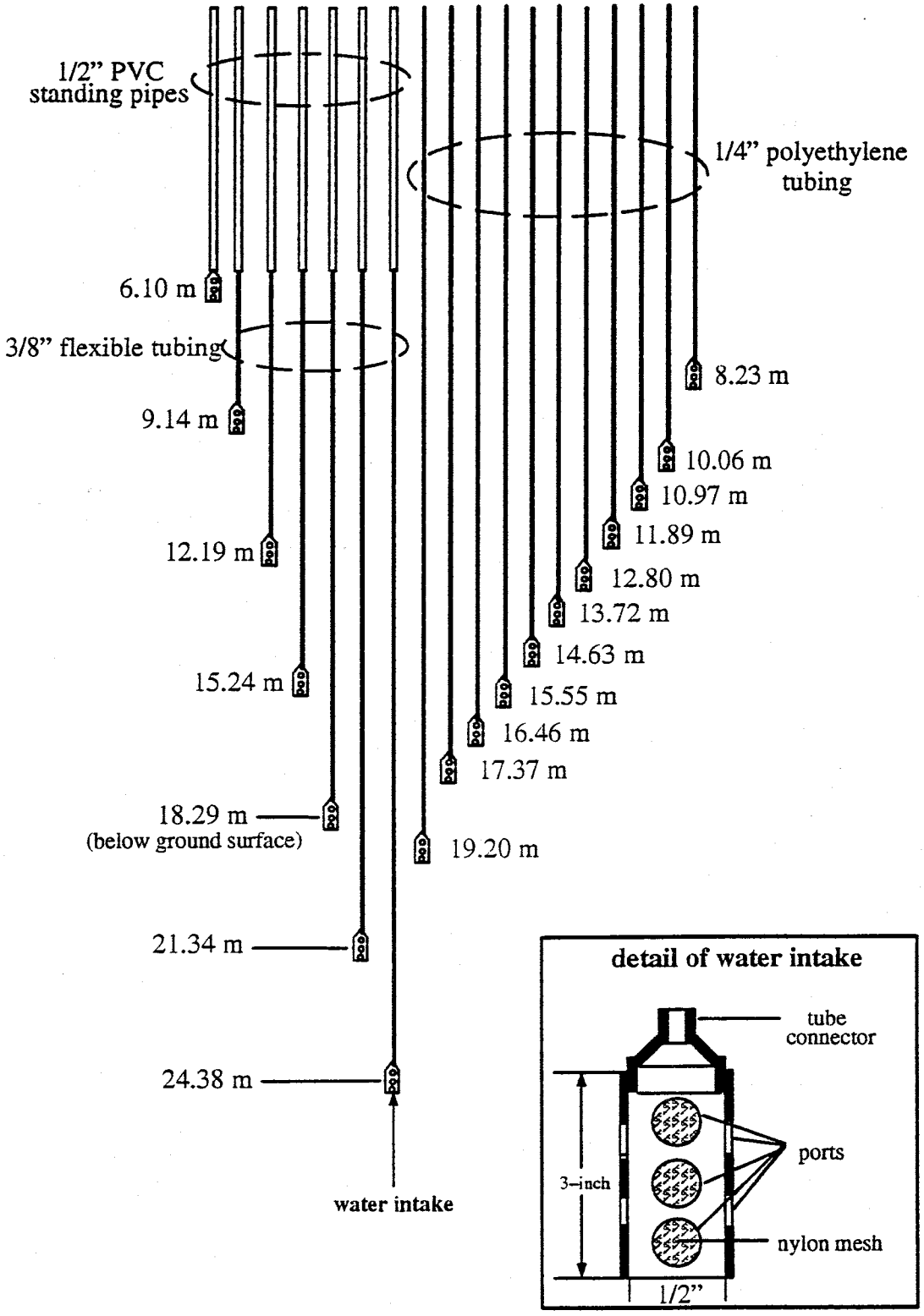

Figure 10. Design of the multilevel samplers/piezometers (MLSP).

8.23, 10.06, 10.97, 11.89, 12.80, 13.72, 14.63, 15.55, 16.46, 17.37, and 19.20 meters BGS. This method eliminated the need for 24 boreholes for piezometers, while more than sufficient amounts of drawdown data for accomplishing the project goals can still be acquired. The drilling for the multilevel samplers/piezometers (MLSP) began on 21 March 1990 using a 18.7 centimeter tricone rotary drill bit. In order to avoid the formation of a wall cake, a foaming agent rather than drilling mud was used along with air lift to remove the drill cuttings. The first borehole was completed to a depth of 25.91 meters BGS and the screen was inserted to a depth of 12.19 meters BGS where it was stopped by an obstruction which might possibly have been caused by caving in the lower portion of the borehole. The screen that is being used for this well is slotted 15.24 centimeter PVC pipe with 0.8 millimeter, machine cut slots. After an unsuccessful attempt to free the screen by drilling below it with a 10.2 centimeter bit, it was decided to use this well to supply water (Well B) for the various project needs. A second borehole, approximately 45.72 meters from the first, was then drilled and completed to a depth of 25.91 meters BGS. However, the high water velocities associated with the air lift technique caused severe caving around the borehole near the surface and this borehole had to be completely abandoned for safety reasons.

In order to avoid the caving problem in future boreholes caused by the air lift technique, it was decided that a 8.3 centimeter hollow stem auger would be used for all future drilling. The piezometers and samplers were designed such that they could be installed through the hollow stem during the drilling procedure. In order to fit the inside diameter of the hollow stem, the 15.24 centimeter PVC casing (originally designed for the multilevel observation wells) was not needed and therefore, was not used. The drilling by hollow stem auger began on 22 May 1990.

It had been hoped that by using the hollow stem auger apparatus, split spoon samples could be taken during the drilling procedure, however, sand rising up in the hollow stem of the auger caused the split spoon to sand lock in the auger. This problem made it impossible to obtain split spoon samples. Without the use of the split spoon, drilling proceeded to 25.91 meters BGS with grab samples being taken from the samples brought up by the auger. The MLSP's were installed without incident, and the annulus was backfilled with native drill cuttings.

Having wished to test the design of this MLSP before proceeding with the installation of the remaining five, it was decided to install the central 15.24 centimeter (Well A) next. Because of the requirement of the 15.24 centimeter casing, the use of the 18.7 centimeter tricone rotary drilling rig that was available for use was unavoidable. In order to keep the borehole open long enough to install the screen while avoiding the potential wall cake problem, a synthetic polymer viscosifier was used in the drilling fluid. The borehole was drilled to 25.91 meters BGS, screened with 15.24 centimeter slotted PVC pipe from 6.10 to 24.38 meters BGS, and cased with 15.24 centimeter solid PVC pipe from the surface to 6.10 meters BGS. After completion, the well was pumped using air lift to remove the drilling fluid and the annulus was backfilled with native drill cuttings. The well was then left for three days to allow the breakdown of any remaining polymer and then developed using air surging and air lift pumping. A pumping test was conducted, but drawdown measurements could not be made in the piezometers from the first MLSP. It was suspected that this was due to the fact that the intake area of each of the piezometers was too small which would lead to easy clogging. After enlarging the intake area (as shown in Figure 9), five additional MLSP's were installed using the 8.3 centimeter hollow stem auger between 3 August and 19 August 1990. The original MLSP had to be completely

abandoned. Drilling resumed on December 14, 1990 and continued into the month of March. During this time, ten fully-screened observation wells were installed at the field site using the same rotary drilling rig and hollow stem augers. During the installation of these ten fully-screened observation wells a technique was developed by which split-spoon samples could be obtained without difficulty. Therefore, it was decided to collect split-spoon samples in order to gain an understanding of the local hydrogeology. In order to avoid the problem of the split-spoon sampler becoming sand locked inside the hollow stem auger as was the problem in trying to sample the boreholes of the MLSP's, a method was devised which consisted of circulating water through the down-hole auger while drilling was in progress as well as keeping the hollow stem full of water while samples were being taken. The circulation of water during the drilling process tended to keep any aquifer material from becoming lodged in between the actual drill stem and the inside walls of the hollow stem auger. Filling the hollow auger with water during the sampling created a significant head at the bottom, open end, of the auger. This head served to inhibit any aquifer material from filling the hollow auger while the drill bit was taken out of the borehole and replaced with the split-spoon sampler. By this process, split-spoon samples were taken in three of the ten boreholes at 1.52 meter intervals. It should be noted that a sieve analysis as well as a hydraulic conductivity determination was performed on each of the soil samples that were collected. The results of this hydraulic conductivity determination will be discussed in a later section.

Prior to the installation of any of the fully-screened observation wells it was planned that each be 24.38 meters in depth; a solid 5.08 centimeter section of PVC pipe for the uppermost 6.10 meters followed by 18.29 meters of slotted 5.08 centimeter PVC pipe. However, in many

instances, installation problems were encountered and the ten fully-screened observation wells extend from the ground surface to a variety of depths; the minimum depth being 20.68 meters and the maximum depth being 25.71 meters BGS. Figure 2 gives a representation of the completion depths and screened intervals for each of the observation wells.

Development of the Fully-Screened Observation Wells

Three available alternatives exist to remove the entrapped fines from the fully-screened Observation wells: **(1)** centrifugal pumping, **(2)** water circulation, and **(3)** air injection. The method of centrifugal pumping is avoided because the significant amount of entrapped fines/debris could cause irreparable damage to the available centrifugal pumps. Thus, in this case, the air and water injection methods were adopted for developing the fully-screened observation wells. In these injection methods, air or water that is injected into the observation wells under high pressure is expected to wash out the entrapped fines/debris. Air or water is pumped into the observation wells under high pressure through pipe that extends down into the observation well to the point at which the sediment is encountered. The air/water conveyance pipe was made out of 1.9 centimeter steel pipe cut into 3.05 meter sections that could be screwed together, allowing sections of pipe to be added as needed. This process is successful in removing the fines/debris from the observation wells and was periodically repeated during the use of the field site to ensure that the fully-screened observation wells remained free of sediment.

Development of the Multilevel Samplers/Piezometers

After installation, piezometers as well as sampling tubes need to be developed in order to improve the hydraulic conductivity between the device intakes and the aquifer. In general, during drilling, the hydraulic conductivity in the zone immediately adjacent to the borehole tends to be reduced due to the disturbance of the aquifer matrix. Development of the devices helps to repair any damage that might have been caused during the drilling process by removing the finer particles which leaves a matrix of well sorted particles and high hydraulic conductivity in the vicinity of the well casing.

The piezometers and samplers in this well field were developed by alternately injecting water under pressure and pumping until there were no noticeable fines being removed by the process. During the injection process the water under pressure expands the aquifer matrix and allows the finer particles to be removed during the pumping process. A manifold system was designed and fabricated in order that several piezometers could be developed simultaneously. Figure 11 shows this manifold system.

A qualitative slug test was used to determine if an individual piezometer had been sufficiently developed. In this type of test the piezometers were filled with water and the rate at which the water level declined was observed and noted. Due to the high hydraulic conductivity of the Sevilleta aquifer and the small bore size of the piezometers, the water levels fell too quickly to allow a quantitative slug test. The extreme smallness of the sampling tubes would not allow any sort of injection to be performed as development procedures. Therefore, pumping was the only alternative and this was done to each of the sampling tubes until the water could be withdrawn at an acceptable rate. This procedure was not entirely successful, however,

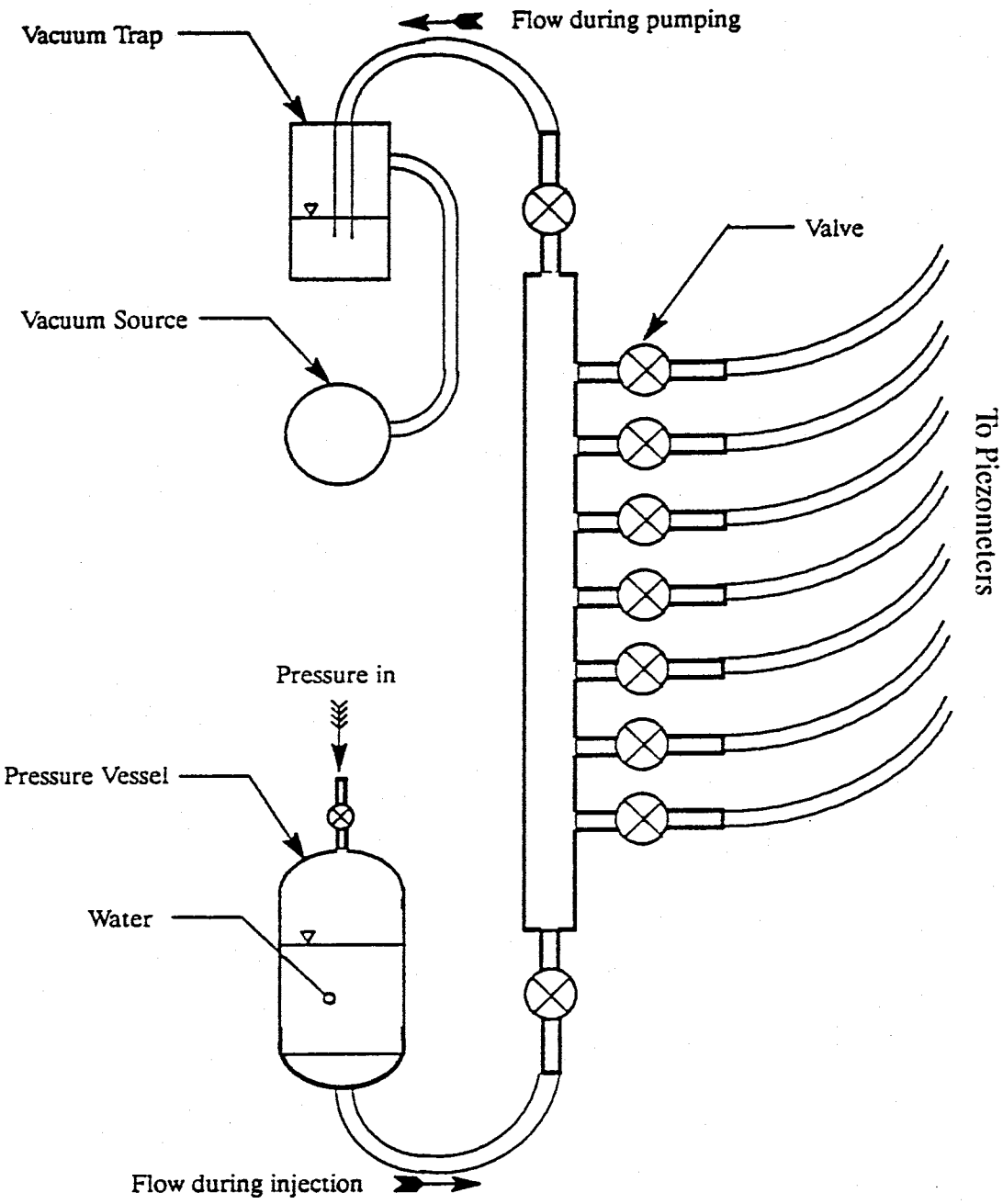

Figure 11. Schematic of the MLSP development manifold.

the majority of the sampling tubes will transmit groundwater at an acceptable rate.

During the installation of MLSP's SE6, SE3, and NE6, the tops of the piezometers were covered to prevent debris generated by the augers from falling into them. During the installation of MLSP's W3 and NE3, the tops were left open and the piezometers were kept filled with water. The piezometers that were not filled with water required substantially more development than did the others due to clogging of the intakes by fine sand and silt. The clogging resulted from water rushing in through the intakes to fill the piezometers. This action forced fine sand and silt from the soupy mix into the borehole and against the screen. This result should be noted during any future installation of piezometers.

A major concern of this project was the effect of back-filling the annulus around the MLSP's with native drill cuttings. The most likely result of this practice would be a reduced hydraulic conductivity in the annulus due to the mixing of grain sizes. A less likely result would be a higher hydraulic conductivity derived by filling the annulus with cuttings from a different, more conductive, portion of the aquifer. A third possibility would be the formation of large unfilled voids around the piezometers or sampling tube screens. This would result in an effective screen length much longer than the actual screen length. The most damaging of these three possibilities is the case of severely reduced hydraulic conductivity. Even a relatively thin layer of low hydraulic conductivity around the intakes would significantly lower the transmissivity measured by that particular piezometer. The last two cases become significant problems only if they are so extensive that they cause too much interconnection between piezometers and/or sampling tubes at different depths.

Pumping tests performed with the fully penetrating central well indicate that the majority of

the piezometers responded independently. The piezometers in MLSP's W3 and SE6 did not and were subsequently abandoned from further use. The fully penetrating pumping test results also show that piezometers at the same depths but different locations respond similarly. If the annulus properties were having a significant effect, random responses at different locations would be expected. From the above results, it has been concluded that the piezometers are measuring the properties of the aquifer rather than those of the annulus.

PRELIMINARY AQUIFER CHARACTERIZATION

Pumping Tests

A few pumping tests were conducted prior to April 1991. These tests, which were of approximately 90 minutes in duration, were undertaken to evaluate the applicability of the MLSP's and other devices at the site and to generate information that could be used to guide future research. From these tests it was determined that a pseudo-steady-state condition was achieved rapidly (approximately a few minutes after pumping begins), that vertical drawdown variations existed, and that a low permeability layer might possibly exist at approximately 11 and 13 meters BGS. Due to these findings it was decided that the aquifer be conceptualized as an upper and a lower strata separated by the low permeability layer at approximately 11 to 13 meters BGS. The upper stratum being unconfined with a finite saturated thickness of approximately 10 meters and the lower stratum being confined and considered to be of infinite thickness because of a lack of information as to where a lower confining layer might exist in the system. A steady-state, three-dimensional well hydraulics theory was used to analyze this preliminary drawdown data in each of the stratum separately.

In all of the pumping tests that were conducted prior to April 1991, two straddle packers were put inside the pumping well. The pumping interval, formed by the distance between the two packers, was kept at 1.52 meters for all of the tests. Because this pumping interval was thought to be relatively short as compared to the aquifer thickness, it was assumed that the pumping well could be considered as a "point" sink in the data analysis. Results of the data analysis indicated that both the upper and the lower strata possessed three-dimensional anisotropy. However, no conclusive properties of the anisotropy were determined due to

uncertainties such as whether a low permeability layer did, in fact, exist, whether the pumping well could be treated as a "point" sink instead of as a "line" sink, why the vertical hydraulic conductivity was the largest in the lower stratum, and other. To deal with these uncertainties, pumping tests carried out after April 1991, used only one single packer. The use of a single packer rather than a pair of straddle packers in the pumping well ensures that the pumping interval is long enough to be considered as a "line" sink without ambiguity.

Qualitative Data Analysis

Analysis of the drawdown data from the previously mentioned pumping tests (post April 1991) confirmed the existence of a low permeability layer at approximately 11 to 13 meters BGS. In pumping tests where a packer was placed in the interval of 11.48 to 13.12 meters BGS and the groundwater was extracted from below the packer, the drawdowns measured above the packer are negligibly small relative to those below the packer, implying the existence of a low permeability layer at approximately 11.48 to 13.12 meters BGS. To further confirm the existence of this low permeability layer a second pumping test was conducted with the packer in the same interval. However, in this test the groundwater was extracted from above the packer. The drawdown profile associated with this second test shows that the drawdowns below the packer are negligibly small relative to those above the packer as would be expected in the instance that a low permeability layer did exist in the previously mentioned region. These tests also indicated that the magnitude of the drawdown in the lower stratum is greater than that of the upper stratum. This fact suggests that the lower stratum of the Sevilleta aquifer is less permeable than the upper stratum.

To assure the location of the low permeability layer, the depth specific data from a third pumping test was used. In this third test the groundwater was extracted from above the packer, which was moved to the interval of 13.12 to 14.76 meters BGS. This packer interval corresponds to the location directly below the proposed low permeability layer. Comparison of the results from this third test and the second test indicate that the overall drawdown variations are similar, and that the magnitude of drawdowns below the packer are essentially identical. This evidence supports the assumption that the low permeability layer exists at approximately 11 to 13 meters BGS.

The vertically averaged drawdowns for the pumping tests during this time period were taken from the fully-screened observation wells W10, W15, NE10, NE15, SE10, and SE15; the locations with respect to the pumping well of which are indicated in Figure 1b. Observation wells W15 and SE15 each extend to a depth below 24 meters BGS, where a highly permeable zone appears to exist. Observation wells W10, NE10, NE15, and SE10 each extend to a depth above this highly permeable zone. Normally, in pumping tests, drawdown decreases as the distance from the pumping well increases. However, a greater magnitude of drawdown is observed at farther distances from the pumping well whenever groundwater was withdrawn from below the packer. This anomalous drawdown profile was not observed whenever the groundwater was withdrawn from above the packer. The existence of a highly permeable zone below 24 meters BGS would justify this anomalous drawdown profile. When pumping takes place from below the packer, this highly permeable zone provides the majority of the groundwater to the pumping well. As a result, a greater magnitude of drawdown is observed at these more distant and deeper observation wells (observation wells W15 and SE15) relative

to the less distant and more shallow observation wells (observation wells W10 and SE10). When pumping from above the packer, this highly permeable zone does not provide a significant amount of groundwater to the pumping well because it is effectively isolated from the upper aquifer in this situation. Therefore, drawdown profiles would be of the typical type in which the drawdown decreases with distance from the pumping well. The existence of the highly permeable zone makes the hydrogeology of the Sevilleta aquifer highly heterogeneous when it is treated as a whole unit. In order to avoid this heterogeneous nature of the aquifer it was decided that the lower stratum would not be used for the tracer tests.

Quantitative Data Analysis

The objective of the preliminary quantitative data analysis was to determine the principal values and directions of hydraulic conductivity anisotropy in the upper stratum in order to get some idea as to the probable behavior of a nonreactive tracer that would be introduced into the system. In a homogeneous, anisotropic aquifer, the principal values and directions of hydraulic conductivity anisotropy are unique and correspond to the eigen-values and eigen-vectors of the hydraulic conductivity tensor, $\underline{K}$, which is symmetrical and commonly expressed as

$$\underline{K} = \begin{vmatrix} K_{11} & K_{12} & K_{13} \\ K_{12} & K_{22} & K_{23} \\ K_{13} & K_{23} & K_{33} \end{vmatrix} \qquad (1)$$

The tensor, $\underline{K}$, can be determined by utilizing the three-dimensional analytical solution for drawdown distributions given by Hsieh and Neuman [1985]. Once $\underline{K}$ is known, the associated

principal values and directions of hydraulic conductivity anisotropy can be identified. The principal hydraulic conductivities will be referred to as K_1, K_2, and K_3 and the associated principal directions will be represented by their compass bearing in a horizontal plane (w) and an angle (v) measured with respect to the horizontal plane.

Determination of the Hydraulic Conductivity Tensor (K)

As stated previously, a line sink/point observation solution was necessary for the proper analysis of the drawdown data that was collected from the Sevilleta field site. To this end, steady-state (i.e. time approached infinity) drawdown at a point, due to a line sink in an infinite aquifer can be derived by combining Equations (18) and (52) from Hsieh and Neuman [1985]. The drawdown at the point (x_1, x_2, x_3) due to pumping from a line sink centered at the origin of the working coordinate system in an infinite aquifer is represented by

$$h = \frac{Q}{8\pi G_{ll}^{1/2}} \ln \frac{\left(\frac{G_{xx}}{G_{ll}} + 2\frac{G_{xl}}{G_{ll}} + 1\right)^{1/2} + \frac{G_{xl}}{G_{ll}} + 1}{\left(\frac{G_{xx}}{G_{ll}} - 2\frac{G_{xl}}{G_{ll}} + 1\right)^{1/2} + \frac{G_{xl}}{G_{ll}} - 1} \tag{2}$$

where,

Q = constant pumping rate,

$G_{ll} = L^T A L$,

$G_{xl} = X^T A L$,

$G_{xx} = X^T A X$,

$L^T = [l_1, l_2, l_3]$,

and l_1, l_2, and l_3 denote the vector components describing the half length of the pumping interval. In this case, l_1 and l_2 are equal to zero and l_3 is the half length of the pumping interval, $X^T = [x_1, x_2, x_3]$, and

$$A = \begin{vmatrix} K_{22}K_{33}-K_{23}^2 & K_{13}K_{23}-K_{12}K_{23} & K_{12}K_{23}-K_{13}K_{22} \\ K_{13}K_{23}-K_{12}K_{33} & K_{11}K_{33}-K_{13}^2 & K_{12}K_{13}-K_{23}K_{11} \\ K_{12}K_{23}-K_{13}K_{22} & K_{12}K_{13}-K_{23}K_{11} & K_{11}K_{22}-K_{12}^2 \end{vmatrix} \quad (3)$$

Although the upper stratum of the Sevilleta aquifer exists under water table conditions, in the preliminary data analysis it was treated as a confined aquifer with a finite thickness. Therefore, the method of image wells was used in order to mathematically deal with the existence of the top and bottom boundaries confining the aquifer. The method of image wells was applied to (2) with the following result

$$h = \frac{Q}{8\pi G_{ll}^{1/2}}\left[\ln\frac{\left(\frac{G_{xx}}{G_{ll}}+2\frac{G_{xl}}{G_{ll}}+1\right)^{1/2}+\frac{G_{xl}}{G_{ll}}+1}{\left(\frac{G_{xx}}{G_{ll}}-2\frac{G_{xl}}{G_{ll}}+1\right)^{1/2}+\frac{G_{xl}}{G_{ll}}-1}+\sum_{i=1}^{\infty}\ln\frac{\left(\frac{(g_{xx})_i}{(g_{ll})_i}+2\frac{(g_{xl})_i}{(g_{ll})_i}+1\right)^{1/2}+\frac{(g_{xl})_i}{(g_{ll})_i}+1}{\left(\frac{(g_{xx})_i}{(g_{ll})_i}-2\frac{(g_{xl})_i}{(g_{ll})_i}+1\right)^{1/2}+\frac{(g_{xl})_i}{(g_{ll})_i}-1}\right] \quad (4)$$

where,

$(g_{ll})_i = G_{ll}-4DLl_3(l_3-m^TL)/m^TKm,$

$(g_{xl})_i = G_{xl}+2Dl_3(d_i-m^T)/m^TKm,$

$(g_{xx})_i = G_{xx}+4D(d_i-m^TX)/m^TKm,$

and

$$D = K_{11}K_{22}K_{33}+K_{12}K_{13}K_{33}-K^2_{12}K_{33}-K_{11}K_{22}-K^2_{23}K_{11}.$$

m is a unit vector normal to the boundary, (in this case it is $[0,0,1]^T$, and d_i = the distance from the origin to image boundary (i). Due to the fact that $m^T = [0,0,1]$ in this case, the following relationships can be obtained

$$m^TX = x_3,$$

$$m^TK = K_{33},$$

$$m^TL = l_3,$$

$$(g_{xl})_i = G_{xl}+2Dl_3(d_i-x_3)/K_{33},$$

and

$$(g_{xx})_i = G_{xx}+4D(d_i-x_3)/K_{33}.$$

Also, due to the fact that $L^T = [0,0,l_3]$, the following relationships can be obtained

$$G_{ll} = l_3l_3a_{13},$$

$$G_{xl} = x_1l_3a_{13}+x_2l_3a_{23}+x_3l_3a_{33},$$

$$(g_{ll})_i = G_{ll},$$

and

a_{ij} = the element of matrix A at row i, and column j.

These nine relationships significantly simplify the calculations of (4). Since the effects of each successive image well decreases, the infinite series can be appropriately approximated by a finite number of terms, N. In this case N was chosen to be 400.

The Levenburg-Marquardt nonlinear least squares algorithm was used to fit the solution to the data. The purpose of the least squares fitting was to find the most probable estimate of model parameters (i.e. K_{11}, K_{12}, K_{13}, K_{22}, K_{23}, K_{33}) by minimizing the merit function which is

defined by

$$\min.\chi = \sum_{i=1}^{n} (h_c(\underline{K}) - h_m)^2 \tag{5}$$

where,

$h_c(\underline{K})$ = the drawdown calculated using the estimate of $\underline{K}$ and the known parameters,

h_m = the measured drawdown,

and

n = the number of measurements used in the computations.

The partial derivatives of (4) with respect to the elements of $\underline{K}$ are the sensitivity coefficients needed for the least squares minimization. They are given as follows

$$\frac{\partial h(\underline{K})}{\partial K_{kl}} = \frac{Q}{8\pi}\left[-\frac{1}{2}G_{ll}^{-3/2}\frac{\partial G_{ll}}{\partial K_{kl}}\ln f(G_{ll},G_{xl},G_{xx}) + G_{ll}^{-1/2}\frac{\partial f(G_{ll},G_{xl},G_{xx}}{\partial K_{kl}}\right.$$

$$\left. + \sum_{i=1}^{N}\left(-\frac{1}{2}G_{ll}^{-3/2}\frac{\partial G_{ll}}{\partial K_{kl}}\ln f(G_{ll},(g_{xl})_i,(g_{xx})_i) + G_{ll}^{-1/2}\frac{\partial \ln f(G_{ll},(g_{xl})_i,(g_{xx})_i)}{\partial K_{kl}}\right)\right] \tag{6}$$

where,

$$f(G_{ll},G_{xl},G_{xx}) = \frac{\left(\frac{G_{xx}}{G_{ll}} + 2\frac{G_{xl}}{G_{ll}} + 1\right)^{1/2} + \frac{G_{xl}}{G_{ll}} + 1}{\left(\frac{G_{xx}}{G_{ll}} - 2\frac{G_{xl}}{G_{ll}} + 1\right)^{1/2} + \frac{G_{xl}}{G_{ll}} - 1} \tag{7}$$

and

$$\frac{\partial \ln f(G_{ll},G_{xl},G_{xx})}{\partial K_{kl}} = \frac{1}{f(G_{ll},G_{xl},G_{xx}} \frac{\partial f(G_{ll},G_{xl},G_{xx})}{\partial K_{kl}} \tag{8}$$

and

$$\frac{\partial f(G_{ll},G_{xl},G_{xx})}{\partial K_{kl}} = \frac{\frac{\partial f_1(G_{ll},G_{xl},G_{xx})}{\partial K_{kl}} f_2(G_{ll},G_{xl},G_{xx}) - \frac{\partial f_2(G_{ll},G_{xl},G_{xx})}{\partial K_{kl}} f_1(G_{ll},G_{xl},G_{xx})}{f_2(G_{ll},G_{xl},G_{xx})^2} \tag{9}$$

and

$$f_1(G_{ll},G_{xl},G_{xx}) = (\frac{G_{xx}}{G_{ll}} + 2\frac{G_{xl}}{G_{ll}} + 1)^{1/2} + \frac{G_{xl}}{G_{ll}} + 1 \tag{10}$$

and

$$f_2(G_{ll},G_{xl},G_{xx}) = (\frac{G_{xx}}{G_{ll}} - 2\frac{G_{xl}}{G_{ll}} + 1)^{1/2} + \frac{G_{xl}}{G_{ll}} - 1 \tag{11}$$

and

$$\frac{\partial f_1(G_{ll},G_{xl},G_{xx})}{\partial K_{kl}} = \frac{1}{2}(\frac{G_{xx}}{G_{ll}} + 2\frac{G_{xl}}{G_{ll}} + 1)^{-1/2}(\frac{\partial \frac{G_{xx}}{G_{ll}}}{\partial K_{kl}} + 2\frac{\partial \frac{G_{xl}}{G_{ll}}}{\partial K_{kl}}) + \frac{\partial \frac{G_{xl}}{G_{ll}}}{\partial K_{kl}} \tag{12}$$

and

$$\frac{\partial f_2(G_{ll},G_{xl},G_{xx})}{\partial K_{kl}} = \frac{1}{2}\left(\frac{G_{xx}}{G_{ll}} - 2\frac{G_{xl}}{G_{ll}} + 1\right)^{-1/2}\left(\frac{\partial \frac{G_{xx}}{G_{ll}}}{\partial K_{kl}} - 2\frac{\partial \frac{G_{xl}}{G_{ll}}}{\partial K_{kl}}\right) + \frac{\partial \frac{G_{xl}}{G_{ll}}}{\partial K_{kl}} \tag{13}$$

and

$$\frac{\partial \frac{G_{xx}}{G_{ll}}}{\partial K_{kl}} = \frac{G_{ll}\frac{\partial G_{xx}}{\partial K_{kl}} - G_{xx}\frac{\partial G_{ll}}{\partial K_{kl}}}{G_{ll}^2} \tag{14}$$

and

$$\frac{\partial \frac{G_{xl}}{G_{ll}}}{\partial K_{kl}} = \frac{G_{ll}\frac{\partial G_{xl}}{\partial K_{kl}} - G_{xl}\frac{\partial G_{ll}}{\partial K_{kl}}}{G_{ll}^2} \tag{15}$$

and

$$\frac{\partial G_{ll}}{\partial K_{kl}} = l_3 l_3 \frac{\partial a_{33}}{\partial K_{kl}} \tag{16}$$

and

$$\frac{\partial G_{xl}}{\partial K_{kl}} = x_1 l_3 \frac{\partial a_{13}}{\partial K_{kl}} + x_2 l_3 \frac{\partial a_{23}}{\partial K_{kl}} + x_3 l_3 \frac{\partial a_{33}}{\partial K_{kl}} \tag{17}$$

and

$$\frac{\partial G_{xx}}{\partial K_{kl}} = \sum_{i=1}^{3} \sum_{j=1}^{3} x_i x_j \frac{\partial a_{ij}}{\partial K_{kl}} \tag{18}$$

and

$$\frac{\partial (g_{xl})_i}{\partial K_{kl}} = \frac{\partial G_{xl}}{\partial K_{kl}} + 2 l_3 (d_i - x_3) \frac{\partial \frac{D}{K_{33}}}{\partial K_{kl}} \tag{19}$$

and

$$\frac{\partial (g_{xx})_i}{\partial K_{kl}} = \frac{\partial G_{xx}}{\partial K_{kl}} + 4 (d_i - x_3) \frac{\partial \frac{D}{K_{33}}}{\partial K_{kl}} \tag{20}$$

Results of the Quantitative Analysis

Data from four pumping tests were analyzed using (4) and the least squares method. A total of four hundred image wells were used for each analysis. In two of the tests the pumping interval penetrated most of the upper stratum with pumping lengths of 6.10 meters and 4.57

meters (i.e. l_3 = 3.05 meters and 2.285 meters respectively for the tests). The remaining two tests were conducted prior to April 1, 1991, and used a pumping interval of 1.52 meters (i.e. l_3 = 0.76 meters). In addition to analyzing each test separately, combinations of the four tests were analyzed, respectively.

The ratio of maximum horizontal to vertical conductivity (i.e. K_1/K_3) was three hundred sixty seven to one; that is , K_1 was three hundred sixty seven times larger than K_3. The ratio of minimum horizontal to vertical conductivity (i.e. K_2/K_3) was thirty to one; that is, K_2 was thirty times larger than K_3. The ratio of maximum horizontal to minimum horizontal conductivity (i.e. K_1/K_2) was twelve to one; that is, K_1 was twelve times larger than K_2. This indicates that the anisotropy of the upper stratum is significant.

As a conclusion, the upper stratum is relatively anisotropic (i.e. the maximum horizontal conductivity was twelve times larger than the minimum horizontal conductivity; the maximum horizontal conductivity was three hundred sixty seven times larger than the vertical conductivity; and the minimum horizontal conductivity was thirty times larger than the vertical conductivity). Also, the vertical direction was a principal direction of anisotropy. So, the two orthogonal, horizontal principal directions were calculated as N 56° W and N 34° E with magnitudes of 1.05×10^{-2} m/s and 8.47×10^{-4} m/s respectively and a vertical conductivity of 2.87×10^{-5} m/s. Figure 12 gives a graphical representation of these results. It should be noted that the preliminary pumping well tracer test calculations were based on these results.

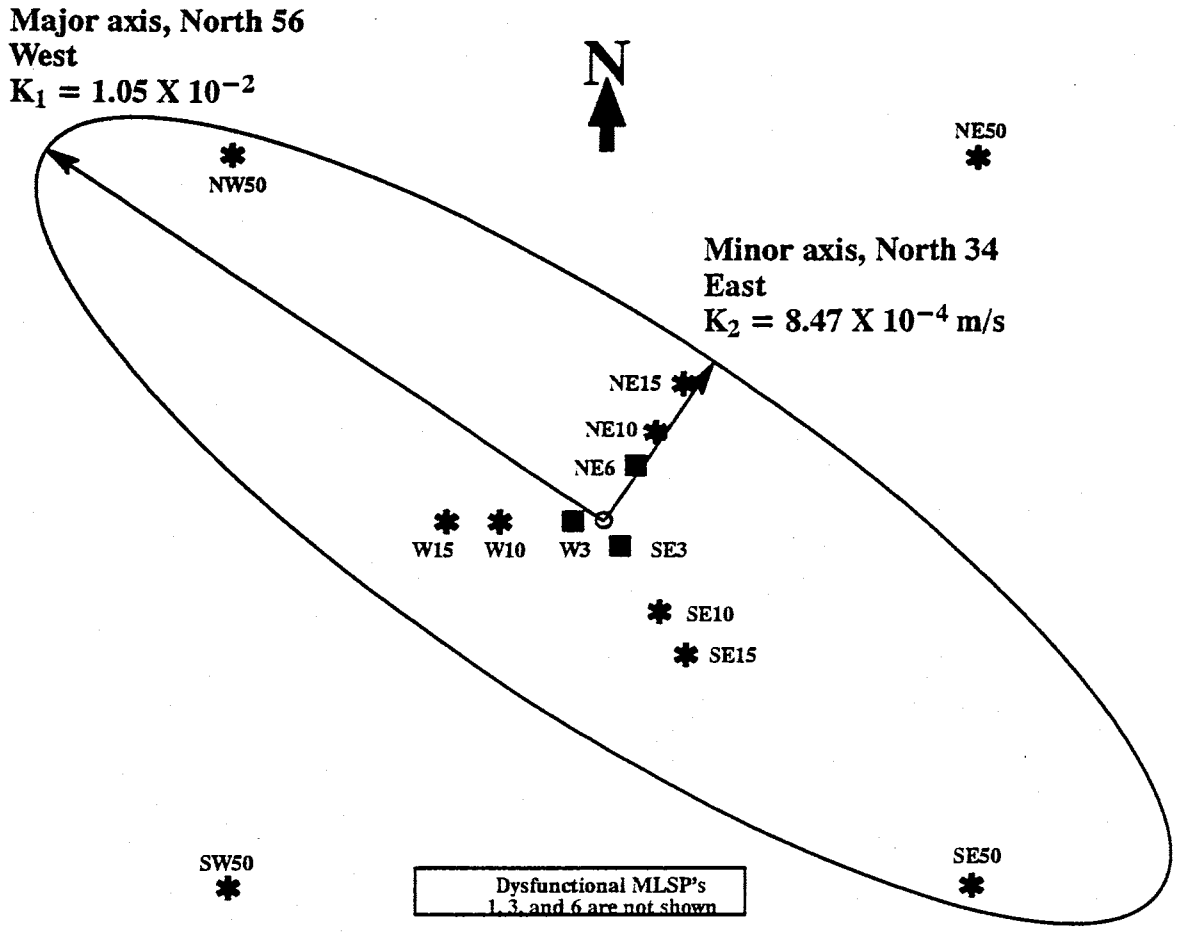

○ – water supply well

✱ – fully–screened piezometers

■ – MLSP's

Figure 12. Preliminary principal directions and values of hydraulic conductivity anisotropy in the upper stratum.

SOIL CLASSIFICATION

Sieve Analysis

The size and shape of soil particles vary over a wide range and in order to categorize soil samples, there must be a method by which the samples can be classified. The most commonly applied method by which soil samples are classified is by the grain-size distribution of the sample. The grain-size distribution of an individual sample is determined by performing a sieve analysis on the sample. A sieve analysis consists of placing a soil sample in the uppermost sieve in a nest of sieves (largest openings are found in the uppermost sieve with progressively smaller openings on lower sieves), and the nest of sieves is vibrated to allow the individual particles to fall through the sieve openings. Then, the weight of the material that is retained on each of the sieves is determined by weighing and the cumulative percent of the sample retained is plotted against the various grain sizes. This plot is known as the cumulative grain-size distribution curve and from this curve the mean grain size, effective grain size, standard deviation (sorting), skewness (degree of asymmetry), and kurtosis (degree of peakedness) can be calculated for use in classifying the sample.

A total of 44 subsurface soil samples were collected from three different boreholes from the Sevilleta research site. The soil samples were collected during the drilling of the three boreholes by split spoon sampling at 1.52 meter intervals and represent a 46 centimeter sampling zone. The research site and the well field layout are shown in Figure 1 and the three boreholes from which the samples were taken are NW50, SE15, and SE50. As can be seen from Figure 1b, the three sampled boreholes make a transect across the research site from northwest to southeast. This was done in order to provide sufficient information to make a subsurface

correlation of the research site.

Prior to performing a sieve analysis, ASTM [1963] states that the samples must be placed into one of three categories: **(A)** sample contains clay and cementing agents, **(B)** sample contains clay, but does not need to be freed of cementing agents or pigments, and **(C)** sample contains no clay, cementing agents, or soluble salts. The 44 soil samples from the Sevilleta research site were found to be of the Type C samples and thus, the following procedures were carried out in preparation for the sieve analysis according to ASTM D422-63 [1963].

1. Dry the sample in air or in a 40 degree Celsius oven. At higher temperatures any clay present may be baked into a bricklike substance, thus making dispersal of the clay difficult. Temperature-sensitive minerals such as halloysite will also be altered at higher temperatures.
2. Break all clumps. Mash with fingers; use wooden or rubber pestle in a mortar; or use a wooden rolling pin. Use enough force to separate the grains, but avoid breaking individual grains.
3. Mix the sample thoroughly and split it to get the desired weight of sample. The exact size of sample that should be used depends on several factors: the size and sorting of the sample, the shape and roundness of the grains, the number of sieves that will be used, and the shaking time. Consequently, exact weights cannot be specified. As a preliminary guide, the following approximate weights are suggested: fine gravel - 500 grams; coarse sand - 200 grams; medium sand - 100 grams; fine sand - 25 to 50 grams. About 15 grams (range from 5 to 25 grams) of material finer than 1/16

millimeter is needed if a pipette or hydrometer analysis is to be made. Another split may be necessary for the analysis of this fine material. Any of several alternate procedures may be used.

4. Weigh the split sample to the nearest 0.01 grams. Record this value on a form for recording sieve analysis information.
5. Build up a nest of clean sieves for the subdivisions desired with the coarsest sieve on top. Half-height sieves will allow a larger number of sieves to be used at one time. A lid should be put on the top and a pan at the bottom of the nest of sieves.
6. Pour the dry sediment onto the top sieve in the nest. Make certain that all of the sediment passes the top sieve.
7. Place the nest of sieves in a Ro-Tap mechanical shaker and shake for 10 minutes.
8. Empty each sieve onto a large sheet of paper. The removal of sand is helped by striking the rim of the sieve with either the palm of the hand or the wooden handle of a sieve brush along the general direction of the diagonals of the wire mesh and brushing the bottom of the sieve with a sieve brush. Use a soft, brass wire brush on sieves coarser than 100 mesh. For sieves finer than 100 mesh, use only a nylon bristle sieve brush. Be careful not to push the wires apart.
9. Weigh each fraction to the nearest 0.01 gram. Make calculations of percent retained for each fraction. The weight of the original sample will be used to calculate percentages.
10. After each use, all of the sieves should be carefully cleaned (see step 8) and stored.

Classification Method

The classification of a soil sample can be determined from a plot of the cumulative percent retained by weight of a sample versus the grain-size. This type of relationship is known as a cumulative distribution curve. Cumulative distribution curves were constructed for each of the samples rather than histograms or frequency curves, which can also be used in soil classification, due to the fact that although the cumulative distribution curve does not yield as good a pictorial representation of the grain-size distribution as a histogram or a frequency curve, its shape is virtually independent of the sieve interval used in the sieving procedure. This was an important consideration because a complete set of sieves was not available for use during the time that this work was done. These curves represent the cumulative percent of sample retained on each of the sieves versus the phi (ϕ) size. The ϕ-size is a convenient convention for the representation of the sediment grain-size that allows the fine fraction of a soil sample to be represented by positive numbers and the coarse fraction to be represented by negative numbers. Boggs [1987] states that by using the ϕ-scale, the grain-size data can be expressed in units of equal value for the purpose of graphical plotting and statistical calculations. Here, ϕ is defined as

$$\phi = -\log_2 d = -3.32\log_{10} d \qquad (21)$$

where, d is the grain-size in millimeters and the symbol, ϕ, follows the trend that as the grain-size gets smaller the ϕ-size gets larger. By using this method, the bother of constantly working with negative numbers is avoided. An example of this relationship is that if a soil sample is found to have a mean grain-size of 0.25 millimeters from (21), the mean grain-size of that sample, in ϕ-units, would be 2.0. The cumulative distribution curves for all of the samples are

given in Figure 13.

The cumulative distribution curves allowed a ϕ-size to be determined corresponding to any cumulative percent retained value from the curves. This information provided the necessary requirements to classify the samples according to size, sorting, and skewness. The classification of all of the samples was done by applying the Udden-Wentworth classification system to the mean grain-size. The classification according to size was based completely upon the mean grain-size of the sample which was defined as

$$M_z = \frac{\phi_{16}+\phi_{50}+\phi_{84}}{3} \tag{22}$$

Therefore, using the soil sample from borehole SE15 from a depth of 17.68 to 18.14 meters BGS from Figure 13b, the value for ϕ_{16} is -0.84, the value for ϕ_{50} is 2.16, and the value for ϕ_{84} is 2.81 which yields a value of 1.37 for M_z which correlates to a medium sand in the classification system shown in Table 1a.

The classification according to sorting was done by applying the criteria shown in Table 1b with the standard deviation of each sample which was defined as

$$\sigma = \frac{\phi_{84}-\phi_{16}}{4}+\frac{\phi_{95}-\phi_{5}}{6.6} \tag{23}$$

Therefore, using the same sample, the value for ϕ_{95} is 3.71 and the value for ϕ_5 is -5.23 which yields a value of 2.26 for σ which correlates to a very poorly sorted sample in Table 1b.

The classification according to the skewness of the sample was done by applying the criteria

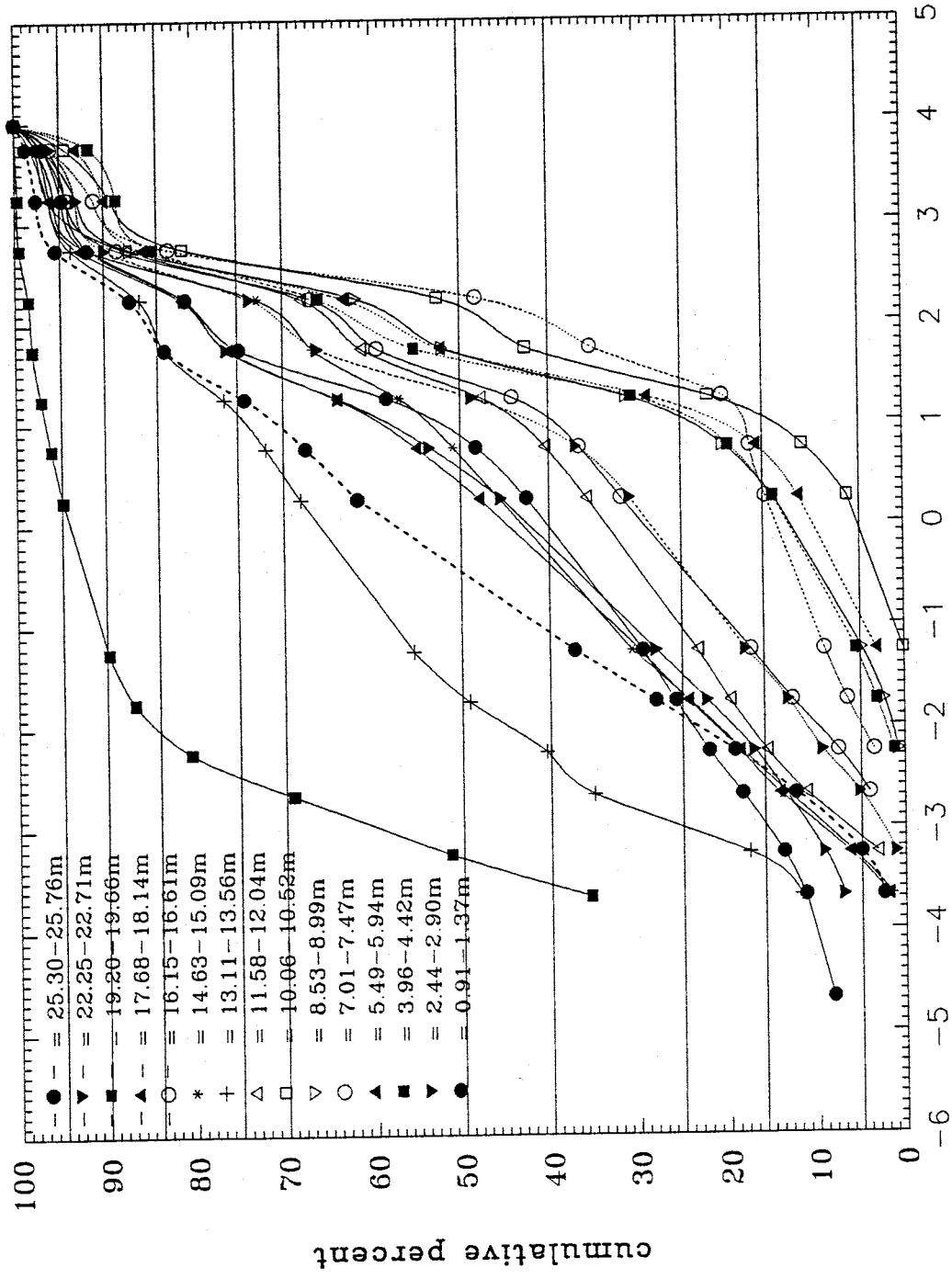

Figure 13a. Cumulative distribution curves for soil samples from NW50.

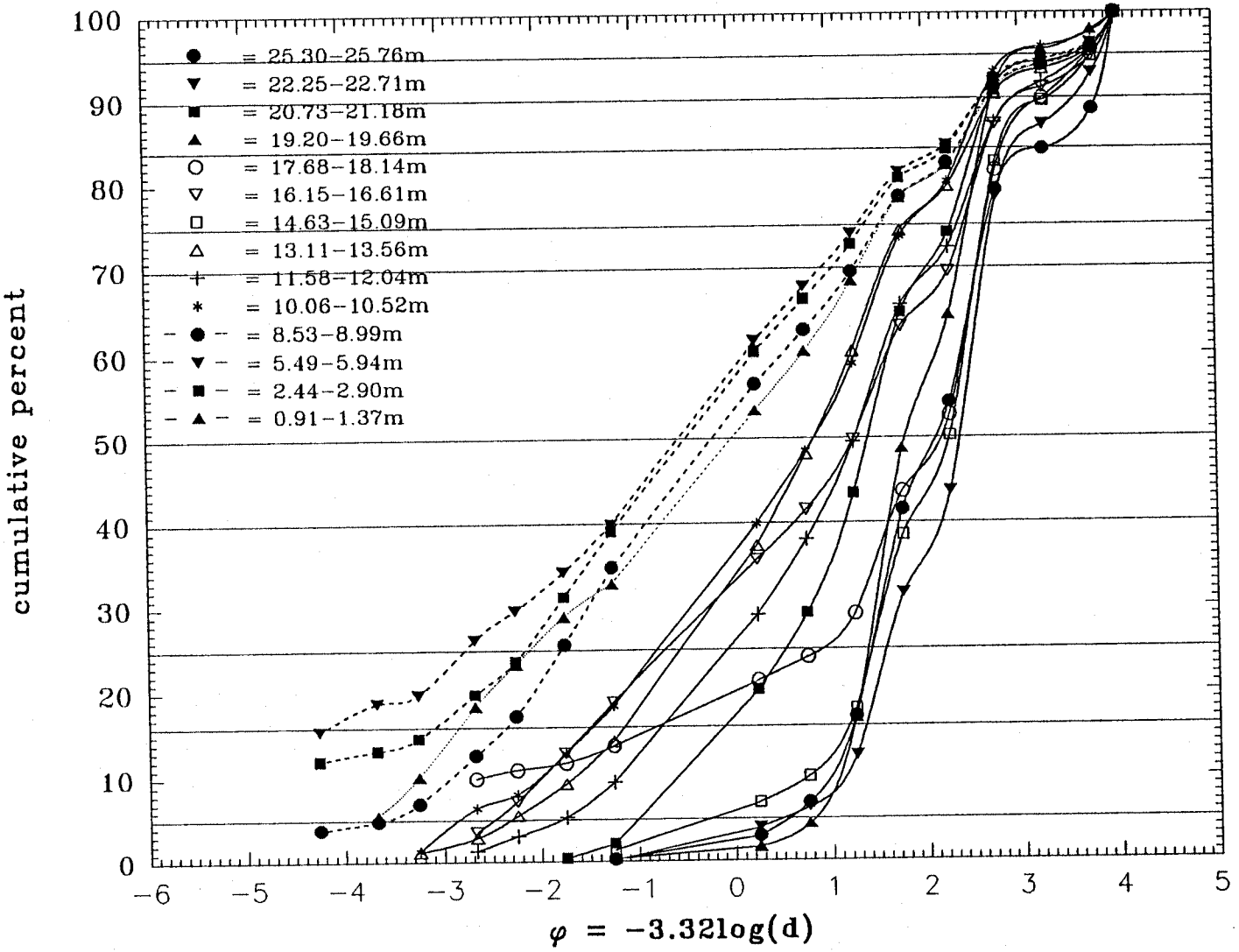

Figure 13b. Cumulative distribution curves for soil samples from SE15.

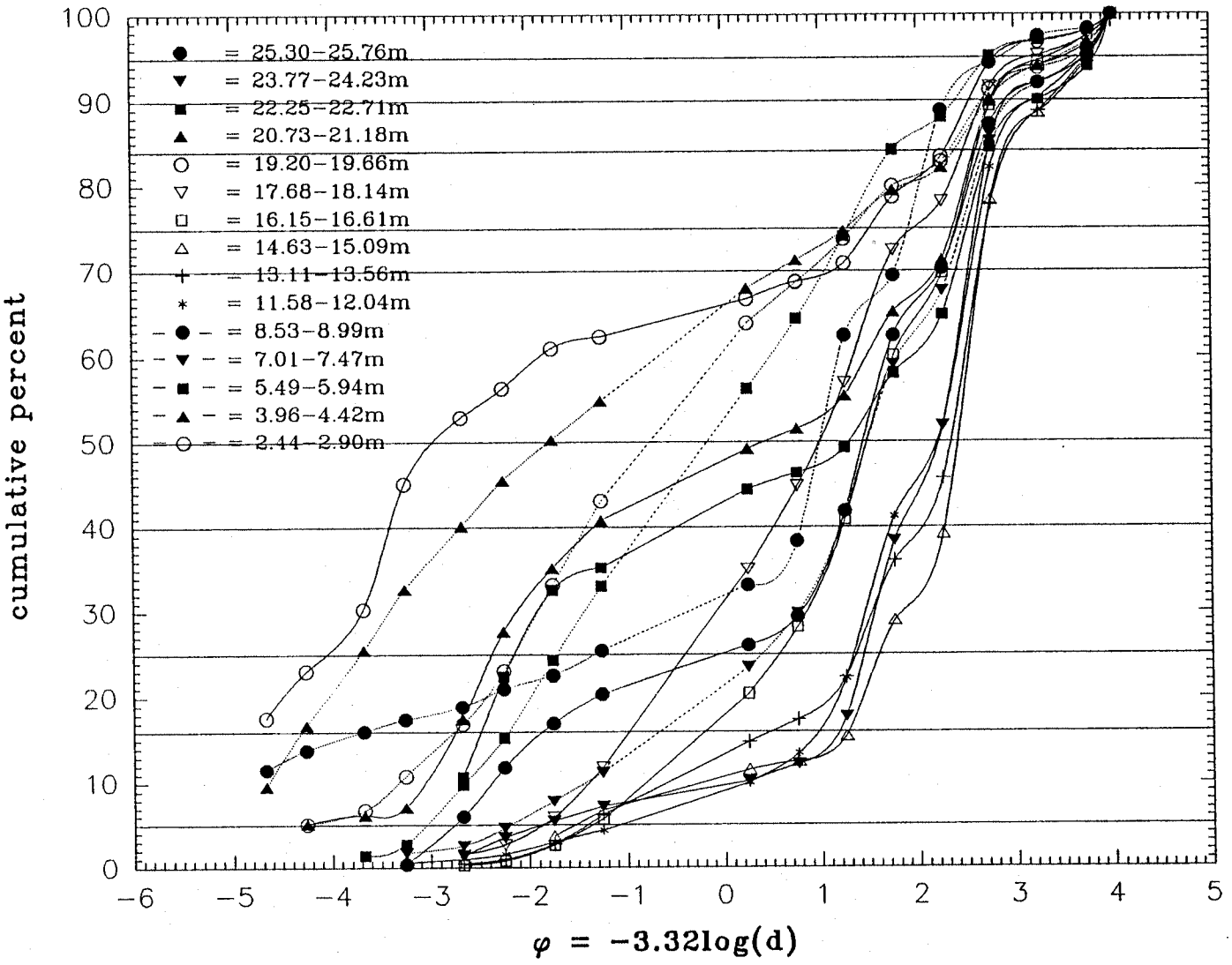

Figure 13c. Cumulative distribution curves for soil samples from SE50.

Table 1. Soil classification by the Udden–Wentworth system.

[from Table 5.1 in Boggs, 1987]

a. Soil classification according to size

d (millimeters)	M_z	Classification
> 4.0	< –2.0	Pebble
2.0 < d < 4.0	–2.0 < M_z < –1.0	Granule
1.0 < d < 2.0	–1.0 < M_z < 0.0	Very Coarse Sand
0.5 < d < 1.0	0.0 < M_z < 1.0	Coarse Sand
0.25 < d < 0.5	1.0 < M_z < 2.0	Medium Sand
0.125 < d < 0.25	2.0 < M_z < 3.0	Fine Sand

b. Soil classification according to sorting

ϕ Standard Deviation	Classification
<0.35	very well sorted
0.35 to 0.50	well sorted
0.50 to 0.71	moderately well sorted
0.71 to 1.00	moderately sorted
1.00 to 2.00	poorly sorted
2.00 to 4.00	very poorly sorted
>4.00	extremely poorly sorted

c. Soil classification according to skewness

Skewness	Classification
> +0.30	strongly fine skewed
+0.30 to +0.10	fine skewed
+0.10 to –0.10	near symmetrical
–0.10 to –0.30	coarse skewed
< –0.30	strongly coarse skewed

shown in Table 1c with the skewness of each sample defined as

$$SK = \frac{(\phi_{84}+\phi_{16}-2\phi_{50})}{2(\phi_{84}-\phi_{16})} + \frac{(\phi_{95}+\phi_{5}-2\phi_{50})}{2(\phi_{95}-\phi_{5})} \quad (24)$$

Again, using the same soil sample, a value of -0.65 for SK is obtained which correlates to a sample that is strongly coarse skewed from Table 1c. These three elements make up the classification that is given in the soil profiles from the three boreholes that are shown in Figure 14.

Porosity Determination

The porosity of a porous medium is defined as the ratio of the volume of the void space to the total volume in that porous medium. The porosity of each of the 44 soil samples from the Sevilleta research site was determined by a water displacement technique. This technique consisted of weighing an empty graduated cylinder then pouring a quantity of the soil sample into the graduated cylinder and reweighing it to obtain the mass of the sample. With the mass and volume of the soil sample known, a known volume of water was added to the graduated cylinder. From this, the volume of the void space in the soil sample was determined. With this information, the porosity of the soil sample was calculated by

$$n = 1 - \frac{\rho_b}{\rho_s} \quad (25)$$

where, ρ_b is the bulk mass density (the mass weight of the soil sample divided by the volume

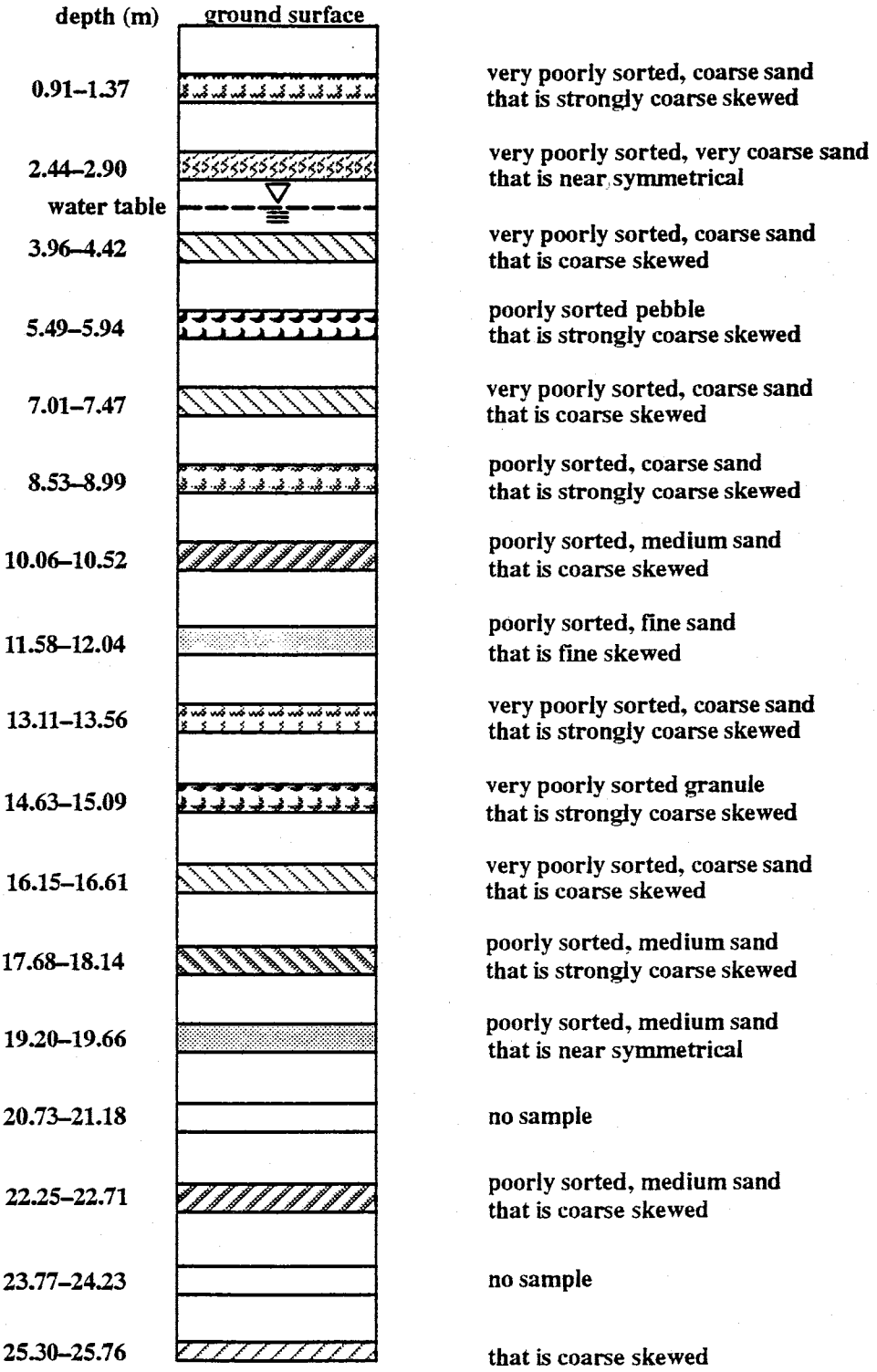

Figure 14a. Soil classification by the Udden–Wentworth system for soil samples from NW50.

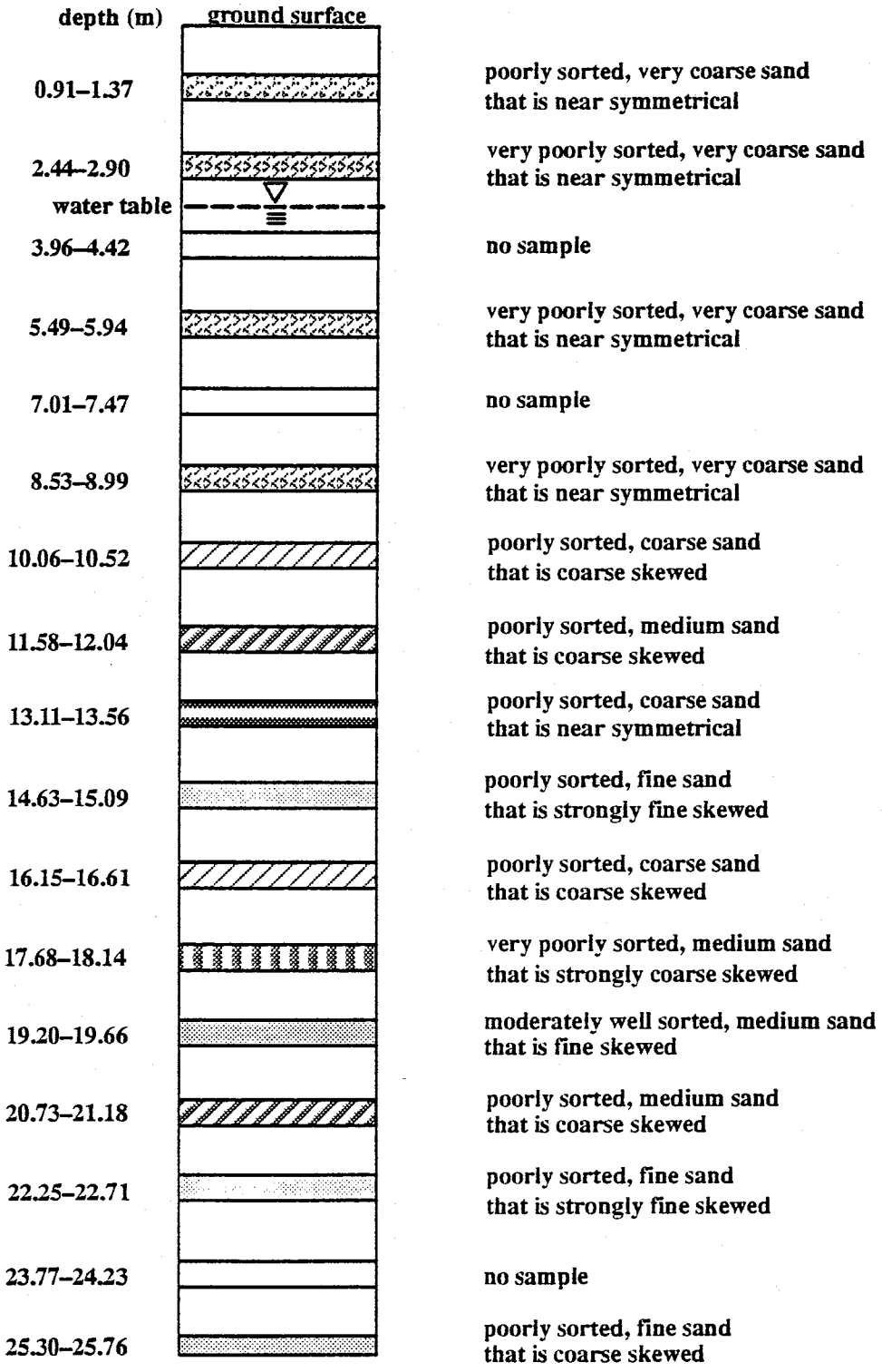

Figure 14b. Soil classification by the Udden–Wentworth system for soil samples from SE15.

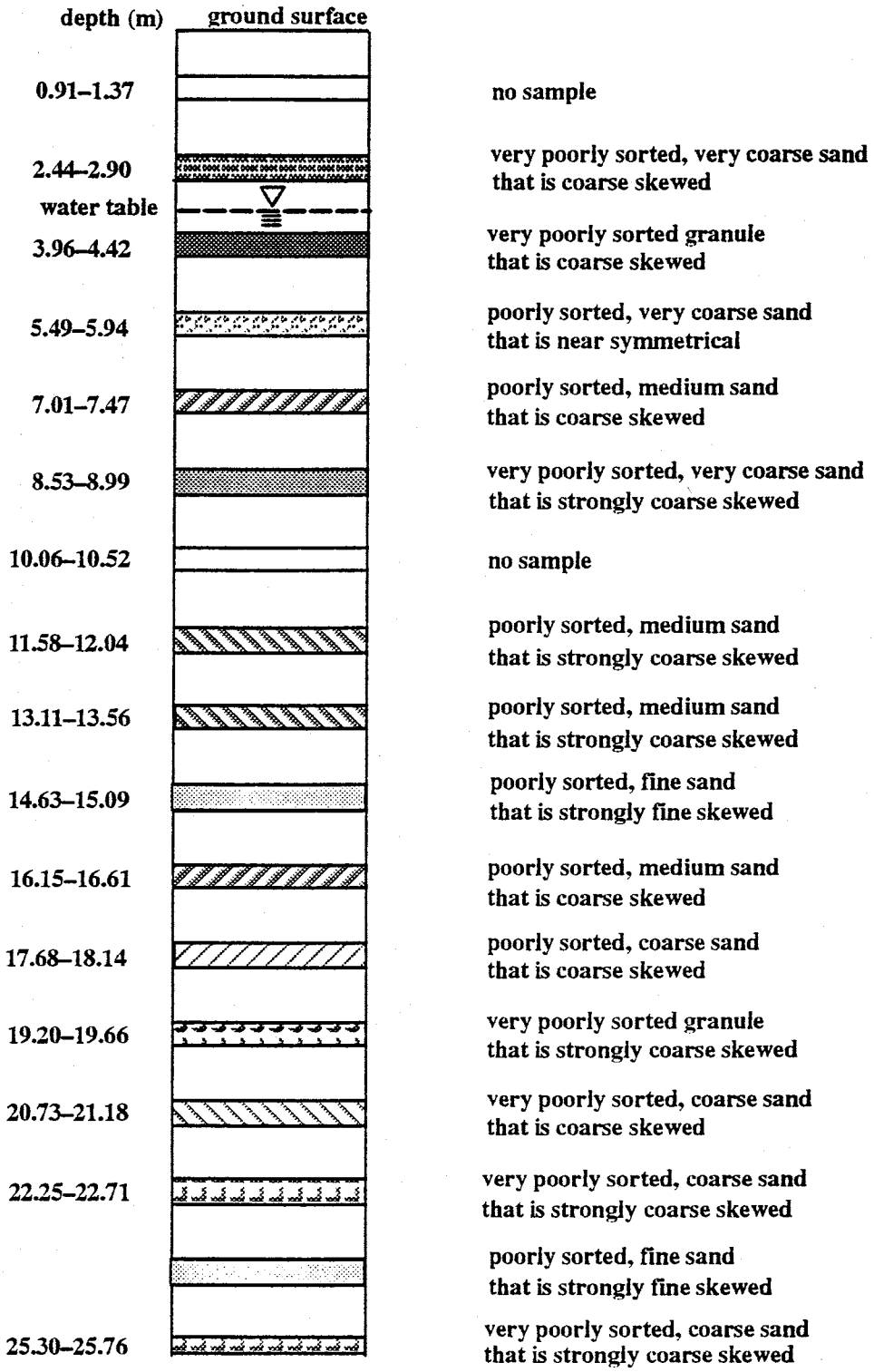

Figure 14c. Soil classification by the Udden–Wentworth system for soil samples from SE50.

of the soil sample) and ρ_s is the particle grain density (the mass of the soil sample divided by the volume of the solid particles, i.e., the volume calculated from the water displacement technique) (Freeze and Cherry, 1979).

The porosities of the 44 soil samples from the Sevilleta research site ranged from a low value of 0.20 to a high value of 0.35. It should be noted that an inherent problem with the laboratory determination of the porosity of a soil sample is that the sample is no longer in its native condition. When the soil sample is removed from the subsurface, the sample is not only disturbed, but all of the overburden pressure is removed. Therefore, porosities determined in the laboratory are typically higher than actual insitu values. Because of this fact, a standard value of 0.25 was used in all of the calculations that required this parameter.

Hydraulic Conductivity Determination

Using the information from the cumulative distribution curves along with a standard value of porosity of 0.25, a computer program developed by Vukovic and Soro [1992] was used to calculate the hydraulic conductivity of each of the 44 soil samples by ten separate methods. The fundamental equation used in each of the ten methods was

$$K = \frac{g}{\nu} C\varphi(n) d_e^2 \qquad (26)$$

where, g is gravitational acceleration, ν is the kinematic coefficient of viscosity, C is a coefficient, φ(n) is the porosity function, and d_e is the effective grain diameter. These parameters vary among the ten methods. The values for each of the parameters for each of the

ten methods along with the domain of applicability for each of the methods are given in Table 2. It should be noted that the domain of applicability of one or more of the methods might be violated by any given soil sample. This serves to screen out the methods that are not applicable to a given soil sample. By following this type of process, the three most applicable methods and thus the most applicable values of hydraulic conductivity were obtained. This was done for each of the 44 soil samples from the Sevilleta research site and the arithmetic average of the three values was calculated and plotted versus depth to show the vertical hydraulic conductivity variation in Figure 15.

The hydraulic conductivity of the soil samples was also determined in the laboratory by performing a constant-head test on each sample. In a constant-head test, a soil sample of length, L, and cross-sectional area, A, is enclosed between two porous plates in a cylindrical tube, and a constant-head differential, H, is set up across the sample. An application of Darcy's law leads to the expression

$$K = \frac{QL}{AH} \tag{27}$$

where, Q is the steady volumetric discharge through the system (Freeze and Cherry, 1979). This test was done for all of the samples and the values of hydraulic conductivity were plotted versus depth as shown in Figure 15. Also shown in Figure 15 is the arithmetic average of the three empirically determined hydraulic conductivity values along with the hydraulic conductivity as determined by the constant-head test versus depth. These three representations serve as a vertical hydraulic conductivity profile for each of the three wells from which the soil samples

Table 2. Empirical equations for estimating hydraulic conductivity.

(from Table 7 of Vukovic and Soro, 1992)

	Author	Value of Coefficient C	Function of Porosity $\phi(n)$	Effective Grain Diameter (d_e)	Domain of Applicability
1	Hazen	6×10^{-4}	$[1+10(n-0.26)]$	$d_e = d10$	$0.1mm < de < 3mm$ $C_u < 5$
2	Slichter	1×10^{-2}	$n^{3.287}$	$d_e = d10$	$0.01mm < de < 5mm$
3	Terzaghi	$10.7\times10^{-3} > Ct$ $Ct > 6.1\times10^{-3}$	$[(n-0.13)/(1-n)^{1/3}]^2$	$d_e = d10$	large–grain sands
4	Beyer	$6\times10^{-4}\log(500/\eta)$	1	$d_e = d10$	$0.06mm < de < 0.6mm$ $1 < C_u < 20$
5	Sauerbrei	3.75×10^{-3}	$[n^3/(1-n)^2]$	$d_e = d17$	sand and sandy clay $d < 0.5mm$
6	Kruger	4.35×10^{-5}	$[n/(1-n)^2]$	$1/d_e=\Sigma \Delta g_i (2)/(d_i^g+d_i^d)$	medium–grain sands $C_u > 5$
7	Kozeny	8.3×10^{-3}	$[n^3/(1-n)^2]$	$1/d_e=3/2\,g_i/d_i+\Sigma \Delta g_i (d_i^g+d_i^d)/(2d_i^g d_i^d)$	large–grain sands
8	Zunker	$0.7\times10^{-4} > Cz$ $Cz > 2.4\times10^{-3}$	$[n/(1-n)]$	$1/d_e=3/2\,g_i/d_i+\Sigma \Delta g_i (d_i^g-d_i^d)/[d_i^g d_i^d(\ln d_i^g-\ln d_i^d)]$	fine and medium grain sands
9	Zamarin	8.3x10	$[n^3/(1-n)^2]$ $\cdot (1.275-1.5n)^2$	$1/d_e=3/2\,g_i+\Sigma \Delta g_i (\ln d_i^g-\ln d_i^d)/(d_i^g-d_i^d)$	large–grain sands
10	USBR	$4.8\times10^{-4}\,d20^{0.3}$	1	$d_e = d20$	medium–grain sands $C_u < 5$

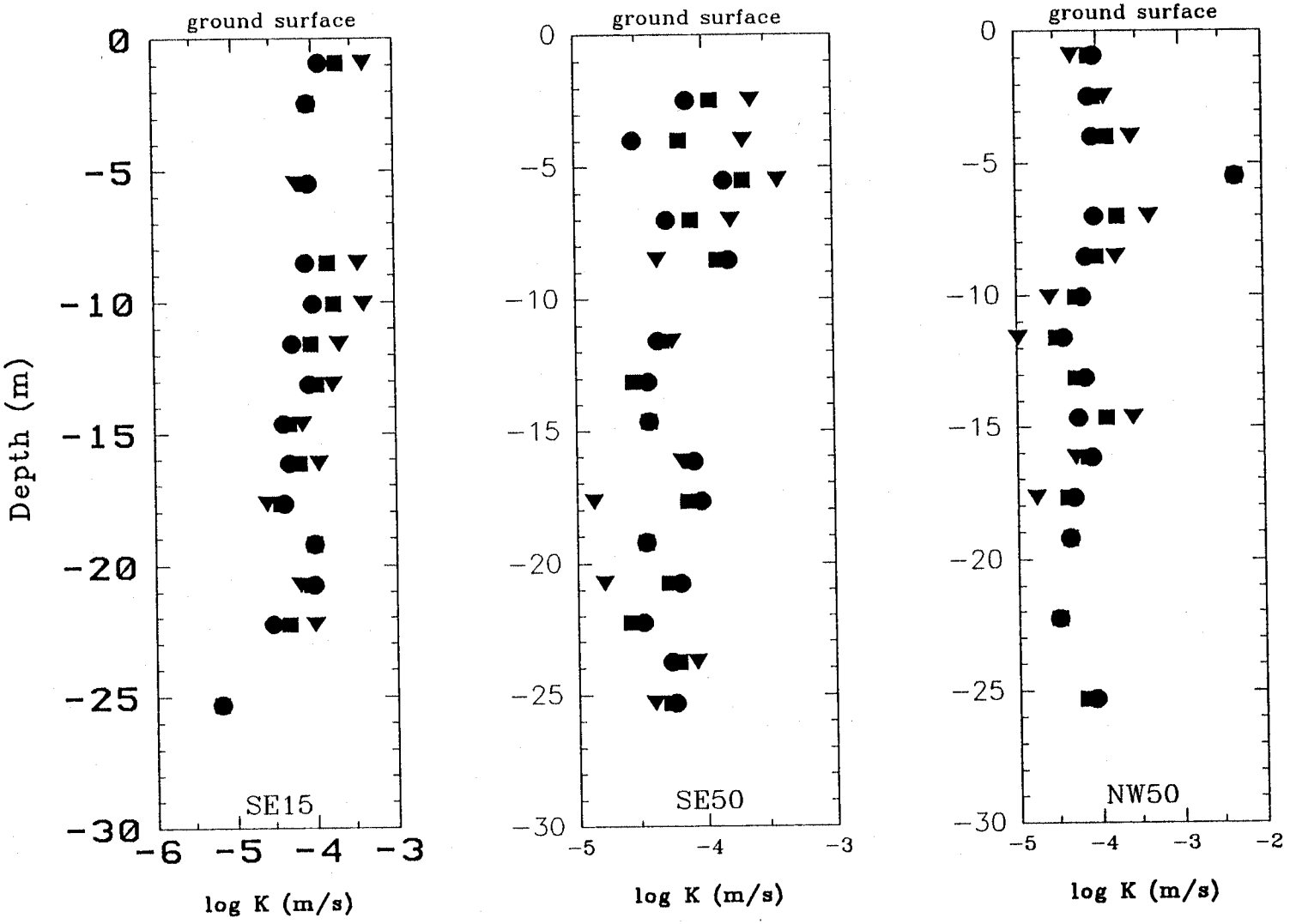

Figure 15. Hydraulic conductivity distribution determined by constant-head test and empirical equations for the soil samples (dots for empirical equations, inverse triangles for constant-head test, and squares for the average of the two methods).

were collected. It should be noted that the hydraulic conductivity as determined by these methods are not insitu values and were used only as reference values when compared to insitu hydraulic conductivity values.

TRACER TEST PROCEDURE

Preliminary Injection Procedure

Prior to conducting a tracer test, information concerning the injection method must be known in order to better ensure that the tracer test is successful. The tracer tests that were conducted at the research site in the Sevilleta National Wildlife Refuge were done so by introducing the tracer (in this case, a premixed solution of bromide) into the aquifer over a finite vertical interval in the 15.24 centimeter diameter Well A. After the tracer was injected into the aquifer, it was transported radially outward from Well A by injecting water into the well from a near-by water supply well (Well B). Sampling of the groundwater began at a predetermined time at the 3, 6, 10, and 15 meter observation points after the tracer was injected and continued for a calculated period of time to ensure that the breakthrough concentration of the tracer was collected. These samples were taken back to the laboratory and analyzed using high performance liquid chromatography (HPLC) for the actual breakthrough curves.

The water supply well that was used in the tracer tests at the Sevilleta research site was Well B located approximately 60 meters to the southeast of Well A. The complete well field layout at the Sevilleta research site is shown in Figure 1b. As stated previously, water will be pumped from Well B into Well A. It was decided to use this method in order to overwhelm the natural groundwater gradient so that the effects of aquifer anisotropy on the radial movement and dispersion of the tracer could be explored. This condition could not be addressed if the regional groundwater gradient was the only source of energy involved in the groundwater movement. By injecting water into Well A to move the tracer radially outward in all directions, it is assumed that the regional groundwater gradient will be an insignificant component in the

groundwater movement.

Due to the fact that previous pumping tests revealed the existence of a low permeability layer at approximately 12 to 14 meters BGS and a highly permeable layer below 24 meters BGS, it was decided that only that portion of the aquifer above the low permeability layer would be used for the tracer tests. This decision was made in order that the assumption of the flow domain consisting of a homogeneous porous media could be realistically made. Therefore, with the static water table at approximately 3.05 meters BGS, the saturated flow regime of the aquifer, b, that was used in all of the calculations is 10 meters. In order to isolate the upper portion of the aquifer for the tracer tests an inflatable packer was put into Well A. At the appropriate depth the packer was inflated and remained in place for the entire duration of each test. A representation of the packer is shown in Figure 16.

A constant injection rate was necessary for the entire duration of each of the tracer tests. To accomplish this, a 3.5 horsepower, centrifugal pump was used to transport the water from Well B to Well A through an impeller driven flow meter. The flow rate was monitored throughout the duration of the tests to ensure that it remained constant. Any fluctuation in the flow rate that occurred during the tests was minimized by taking the arithmetic average of all of the flow rates that were recorded during the test.

It was assumed that a radially elliptical flow field would exist for the entire duration of the tracer tests. Therefore, an inherent assumption was that there would be an insignificant amount of interference between Well A and Well B. To verify that there would be an insignificant amount of interference between the two wells, the Theis equation was applied for an estimation of the aquifer parameters at the Sevilleta research site. The two wells in question are

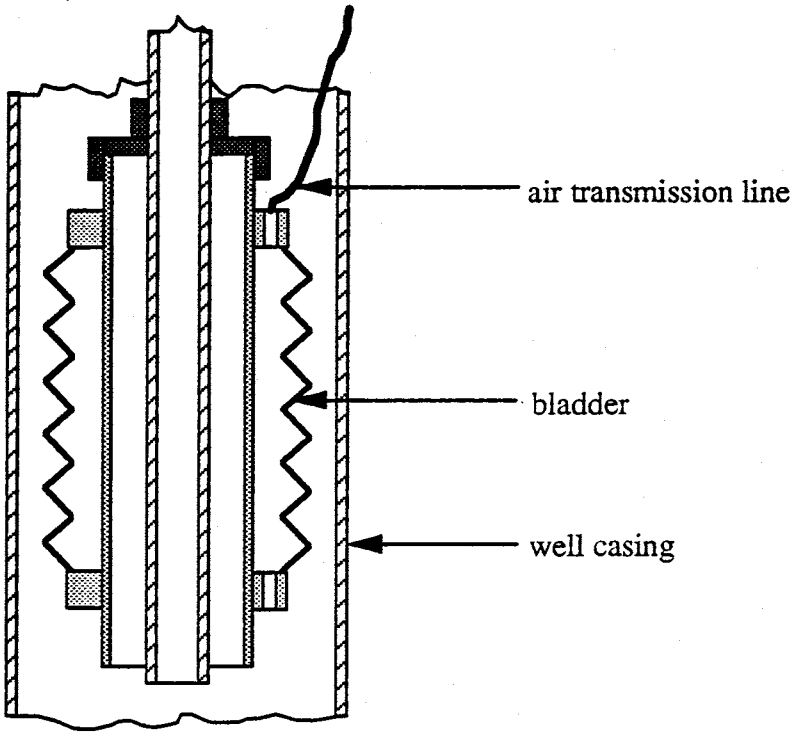

Figure 16a. Schematic of the inflatable packer (uninflated).

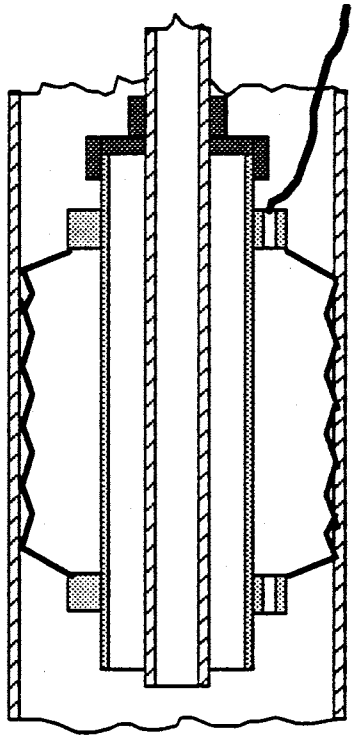

Figure 16b. Schematic of the inflatable packer (inflated).

approximately 60 meters from one another. Therefore, because one well produces a cone of depression and one produces a cone of mounding water, a radius of 25 meters was assumed and the amount of drawdown and mounding was calculated for this distance. By assuming a flow rate, Q, of 3.154×10^{-3} m^3/s and setting the specific yield, S_y, equal to 0.155, which is the mean value based on Freeze and Cherry [1979], and taking the hydraulic conductivity, K, as 9.95×10^{-3} m/s, which is the calculated value in the direction of the two wells based upon the preliminary principle values of hydraulic conductivity, the drawdown and mounding at 25 meters reaches approximately 1.7 centimeters after 103 hours of pumping. This is an acceptable amount of interference for wells A and B. However, it should be noted that this is only an estimate of the actual conditions that exist at the Sevilleta research site.

Preliminary Collection Procedure

The design and layout of the MLSP's at the Sevilleta research site is such that the bromide tracer can be collected at any one of fifty-five depth-specific sampling points and seven vertically averaged sampling points within the aquifer. The depth-specific sampling points are incorporated into the design of the MLSP's and the vertically averaged sampling points are derived from the vertically averaged observation wells as well as Well A that have been installed at the Sevilleta research site. In the preliminary tracer tests, only the MLSP's that have yielded reliable drawdown data in response to pumping tests were used as sampling points; that is, MLSP's SE3, W3, and NE6. Each of the MLSP's contain eleven depth-specific sampling tubes. So, under these limitations, the number of sampling points was effectively reduced to thirty-three. The reader is referred to Figure 1b for the spatial layout of the individual MLSP's and

to Figure 10 for the design of the individual sampling tubes. It has been mentioned that, in conducting the tracer tests, the upper portion of the aquifer will be isolated from the rest of the aquifer by placing an inflatable packer at approximately 12 to 14 meters BGS. Isolating the upper portion of the aquifer at 12 to 14 meters BGS further reduces the effective number of sampling points that can be used from eleven to five for each MLSP. The sampling tubes that are open to the aquifer at depths of 8.23, 10.06, 10.97, 11.89, and 12.80 meters BGS are the five that were monitored during the tracer tests. The four uppermost of these sampling points represent points within the upper aquifer while the sampling point at 12.80 meters BGS corresponds to a point immediately below the proposed low permeability layer. This deepest sampling point will be monitored in order to substantiate the existence of the low permeability layer. Therefore, in the preliminary tracer tests, the maximum number of depth-specific sampling points was limited to fifteen.

It is necessary to obtain the groundwater samples from the observation points simultaneously. Therefore, a sampling manifold was developed to facilitate this procedure and is shown in Figure 17. This manifold system allowed for the simultaneous sampling of as many as ten individual observation points using a single vacuum pump. The fact that this manifold system allows for the simultaneous sampling of many observation points with a single vacuum pump greatly reduced the cost of the tracer tests as well as greatly simplifying the data analysis procedure. The design of this sampling manifold is a variation of the sampling manifold described by Hitchman [1988].

The sampling manifold developed at New Mexico Tech uses ten 60 milliliter, polyethylene syringe barrels as collection chambers which are interconnected to a vacuum source by 0.64

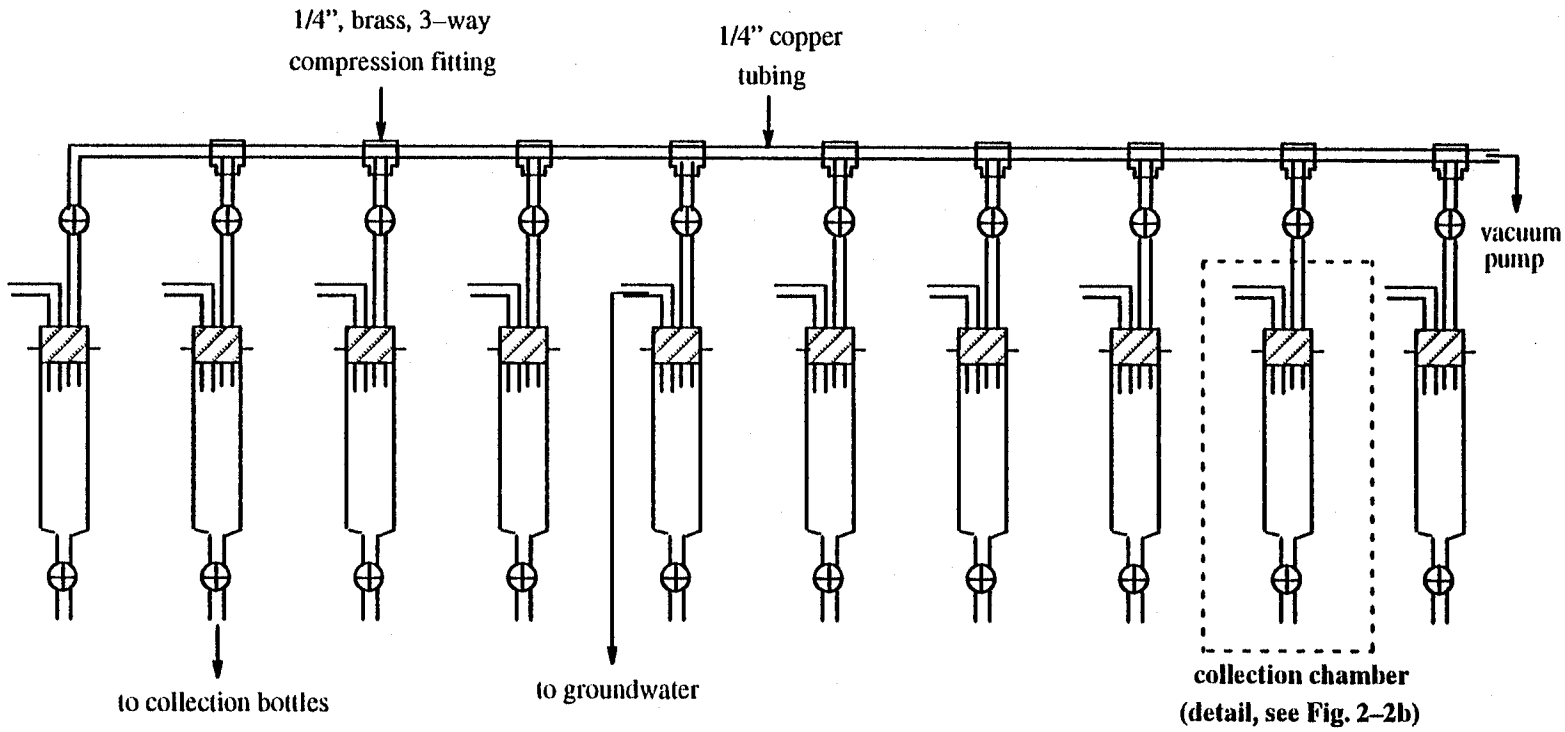

Figure 17a. Design of the groundwater sampling manifold system.

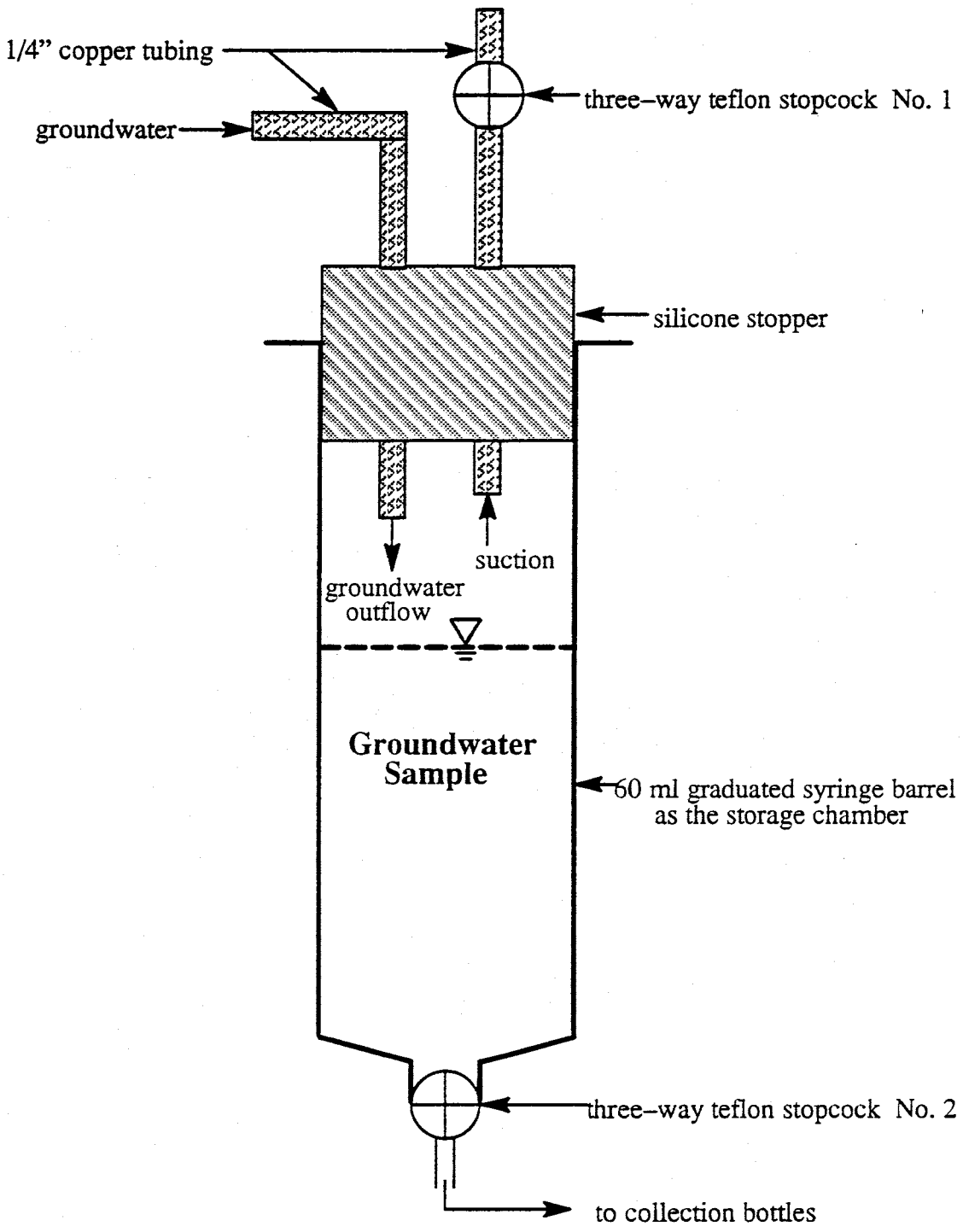

Figure 17b. Detail of the collection chamber.

centimeter copper tubing. It was decided to use copper tubing because of its rigidity and its resistance to ultraviolet light which becomes a serious problem with polyethylene tubing when it is exposed for extended periods of time such as under field conditions. Another reason that copper tubing was used in the construction of the manifold is that it has been verified that copper will not sorb any of the bromide tracer as it is collected (Bowman, 1984). For each of the ten collection chambers there are two, three-way, teflon stopcocks incorporated into the system. The first stopcock allows the vacuum suction to bypass any combination of the collection chambers. The second stopcock allows the collected samples to be extracted from the collection chamber. Because each of the collection chambers must be able to act independently of the others, the ten individual units were incorporated into the single system using brass compression fittings. Again, the reader is referred to Figure 16 where the sampling manifold design is shown in detail. The sampling manifold has been successfully tested in the laboratory as well as at the Sevilleta research site employing an electric, carbon vein, vacuum pump, powered by a gasoline generator, as the source of the vacuum.

The operation of the sampling manifold was made as simple as possible. Ten of the depth-specific sampling tubes from the MLSP's are connected to the manifold collection chambers and the vacuum pump is connected to the manifold at the proper location as shown in Figure 16a. Then, with stopcock #1 in the open position and stopcock #2 in the closed position, the vacuum pump is turned on, thus applying a negative pressure to the ten depth-specific sampling tubes. When a collection chamber fills, stopcock #1 of that chamber is turned to the closed position which causes the suction to bypass that particular chamber and stopcock #2 is turned to the open position allowing the sample to be drained from the collection chamber into a container that is

transported back to laboratory for analysis. In order to obtain a representative sample of the groundwater in the aquifer at any given time, the residual water that is contained inside each of the sampling tubes must be removed. Therefore, prior to the collection of any groundwater samples, one to two pore volumes of groundwater was removed from the sampling tubes that were sampled (Pickens et al., 1978). This procedure helped to ensure that a representative groundwater sample was being obtained from the aquifer.

A collection method that greatly reduced the logistics of the tracer tests was developed for this research as well. In the preliminary tracer tests it was decided that each of the ten sampling tubes that were used would be sampled at approximately sixty different times. By following this guideline, the breakthrough curve was very well delineated. However, sampling ten points, sixty times each, translated to a total of six hundred samples; each of which was unique with respect to time and location. Keeping track of these six hundred samples seemed to pose a serious problem concerning any conventional book-keeping that would be involved. Therefore, it was decided to construct sampling trays for the collection procedure. Each of the sampling trays contained ten, 30 milliliter high density polyethylene (HDPE) bottles in fixed positions corresponding to the positions of the collection chambers. Prior to use, each of the HDPE bottles was thoroughly rinsed, filled with ultra-pure water and allowed to stand for approximately one week, emptied, rinsed one to two times with tap water, and lastly, rinsed with ultra-pure water. After drying, the bottles were capped and not opened until used (Ground Water Manual, 1981). This procedure was also used for the polyethylene collection chambers. At a given collection time, the collection chambers were emptied into the HDPE bottles and the entire sampling tray was removed and the time at which the samples were collected was recorded

on the tray. Then a new tray replaced the used one for the subsequent sampling time. By prelabeling the collection trays and the collection chambers in the manifold from one to ten, and making sure that these numbers correspond for each sampling period, the information concerning the location of each of the samples was recorded only once due to the fact that this will not change during a given tracer test. Therefore, the only variable among the six hundred samples was the time at which the samples were collected and this information was recorded on each on the collection trays.

Background Groundwater Analysis

In order to ensure that bromide was an acceptable groundwater tracer for use at the Sevilleta research site, an analysis of the native aquifer water was made. Eleven samples of the Sevilleta aquifer water were taken from different locations within the well field and taken back to the laboratory for analysis using HPLC. The eleven samples were collected and analyzed in order to determine if there was any background bromide concentration in the groundwater and to determine if there was any spatial variation of the groundwater chemistry within the boundaries of the research site. The samples that were analyzed were collected from wells NW50, SW50, NE50, SE50, W10, W15, NE10, NE15, SE10, SE15, and Well A. The reader is referred to Figure 1b for the locations of these wells.

Prior to the analysis of the background water, it was anticipated that there would be three primary anions present consisting of chloride (Cl^-), nitrate (NO_{32-}), and nitrite (NO_{3-}). Following this assumption, a strong anion exchange column was installed and a mobile phase for the HPLC analysis was developed that would provide satisfactory separation between bromide (Br^-) and the

three expected background anions. Figure 18 shows an HPLC run of a solution containing the three anions that were expected to be present in the native aquifer water as well as bromide, using the mobile phase that will be used for any future analysis. In Figure 18 it has been verified that peak #1 represents nitrite, peak #2 represents bromide, and peak #3 represents a combination of nitrate and chloride. The combination of nitrate and chloride does not present a problem because, in conducting the tracer tests, bromide is the only anion of interest. It should also be noted that the interference that is present at the base of peak #2 and #3 in Figure 18 will not cause additional problems in the analysis due to the fact that the concentration of any peak is calculated based on the height of the peak and not the area under the peak.

The analysis of the eleven samples taken from the Sevilleta research site revealed that there was no noticeable spatial variation in water chemistry within the boundaries of the research site. A typical result from the HPLC analysis is shown in Figure 19. This sample was taken from Well A and, as in all eleven samples, contains three distinct peaks. The first peak has not been identified, however, peak #2 represents the natural bromide concentration, and peak #3 represents the combination of natural chloride and nitrate that is present. The background bromide concentration has been determined to be approximately 0.3 milligrams per liter (mg/l). Therefore, in conducting the tracer tests, a concentration of 0.5 mg/l was set as the lower limit of reliability for tracer detection. Figure 20 represents the result of an HPLC run of the native Sevilleta aquifer water with 20 mg/l of bromide added to it. Peak #3 represents the bromide at 20 mg/l and serves to show that the added bromide tracer quickly overwhelms the natural concentration of bromide.

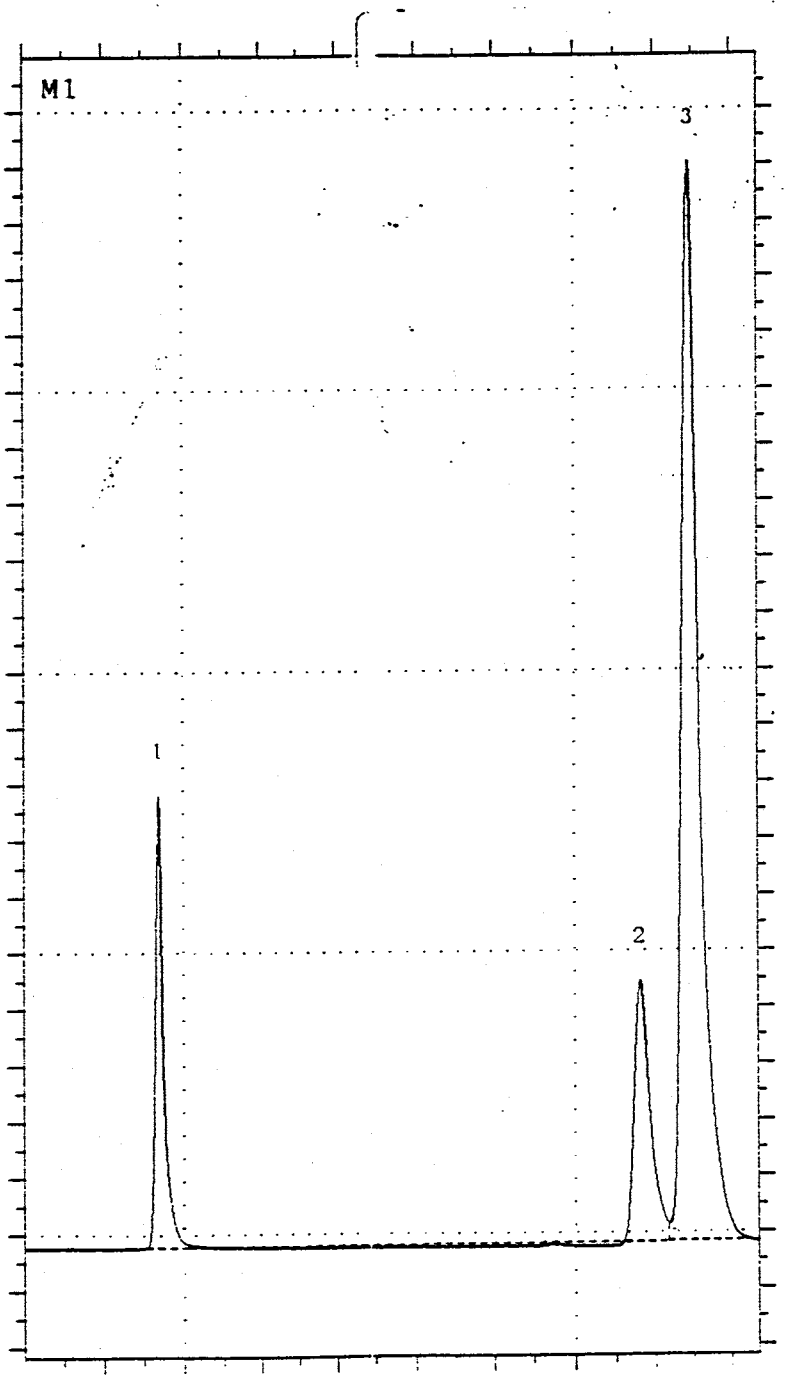

Figure 18. HPLC analysis of chloride, nitrate, nitrite, and bromide.

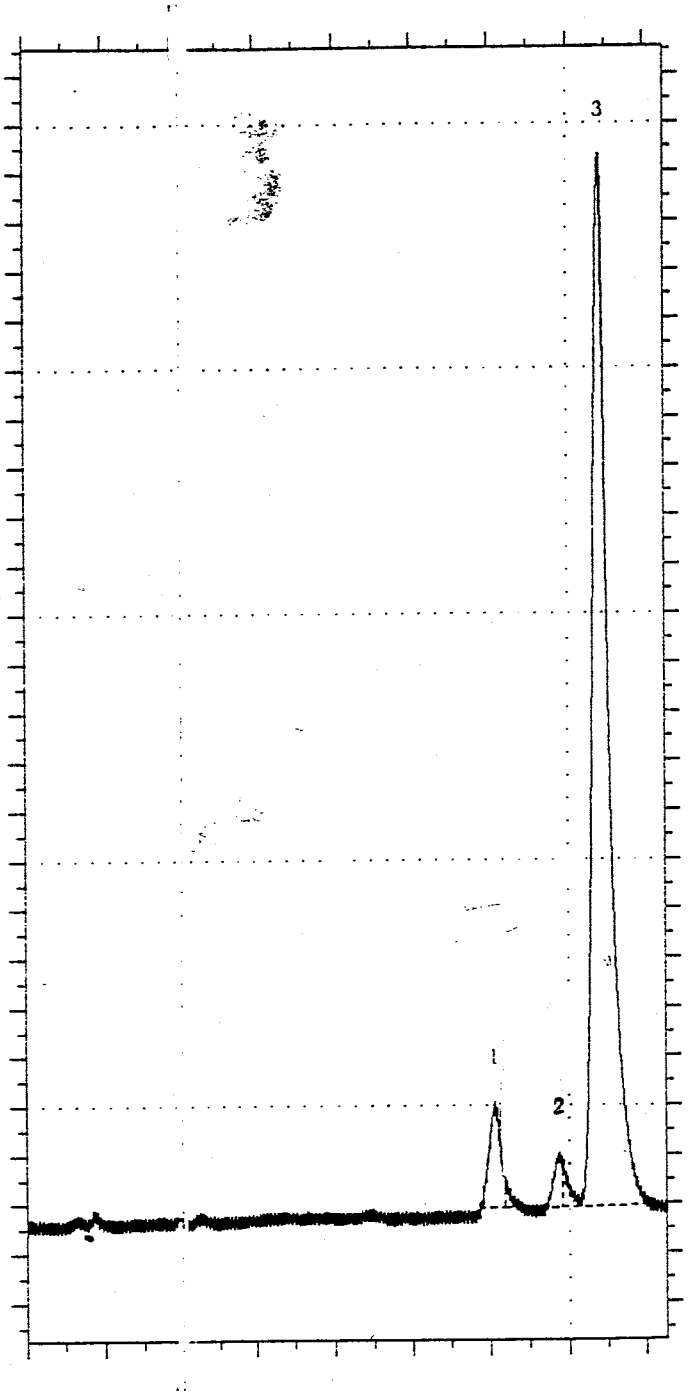

Figure 19. HPLC analysis of the native Sevilleta groundwater.

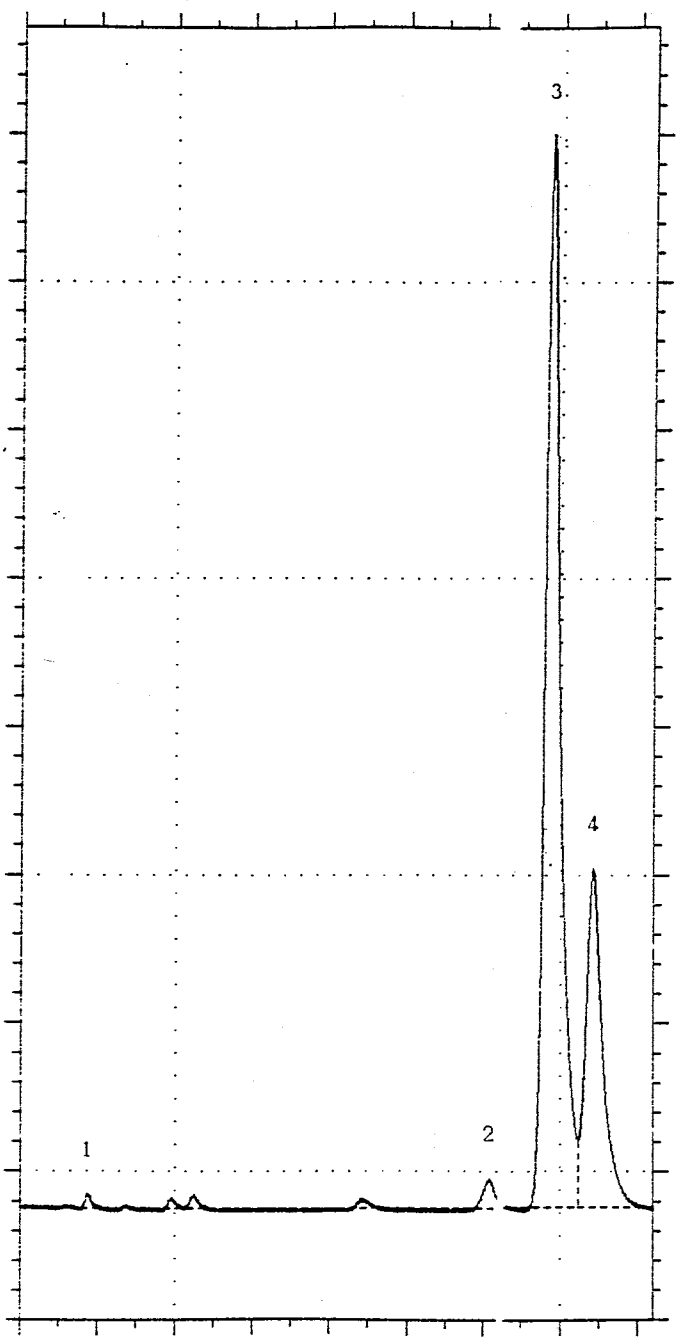

Figure 20. HPLC analysis of the native Sevilleta groundwater spiked with 20 mg/l bromide.

HPLC Analysis

The HPLC automated data analysis system include a Waters 501 pump, a Perkin-Elmer ISS200 autosampler, a Waters 481 spectrophotometer, and a Waters 745 data module. The mobile phase that was used was a 0.025 molar solution of potassium dihydrogen phosphate adjusted to a pH of 2.7 and containing 18% acetonitrile as an organic modifier. The HPLC method that was employed for the groundwater analysis was reported as having a lower detection limit (LDL) of 0.2 mg/l, meaning that below this concentration the HPLC does not yield reliable results concerning the reported concentrations. Also, the HPLC was found to have an upper detection limit (UDL) of approximately 200 mg/l, meaning any samples suspected of having concentrations higher than 200 mg/l were diluted accordingly in order to obtain reliable actual concentrations.

Maximum Allowable Tracer Concentration

In conducting pumping well tracer tests, differences in density between the injected mass of tracer and the natural aquifer water must be taken into account. Typically, one would like to introduce a tracer into an aquifer system in as high a concentration as possible in order to ensure that the equipment that is to be used to detect the tracer, after being injected into the aquifer, can do so even with the dilution that occurs between the injection point and the observation points. For this particular case, high performance liquid chromatography (HPLC) was used to analyze the samples that were obtained from the observation points. However, at excessively high concentrations, a mass of tracer may sink to the bottom of the aquifer preferentially due to the difference in density between the injected tracer mass and the natural aquifer water. This

effect would not reflect the actual flow field in the aquifer system nor the mechanisms that are acting on the tracer within the aquifer.

An estimate as to the maximum allowable concentration of tracer that could be introduced into the aquifer at the Sevilleta research site without introducing a significant artificial vertical flow component due to density differences was made. In this case the maximum allowable concentration of tracer was calculated based upon a conservative, worst case scenario. The scenario that was followed was one in which the natural groundwater gradient was used to determine the horizontal velocity of the aquifer water. This was a conservative assumption due to the fact that a gradient of much higher magnitude was imposed by injecting water into the system, thereby causing higher groundwater velocities for the actual tracer tests. The calculations are based on a model for a vertically oriented cylinder of migrating fluid in a different fluid background by Yih [1965] under the assumptions that no mixing occurs between the cylinder of migrating fluid and the background fluid and that no interfacial tension exists between the cylinder of injected fluid and the background fluid. For this case, it was decided that the vertical velocity of the tracer, $V_{z(tracer)}$, had to be less than or equal to one tenth of the horizontal velocity of the aquifer water, $V_{h(water)}$, in order to be confident that there would be no significant artificial vertical flow component produced by density effects, or

$$V_{z(tracer)} \leq 0.1 V_{h(water)} \tag{28}$$

Also, from Yih [1965; Eq. 47], it was found that

$$V_{z(tracer)} = \frac{\mu_{water}}{\mu_{tracer}} V_{z(water)} + \frac{k\Delta\rho g\alpha}{\mu_{tracer}} \quad (29)$$

where, V_z is the vertical velocity, V_h is the horizontal velocity, μ is the dynamic viscosity, k is the intrinsic permeability, ρ is the density, g is the gravitational acceleration, and α is the direction cosine of the Z-axis of the cylinder. In this case, the value of α is equal to 1. Also, from Yih [1965; Eq. 53] it was found that

$$V_{h(tracer)} = \frac{2\mu_{water}}{\mu_{tracer}+\mu_{water}} V_{h(water)} + \frac{k\Delta\rho g\beta}{\mu_{tracer}+\mu_{water}} \quad (30)$$

where, β is the direction cosine of the X-axis of the cylinder. In this case, the value of β is equal to 0. Under the assumption that $V_{z(water)} = 0$, (29) was simplified to

$$V_{z(tracer)} = \frac{k\Delta\rho g\alpha}{\mu_{tracer}} \quad (31)$$

Multiplying the right side of (31) by ρ/ρ yields

$$V_{z(tracer)} = \frac{k\rho\Delta\rho g\alpha}{\rho\mu_{tracer}} \quad (32)$$

and realizing that

$$K_z = \frac{k\rho g}{\mu} \tag{33}$$

(32) was simplified to

$$V_{z(tracer)} = \frac{K_{z(water)}\Delta\rho}{\rho} \tag{34}$$

where, K_z is the vertical hydraulic conductivity. Also, (30) was simplified to

$$V_{h(tracer)} = \frac{2\mu_{water}}{\mu_{tracer}+\mu_{water}} V_{h(water)} \tag{35}$$

The pumping tests and subsequent data analysis that were conducted during the summer of 1991 yielded information that allowed for a preliminary determination of the principle values and directions of horizontal hydraulic conductivity at the Sevilleta research site which resulted in

$K_{h(max)} = 1.05\text{x}10^{-2}$ m/s with a direction of N 56° W

$K_{h(min)} = 8.47\text{x}10^{-4}$ m/s with a direction of N 34° E

These same tests also yielded information that allowed for the determination of the hydraulic conductivity in the vertical direction which resulted in

$K_{z(water)} = 2.87\text{x}10^{-5}$ m/s

All of the calculations of the three principle values and directions of hydraulic conductivity were done by Holmes (1991, personal communication). The determination of the maximum allowable concentration employed an effective hydraulic conductivity rather than either of the principle hydraulic conductivities. The effective hydraulic conductivity was calculated by

$$K_{h(water)} = \sqrt{K_{h(\max)} K_{h(\min)}} = 2.98x10^{-3}\ m/s \tag{36}$$

The regional hydraulic gradient at the Sevilleta research site was calculated in August of 1991 to be

$$\frac{\partial h}{\partial l} = 8.33x10^{-3}\ m/s \tag{37}$$

This information allowed for the horizontal velocity of the aquifer water to be calculated by

$$V_{h(water)} = K_{h(water)} \frac{\partial h}{\partial l} = 2.48x10^{-5}\ m/s \tag{38}$$

then, from (28), the vertical velocity of the tracer was

$$V_{z(tracer)} \leq V_{h(water)} \leq 2.48x10^{-6}\ m/s \tag{39}$$

Taking the result from (34) and applying it to (39) leads to

$$\frac{K_{z(water)}\Delta\rho}{\rho} \leq 2.48x10^{-6}\ m/s \tag{40}$$

where, $\Delta\rho$ is the maximum allowable density of the injected mass. Therefore, the maximum allowable density of the injected tracer mass was calculated by

$$\Delta\rho \leq \frac{V_{z(tracer)}\rho}{K_{z(water)}} \tag{41}$$

A sample of the groundwater from the Sevilleta research site was collected and taken back to the laboratory and analyzed in order to determine its density. The analysis of this sample showed that

$$\rho_{Sevilleta} = 0.9980\ g/cm^3 \tag{42}$$

The temperature at which this measurement was made was 22.8° Celsius, which was the approximate temperature of the aquifer water. The CRC Handbook of Chemistry and Physics 71st edition (Lide, pp.6-8) gives the density of pure water at various temperatures and by linear interpolation, the density of pure water at 22.8°C is

$$\rho_{22.8} = 0.99749\ g/cm^3 \tag{43}$$

This implies that the density of the groundwater at the Sevilleta research site at standard temperature and pressure (STP) was

$$\rho_{STP} = 1.0005\ g/cm^3 \tag{44}$$

The injection technique that was used for the tracer tests was such that the tracer solution was mixed to the desired concentration in the laboratory using pure water. The calculations that follow were based on a tracer mass with a temperature of 22.8°C. However, considering that the tracer tests were conducted during the months of May through August, the tracer mass, most probably, had a higher temperature and thus a lower density. By assuming a temperature of 22.8°C, the resulting calculation of the maximum allowable tracer concentration was a conservative estimate. So, from (41), the maximum allowable tracer concentration was calculated to be

$$\Delta\rho \leq 8.619x10^{-2}\ g/ml \tag{45}$$

Making a standard conversion to milligrams per liter (mg/l) yields

$$C_{max} \leq 86194\ mg/l \tag{46}$$

Tracer Travel Time

It was established from the preliminary pump tests of 1991 that the aquifer at the Sevilleta research site was anisotropic in nature with the principle values and directions of horizontal hydraulic conductivity being

$K_{h(max)}$ = 1.05×10^{-2} m/s with a direction of N 56° W

$K_{h(min)}$ = 8.47×10^{-4} m/s with a direction of N 34° E

Therefore, the time required for the groundwater front to move from the injection point (Well A) to the observation point at 3, 6, 10, and 15 meters radial distance was determined taking the anisotropy into consideration. The process of heat conduction in solids was adopted in order to determine the velocity of the groundwater front under anisotropic conditions. The governing equation was taken from Carslaw and Jaeger [1978] as

$$h(x,y,t) = -\frac{Q}{4\pi b\sqrt{K_x K_y}}\ln(r^2\omega) \tag{47}$$

where, K_x and K_y are the principle values of horizontal hydraulic conductivity and

$$\omega = \frac{\cos^2\theta}{K_x} + \frac{\sin^2\theta}{K_y} \tag{48}$$

where, θ is the angle between a given direction and the direction of maximum horizontal hydraulic conductivity. It was verified that the velocity of the groundwater front could be determined from

$$\{V\} = \underline{K}\{\nabla h\} \tag{49}$$

where,

$$K_{rr} = K_x\cos^2\theta + K_y\sin^2\theta \tag{50}$$

$$K_{r\theta} = -K_x\cos\theta\sin\theta + K_y\cos\theta\sin\theta \tag{51}$$

and

$$K_{\theta\theta} = K_x\sin^2\theta + K_y\cos^2\theta \tag{52}$$

Carrying out the necessary operations yielded a result of

$$V_r = \frac{Q}{2\pi br\omega\sqrt{K_xK_y}} \tag{53}$$

and

$$V_\theta = 0 \tag{54}$$

where, V_θ is the angular velocity. However, in dealing with fluid flow through a porous medium, the porosity of the medium must be incorporated into any velocity determination. Doing this and realizing that (53) could be reduced to an ordinary, separable, differential equation, the travel time required for the groundwater front to move any distance were easily calculated by

$$t = \frac{r^2 - C}{2\lambda} \tag{55}$$

where,

$$\lambda = \frac{Q}{2\pi bn\omega\sqrt{K_x K_y}} \tag{56}$$

and C is a constant of integration that was determined, from the boundary conditions of the tracer tests (t = 0 at r = 0.0762 m), where r is the radius of the well, to be

$$C = 2.903x10^{-3}\ m^2 \tag{57}$$

A pumping rate of approximately 3.785×10^{-3} m^3/s was maintained for each of the tracer tests. Therefore, the travel time in each of the three directions to a distance of 6 meters was calculated to be 7.86 hours in the west direction, 21.31 hours in the northeast direction, and 5.23 hours in the southeast direction. The travel time is linearly dependent on the pumping rate. Therefore, any fluctuation in the flow rate would translate to a linear increase or decrease in the travel time. This information led to the decision that, in order to obtain breakthrough curves from the 10 and 15 meter observation wells, a tracer test would need to be at least 84 hours in duration.

Experimental Procedure

The actual pumping well tracer test took place from 19:20 on August 6, to 18:00 on August

10, 1992, was 95.33 hours in duration, and the packers were placed in Well A in the interval from 12.19 to 14.63 meters BGS. This test was of the circulation type in which groundwater was pumped from Well B and injected into Well A through a water conveyance pipe line and a potassium bromide solution at 268000 mg/l bromide was used as the groundwater tracer. The circulation and tracer injection systems are shown in Figure 5. The bromide solution, at the highest possible concentration of 268000 mg/l, was stored in a constant-head tank and was released into the water conveyance pipe at a constant rate, q, through the tracer injection valve. A total of 300 liters of 268000 mg/l bromide solution was introduced into the aquifer. The tracer injection started at 08:41 on August 7, 1992 and continued for 83 minutes, providing a tracer injection rate of 3.62 liter/minute (i.e., $q = 3.62$ l/min). A total of 1573 groundwater samples were collected from various locations throughout the duration of the test. A total of 132 groundwater samples were collected from Well A at three depths from 08:41 to 11:55 on August 7 at twenty minute intervals. These groundwater samples, shown in Figure 6, indicated that the bromide tracer was relatively uniformly mixed inside Well A and was diluted to an average concentration of 4338 mg/l during the tracer injection period. A total of 60 depth-specific groundwater samples were collected from W3 at two depths from 12:11 on August 7 to 23:12 on August 9 in one hour intervals. A total of 560 depth-specific groundwater samples were collected from SE3 at ten depths from 12:11 on August 7 to 22:14 on August 9 in one hour intervals. A total of 90 depth-specific groundwater samples continued to be collected from SE3 from the five lower depths from 23:40 on August 9 to 18:02 on August 10 in one hour intervals. A total of 350 depth-specific groundwater samples were collected from well NE6 at five depths from 17:06 on August 7 to 18:02 on August 10 in one hour intervals. A total of 201 vertically-

averaged groundwater samples were collected from W10, SE10, and NE10 from 20:40 on August 7 to 18:02 on August 10 in one hour intervals. A total of 120 vertically-averaged groundwater samples were also collected from W15, SE15, and NE15 from 00:20 on August 9 to 18:02 on August 10 in one hour intervals. All of the groundwater samples were filtered through a 0.45 micron nylon filter prior to analysis by HPLC. The resulting bromide breakthrough curves from the various observation points are shown in Figures 7, 8, 21, 22, and 23. The analysis of the depth-specific groundwater samples is not within the scope of this paper. The reader is referred to Chen et al. [1993] for information regarding this aspect of the research.

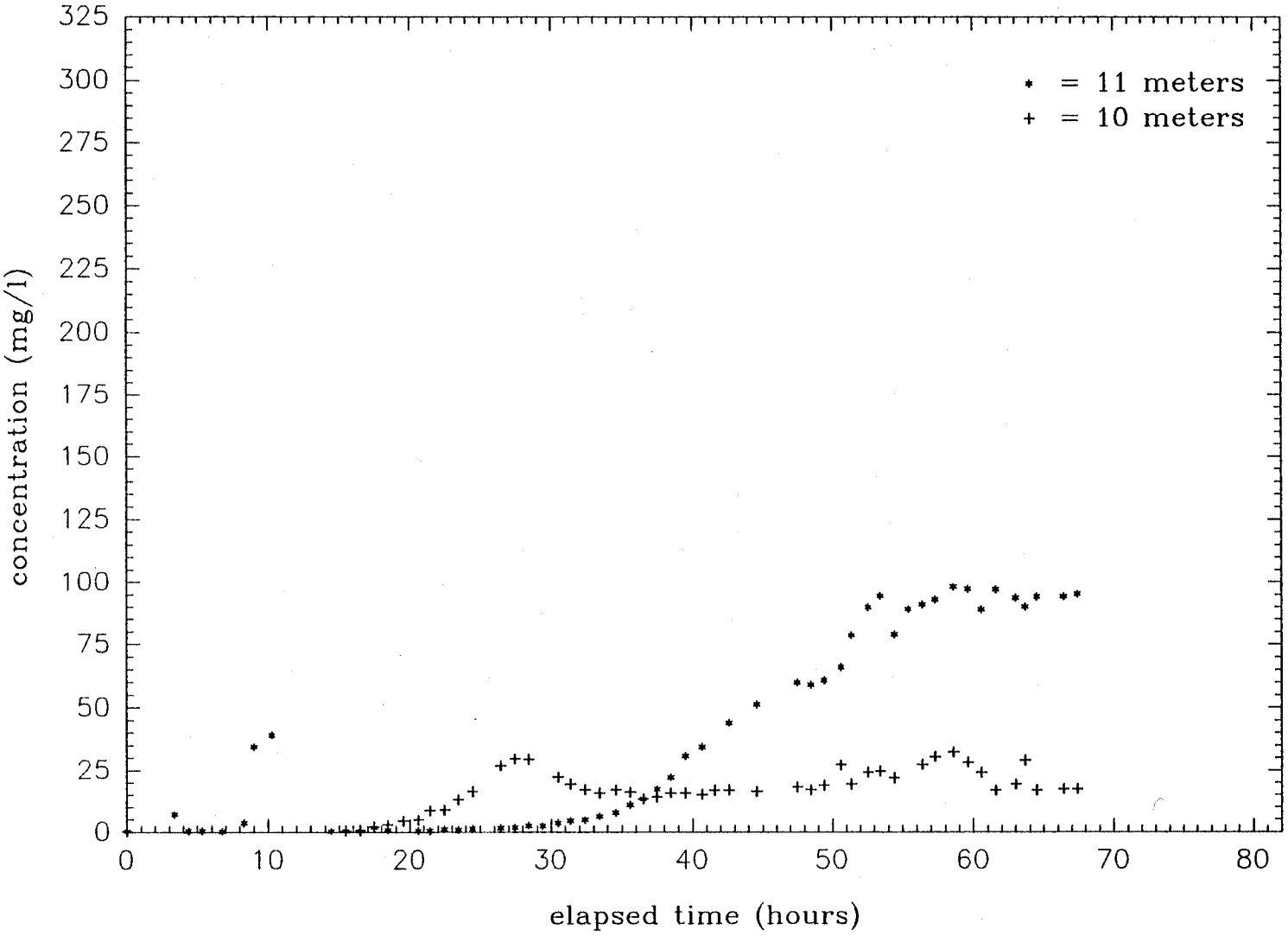

Figure 21. Bromide concentrations measured at W3.

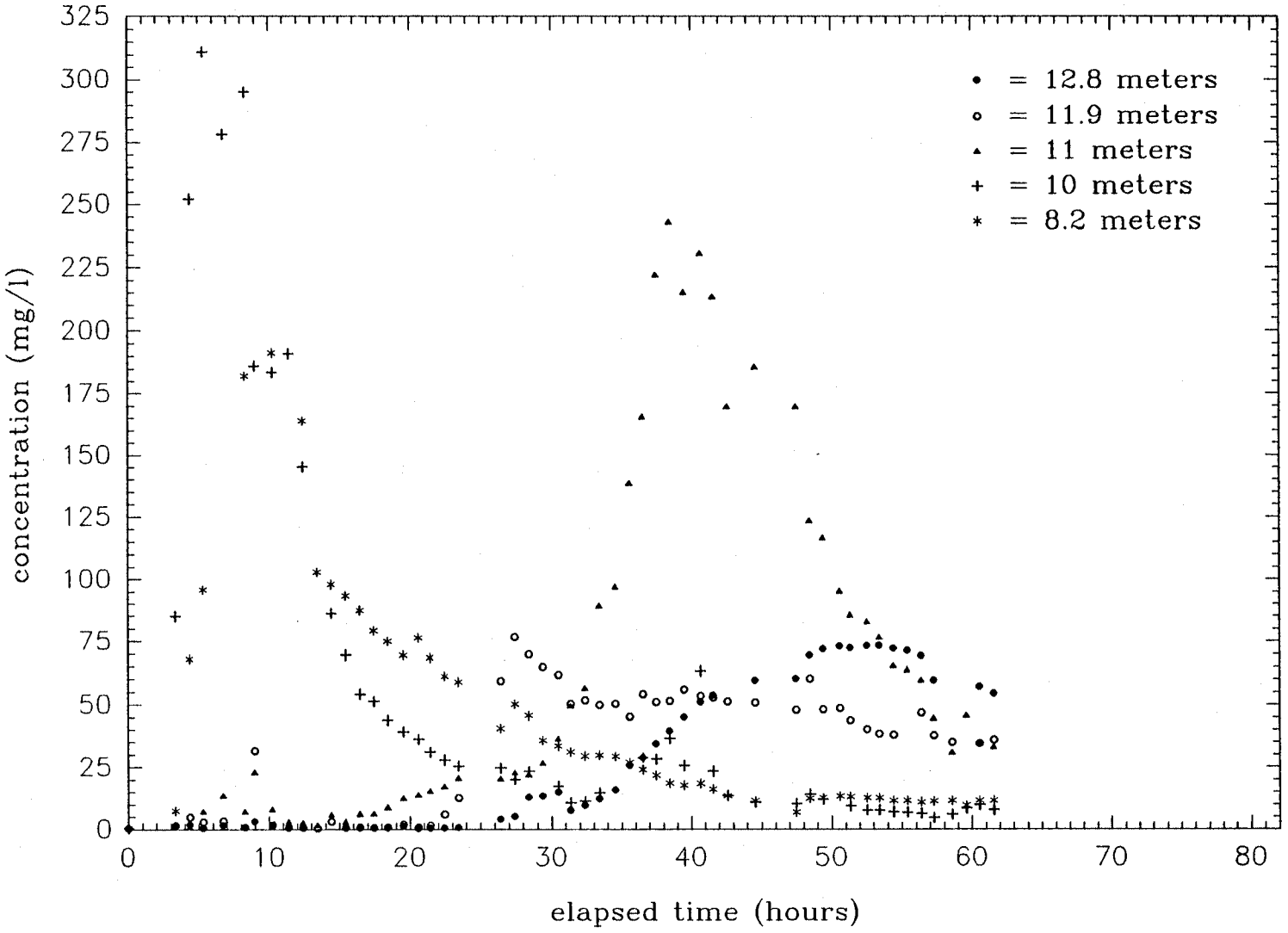

Figure 22a. Bromide concentrations measured at the upper SE3.

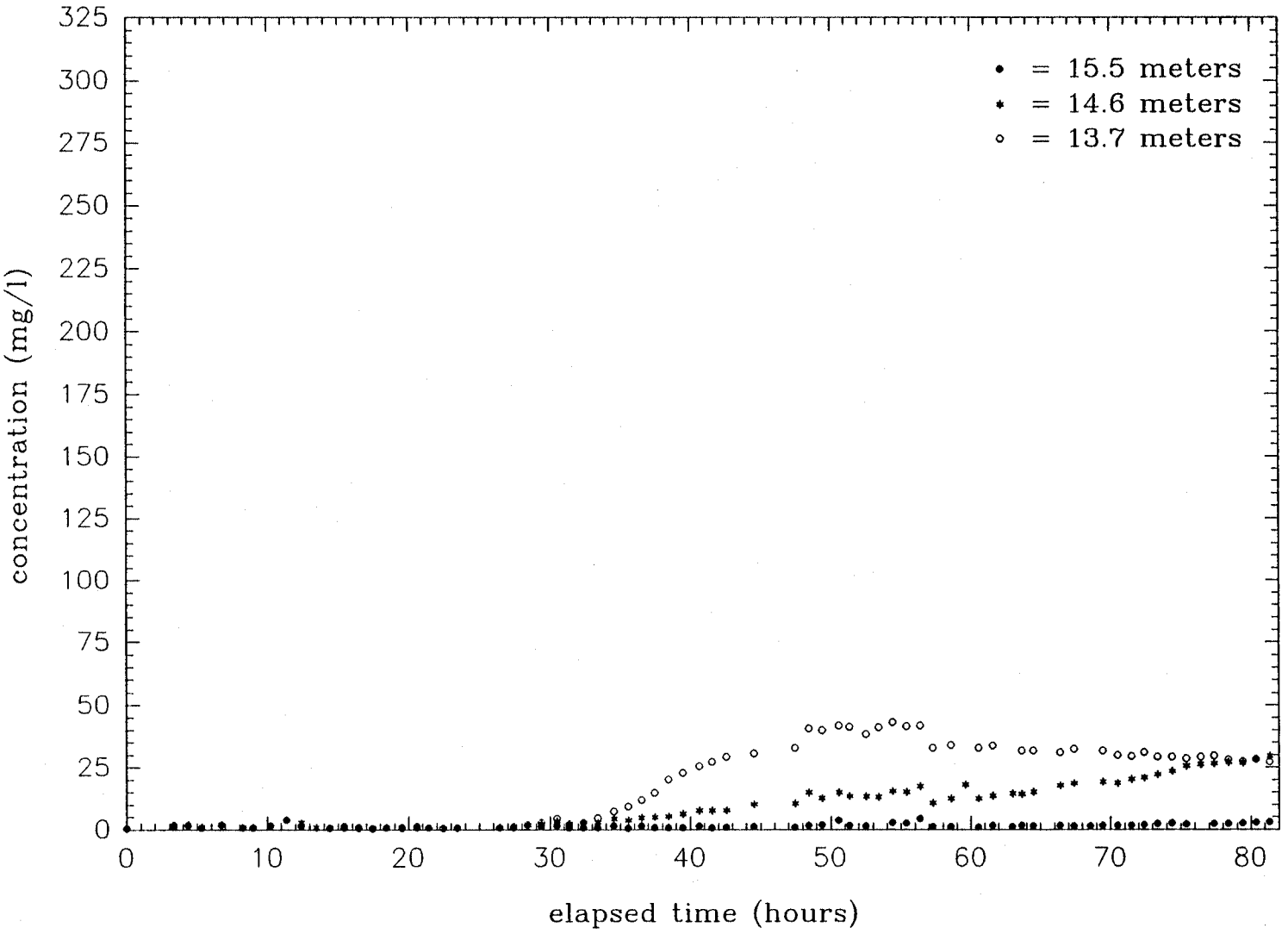

Figure 22b. Bromide concentrations measured at the lower SE3.

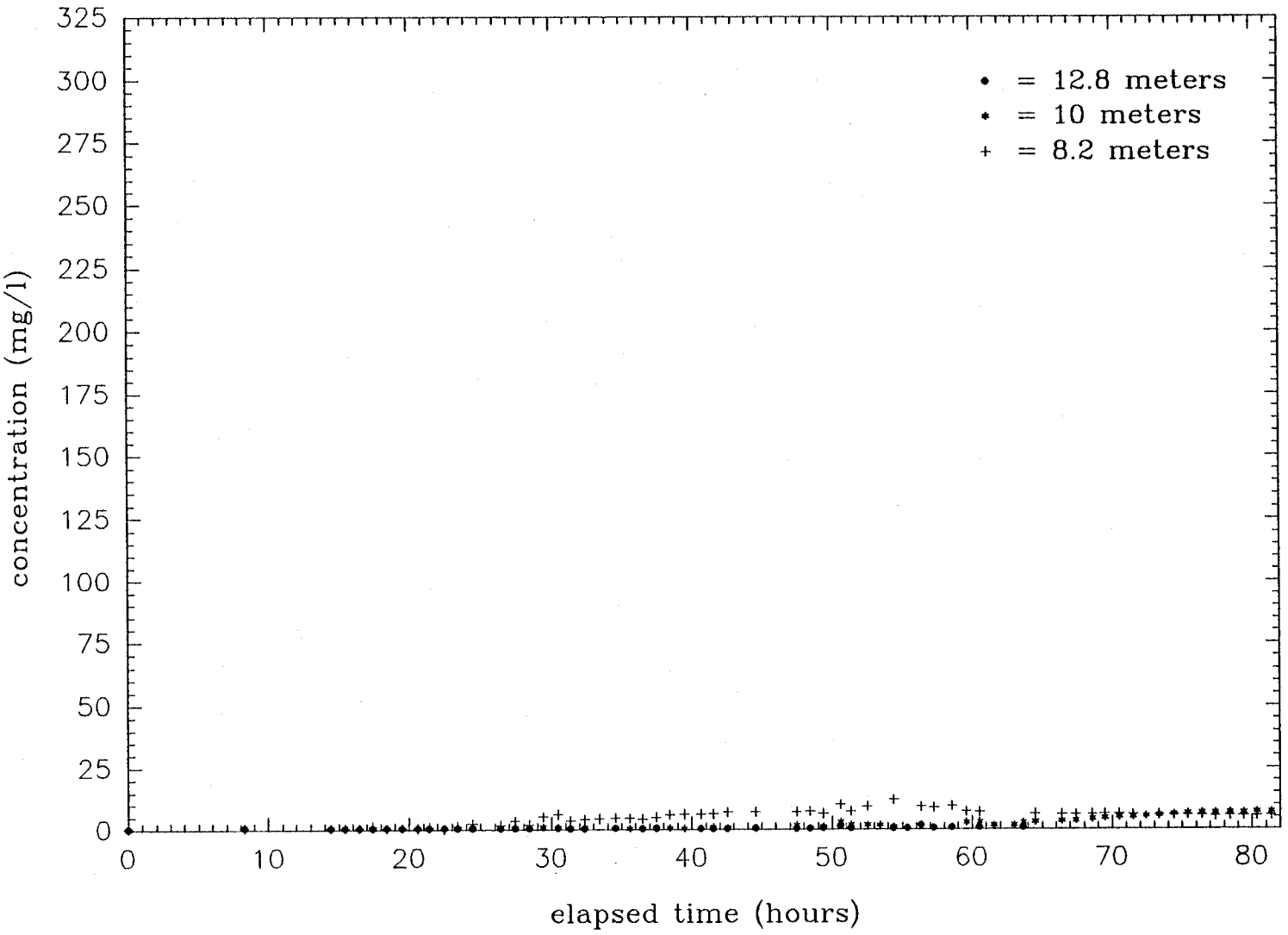

Figure 23. Bromide concentrations measured at NE6.

MODEL AND SOLUTIONS

As shown in Figure 3, the physical conceptualization of this model is one in which the solute is transported horizontally through the saturated flow regime by advection and dispersion and vertically up into the unsaturated zone by molecular diffusion. The assumptions made for this model are as follows: (1) the saturated flow regime is homogeneous and anisotropic, has a uniform thickness, and is located in a horizontal plane, (2) the unsaturated zone overlying the saturated flow regime is considered to be of infinite vertical extent due to the slow velocities associated with the groundwater movement in this zone, (3) the tracer movement from the saturated flow regime into the unsaturated zone can be accounted for by one-dimensional molecular diffusion, and (4) the tracer is transported within the saturated flow regime by means of advection and longitudinal mechanical dispersion only.

Groundwater Flow Field Approximation

The two-dimensional groundwater flow field under an anisotropic condition consists of two components; the radial velocity, v_r, and the angular velocity, v_θ. These two components are assumed to exist under the pseudo-steady-state in which the drawdown is temporal while its gradient is steady-state. Therefore, in polar coordinates, the groundwater flow field due to pumping can be expressed as

$$\begin{Bmatrix} v_r \\ v_\theta \end{Bmatrix} = -\underline{\underline{K}} \begin{Bmatrix} \partial h/\partial r \\ \frac{1}{r}\partial h/\partial \theta \end{Bmatrix} \tag{58}$$

where,

$$\underline{\underline{K}} = \begin{bmatrix} K_{rr} & K_{r\theta} \\ K_{r\theta} & K_{\theta\theta} \end{bmatrix} \tag{59}$$

and the elements of the planar anisotropy tensor are defined as

$$K_{rr} = K_x \cos^2\theta + K_y \sin^2\theta \tag{60a}$$

$$K_{r\theta} = (K_y - K_x)\frac{\sin 2\theta}{2} \tag{60b}$$

and

$$K_{\theta\theta} = K_x \sin^2\theta + K_y \cos^2\theta \tag{60c}$$

Here, K_x and K_y are the principal magnitudes of hydraulic conductivity and

$$\theta = \arctan\left(\frac{y}{x}\right) \tag{61}$$

where, x and y are coincident with the principal directions of the aquifer anisotropy. Without the loss of generality, field observations suggest that the large-time drawdown for estimating the horizontal flow field can be adequately investigated by using the steady-state expression of the logarithmic approximation of the Theis solution. As indicated in Carslaw and Jaeger [1959; pp. 44-45], the steady-state drawdown field under an anisotropic condition is described by

$$h(x,y) = -\gamma \ln\left(\frac{x^2}{K_x}+\frac{y^2}{K_y}\right) = -\gamma \ln\left[r^2\left(\frac{\cos^2\theta}{K_x}+\frac{\sin^2\theta}{K_y}\right)\right] \tag{62}$$

where,

$$\gamma = \frac{Q}{4\pi b\sqrt{K_x K_y}} \tag{63}$$

$$r = \sqrt{x^2+y^2} \tag{64}$$

and Q is the injection rate and b is the aquifer thickness. In a straightforward manner, v_r and v_θ can be determined by taking the partial derivatives of (62) with respect to r and θ and applying the results to (58). Doing so, it was found that v_θ is equal to zero and

$$v_r = \frac{A}{r\omega} \tag{65}$$

where,

$$A = \frac{Q}{2\pi b n_1} \tag{66}$$

and

$$\omega = k\sin^2\theta + \frac{\cos^2\theta}{k} \quad ; \quad k = \sqrt{\frac{K_x}{K_y}} \tag{67}$$

In (66), n_1 is the porosity of the saturated flow regime and in (67), k is the eccentricity of the planar anisotropy ellipse and ω is the anisotropy factor. Under isotropic conditions, both k and ω are equal to one. Under anisotropic conditions, k is always greater than one and the larger the value of k, the more significant the anisotropy. The condition of v_θ being equal to zero indicates that there is no groundwater movement across any adjacent radial pathlines. These pathlines are not symmetric but are radially diverging with respect to the pumping well, as depicted by (65).

Solute Transport Model with Boundary Conditions

The mathematical structure and nature of the dispersion coefficient tensor has been discussed, in detail, by Scheidegger [1961], Bachmat and Bear [1964], Bear [1971], and others for homogeneous and isotropic conditions, by Fattah and Hoopes [1985] for homogeneous and anisotropic conditions, and by Gelhar and Axness [1983] and Neuman et al. [1987] for heterogeneous and anisotropic conditions. Fattah and Hoopes [1985] found that the longitudinal dispersion coefficient was a second-rank tensor whose principal axes were collinear with those of $\underline{\underline{K}}$ and whose eccentricity was equal to that of $\underline{\underline{K}}$. The transverse dispersion coefficient was also a second-rank tensor whose principal axes were orthogonal to those of $\underline{\underline{K}}$ and whose eccentricity increased with increasing seepage velocity. Neuman et al. [1987] investigated

Fickian dispersion in a statistically anisotropic porous medium characterized by a spherical covariance of log-hydraulic conductivities. They showed that the dispersivity tensor was symmetric and second-rank,a nd became diagonal when the mean seepage velocity was parallel to any of the three principal coordinates of statistical anisotropy. At small Peclet numbers, all of the three principal elements increase linearly with anisotropy. At sufficiently large Peclet numbers, the largest principal element becomes a constant whereas the other two decrease inversely with the Peclet number. The asymptotic dispersivity tensor at large Peclet numbers has only one nonzero, constant principal element, which represents the longitudinal dispersivity. Under this asymptotic condition, regardless of the mean seepage velocity orientation, the longitudinal dispersivity always lies in the same direction as the mean seepage velocity. In these analyses, the groundwater velocity was assumed to be uniform with a constant mean. This condition is difficult to achieve in an asymmetric, diverging flow field such as the case in this study. Therefore, the findings regarding the dispersivity or dispersion coefficient reported by these authors may not be applicable here. Here, the longitudinal dispersivity, a_L, is assumed to be constant and always lies in the same direction as that of v_r.

Using the mass balance principal, the governing equation for solute transport from an injection well into a homogeneous and anisotropic unconfined aquifer subject to the flow field discussed above can be developed as

$$\frac{a_L}{r}\frac{\partial^2 C_1}{\partial r^2} - \frac{1}{r}\frac{\partial C_1}{\partial r} + \frac{a_T}{r^3}\omega\frac{\partial}{\partial\theta}\left(\frac{1}{\omega}\frac{\partial C_1}{\partial\theta}\right) + \frac{\omega_1^2}{l}\frac{\partial C_2}{\partial Z}\Big|_{z=0} = \frac{\partial C_1}{\partial t} \qquad (68)$$

where, C_1 is the dimensionless resident concentration in the saturated flow regime, C_2 is the

dimensionless resident concentration in the unsaturated zone, a_L is the longitudinal dispersivity of the saturated flow regime, a_T is the transverse dispersivity of the saturated flow regime, ω_i is a dimensionless ratio expressing the effect of diffusive losses to the injection effect, where i = 1 and 2, 1 is the dimensionless saturated thickness defined as b/a_L, and z is the vertical distance. Here, i = 1 implies the saturated flow regime and i = 2 implies the unsaturated zone. Chen et al. [1993] showed that the third term of (68), which accounts for angular dispersion, can be neglected when the anisotropy eccentricity of an aquifer is less than 2 without introducing significant error into the solution. Therefore, for an anisotropy eccentricity of 1.13, this term was dropped from (68) and the complete mathematical model, in dimensionless form, is

$$\frac{\partial^2 C_2}{\partial \xi^2} = \frac{1}{\omega_2^2}\frac{\partial C_2}{\partial \tau} \qquad 0 \le \xi \le \infty \tag{69}$$

$$C_2(0,\tau) = C_1(\rho,\tau) \tag{70a}$$

$$C_2(\infty,\tau) = 0 \tag{70b}$$

$$\frac{1}{\rho}\frac{\partial^2 C_1}{\partial \rho^2} - \frac{1}{\rho}\frac{\partial C_1}{\partial \rho} + \frac{\omega_1^2}{l}\frac{\partial C_2}{\partial \xi}\Big|_{\xi=0} = \frac{\partial C_1}{\partial \tau} \qquad \rho_0 \le \rho \le \infty \tag{71}$$

$$C_1 - \frac{\partial C_1}{\partial \rho} = 1 \quad at\ \rho_0 \quad 0 \le \tau \le \tau_0 \tag{72a}$$

$$C_1(\infty,\tau) = 0 \tag{72b}$$

$$C_1(\rho,0) = C_2(\xi,0) = 0 \tag{73}$$

where, τ is the dimensionless time defined as $(At)/(a_L^2)$, τ_0 is the dimensionless tracer injection duration defined as $(At_0)/(a_L^2)$, ξ is the dimensionless vertical distance defined as z/a_L, ρ is the dimensionless radial distance defined as r/a_L, ρ_0 is the dimensionless well radius defined as r_w/a_L. Here, the ω_i terms are defined by

$$\omega_1 = \omega_2 \sqrt{\frac{n_2}{n_1}} \tag{74a}$$

and

$$\omega_2 = \sqrt{\frac{D_{m2}}{A}} \tag{74b}$$

where, n_2 is the porosity of the unsaturated zone and D_{m2} is the effective molecular diffusion coefficient of the unsaturated zone. This model is mathematically identical to that of Chen

[1985] with the exception that a Cauchy (third-type) boundary is applied at the injection well as in Chen [1987].

Laplace Transform

Application of the Laplace transform with respect to τ in (69)-(73) yields

$$\frac{d^2G_2}{d\xi^2} = \frac{p}{\omega_2^2}G_2 \tag{75}$$

$$G_2(0,p) = G_1(\rho,p) \tag{76a}$$

$$G_2(\infty,p) = 0 \tag{76b}$$

$$\frac{1}{\rho}\frac{d^2G_1}{d\rho^2} - \frac{1}{\rho}\frac{dG_1}{d\rho} + \frac{\omega_1^2}{l}\frac{dG_2}{d\xi}\Big|_{\xi=0} = pG_1 \tag{77}$$

and

$$G_1 - \frac{dG_1}{d\rho} = \frac{\exp(-p\tau_0)}{p} \quad at\ \rho_0 \tag{78}$$

Equation (78) is derived from Abramowitz and Stegun [1970; Eq. 29.3.63, p. 1025] for a slug

tracer injection of finite duration. Here, p is complex and represents the transform parameter and G is the Laplace transform of C as defined by

$$G = \int_0^\infty \exp(-p\tau)C(\rho,\tau)d\tau$$

The solution of (77) subject to the given boundary conditions is

$$G_1 = \exp(\frac{\rho-\rho_0}{2})[\frac{\exp(-p\tau_0)}{p}]\frac{Ai(Y)}{(\frac{1}{2})Ai(Y_0)-p^{1/3}Ai'(Y_0)} \qquad (79)$$

where, Ai is the Airy function, Ai' is the first derivative of the Airy function, and the arguments are defined by

$$Y = (p+\alpha\sqrt{p})^{1/3}\frac{1}{\rho+4(p+\alpha\sqrt{p})} \qquad (80a)$$

and

$$Y_0 = (p+\alpha\sqrt{p})\frac{1}{\rho_0+4(p+\alpha\sqrt{p})} \qquad (80b)$$

where,

$$\alpha = \frac{n_2 \omega_2}{n_1 l} \tag{81}$$

Here, α is defined, however, its magnitude is determined through curve fitting procedures. The purpose of the curve fitting procedure is to determine the values of a_L and α that produce the best fit to the observed data. The solution for G_2, which would be the Laplace domain solution for the unsaturated zone, is not presented here due to the fact that there were no solute concentration observations made in the unsaturated zone.

Solution Verification

As shown in Chen [1985; Eq. (A6)], realizing that A_2 goes to zero

$$G_1 = A_1 \exp(\frac{y}{2}) A_i(\beta^{1/3} y) \tag{82}$$

where, A_1 is a coefficient dependent on the prescribed boundary conditions, and

$$y = \rho + (4\beta)^{-1} \tag{83}$$

and

$$\beta = p + \alpha p^{1/2} \tag{84}$$

Therefore,

$$G_1 - \frac{dG_1}{d\rho} = \frac{\exp(-p\tau_0)}{p} \quad at \quad \rho = \rho_0 \tag{85}$$

So,

$$G_1 - \frac{dG_1}{d\rho}\Big|_{\rho_0} = A_1 \frac{1}{2}\exp(\frac{y}{2})\frac{dy}{d\rho}Ai(\beta^{1/3}y) + Ai\exp(\frac{y}{2})\frac{dAi(\beta^{1/3}y)}{d\rho}$$

$$= A_1\exp(\frac{y_0}{2})[\frac{1}{2}Ai(\beta^{1/3}y_0) + Ai'(\beta^{1/3}y_0)] \tag{86}$$

Rearranging,

$$\frac{\exp(-p\tau_0)}{p} = A_1\exp(\frac{y_0}{2})Ai(\beta^{1/3}y_0) - A_1\exp(\frac{y_0}{2})[\frac{1}{2}Ai(\beta^{1/3}y_0) + Ai'(\beta^{1/3}y_0)]$$

$$= A_1\exp(\frac{y_0}{2})[Ai'(\beta^{1/3}y_0) + \frac{1}{2}Ai(\beta^{1/3}y_0)] \tag{87}$$

Therefore,

$$G_1 = \exp(\frac{y-y_0}{2})[\frac{\exp(-p\tau_0)}{p}]\frac{Ai(\beta^{1/3}y_0)}{Ai'(\beta^{1/3}y_0) + \frac{1}{2}Ai(\beta^{1/3}y_0)} \tag{88}$$

Flux Concentration

The solution for the flux-concentration is obtained by applying the following transformation

$$C_f = C_r - \frac{\partial C_r}{\partial \rho} \tag{89}$$

where, C_f is the dimensionless flux-concentration and C_r is the dimensionless resident concentration. Therefore, the Laplace domain solution for the flux-concentration is

$$G_{1f} = \exp\left(\frac{\rho - \rho_0}{2}\right)\left[\frac{\exp(-p\tau_0)}{p}\right]\frac{\left(\frac{1}{2}\right)Ai(Y) + p^{1/3}Ai'(Y)}{\left(\frac{1}{2}\right)Ai(Y_0) - p^{1/3}Ai'(Y_0)} \tag{90}$$

There was no attempt made to obtain the analytical inversion from the Laplace domain to the real time domain for (79) and (90). The Talbot [1979] method of numerical inversion was applied to obtain the real time domain solutions to (79) and (90). The parameters that were used in the model are as follows: Q = 13.4 m^3/hr, b = 10 m, r_w = 0.076 m, r = 10 m, n_1 = 0.25, C_0 = 4338 mg/l, t_0 = 1.38 hours.

RESULTS AND DISCUSSIONS

The data analysis of the vertically-averaged groundwater samples primarily means to find a_L and α by fitting the radial dispersion solutions, (79) and (90), to the field data. The best fit results obtained from the model as compared to the field data are shown in Figures 24 and 25 which give both the resident and flux-concentrations under both isotropic and anisotropic conditions. Also, as shown in Figures 7 and 8, the highest peak of bromide concentration appears in the SE direction and the lowest (practically zero) appears in the W direction. This trend is inconsistent with the principal directions of the aquifer anisotropy where SE is almost collinear with the minor semi-axis of the anisotropy ellipse. It would seem that the smallest peak should exist along this direction since the hydraulic conductivity is the smallest in the SE direction. However, the comparison of the peak arrival times for SE10 and NE10 indicate that the breakthrough of NE10 is, indeed, earlier than that of SE10, supporting the theory that the groundwater flows slower in the SE direction. Therefore, a possible explanation for the higher concentration peak at SE10 is that the dispersivity in the SE direction is smaller than that in the NE direction. Indeed, the curve-fitting results shown in Figures 24 and 25 indicate that the dispersivity in the SE direction (a_L = 0.6 m) is smaller than that in the NE direction ($a_L \approx$ 1.3 m). No curve-fitting attempt was made on the field data in the W direction due to the extremely low concentrations.

The two-dimensional analysis of the vertically-averaged concentration data indicates that the pertinent fitted parameters (i.e., the longitudinal dispersivity and the molecular diffusion parameter) can be constant along a single radial direction with respect to the injection well. However, the results indicate that a directional dependence exists between the magnitude of these

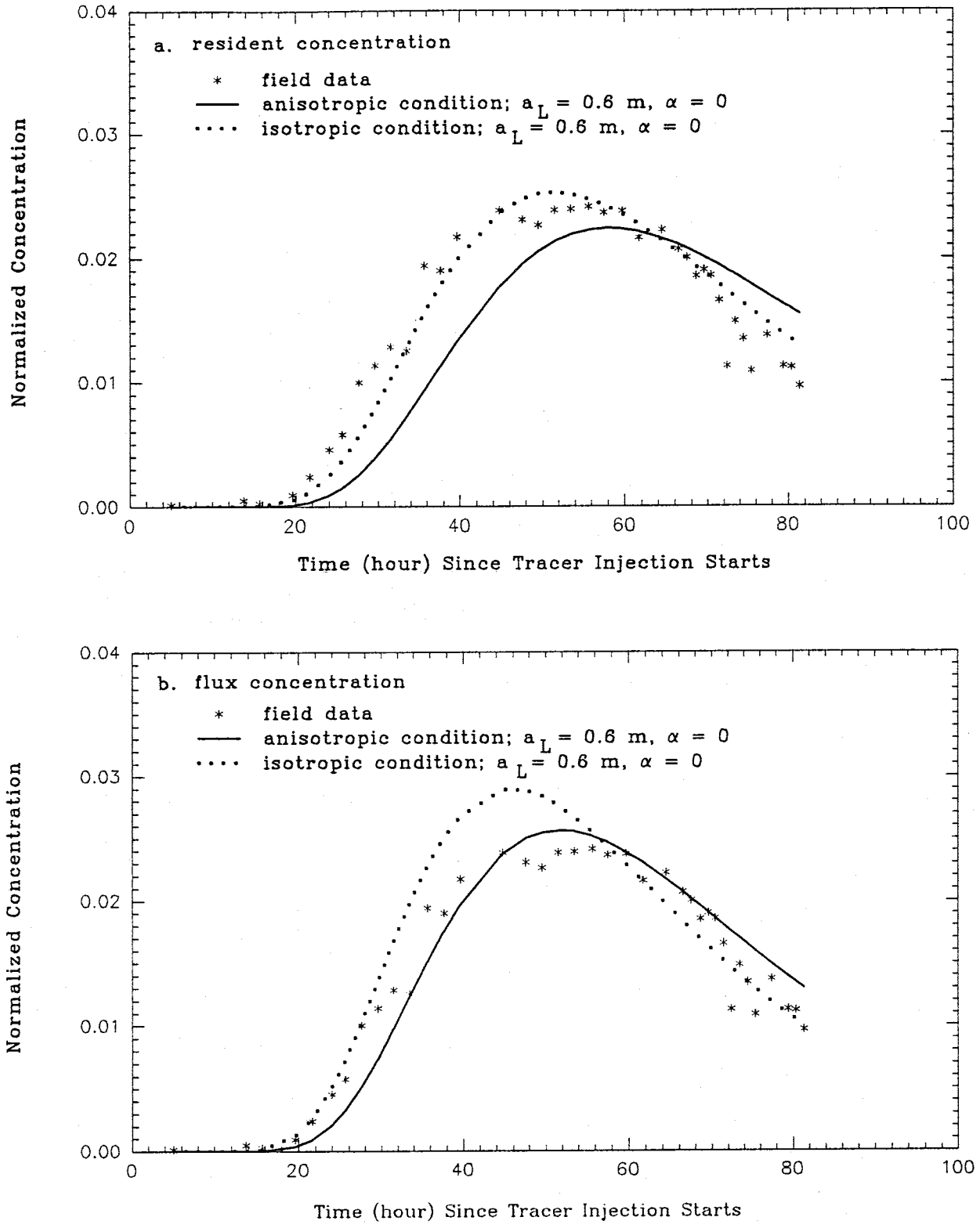

Figure 24. Normalized bromide concentrations from SE10 fitted by a two-dimensional radial dispersion solution.

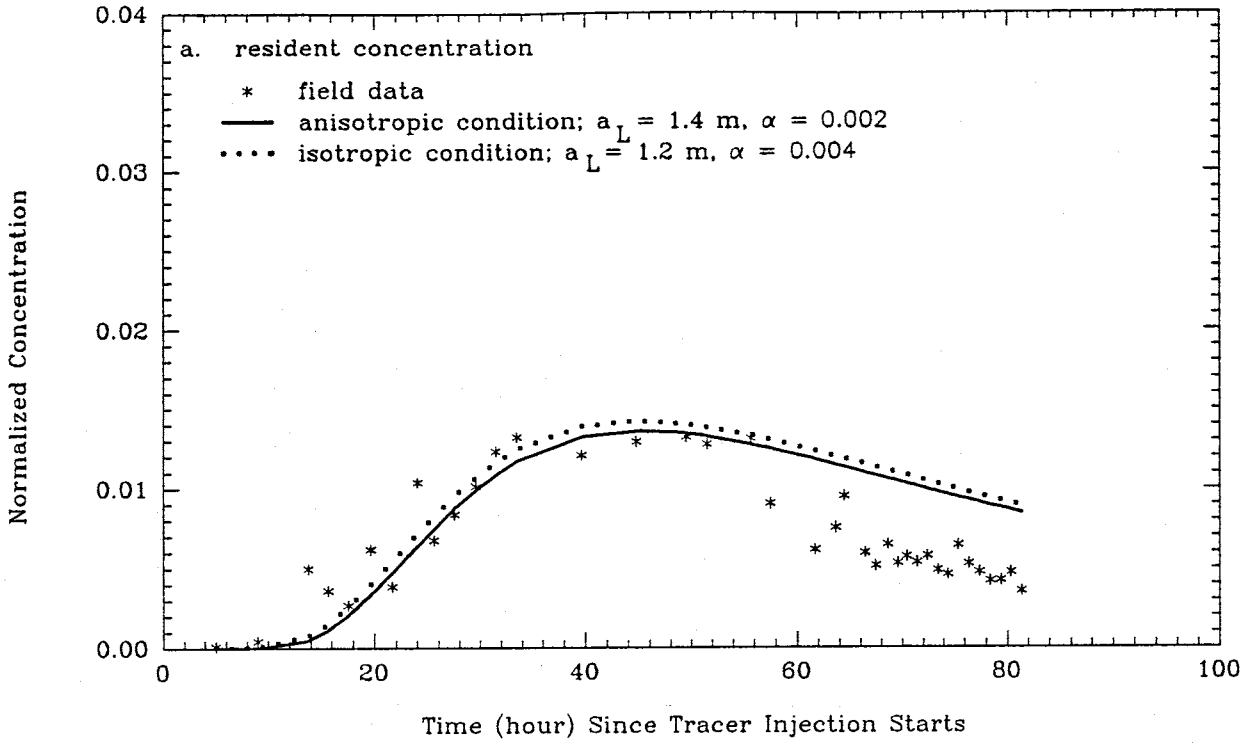

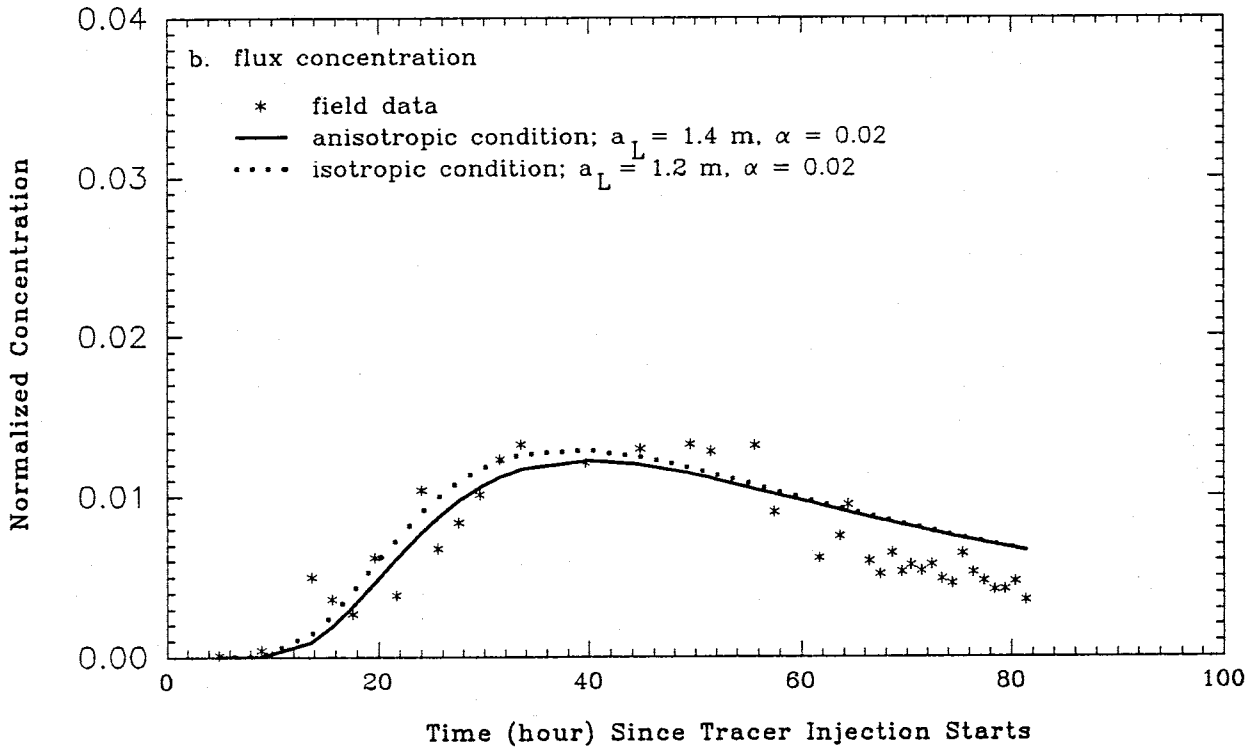

Figure 25. Normalized bromide concentrations from NE10 fitted by a two-dimensional radial dispersion solution.

fitted parameters and the radial direction. An exact relationship between the magnitude of the fitted parameters and the radial direction could not be determined due to insufficient field data. The fact that the fitted parameters can be constant along a single radial direction can be attributed to the condition that the complicated vertical groundwater velocity variation caused by possible layering effects are significantly buffered, if not eliminated, through the vertical mixing mechanism that occurs across the relatively long screened intervals of the observation wells.

The model results, through the curve fitting procedure depicted in Figures 24 and 25, show that the incorporation of the aquifer anisotropy into the radial dispersion solution is an important element in the analysis of pumping well tracer test data. Both anisotropic and isotropic model results are given in Figures 24 and 25. In order to obtain comparable fits, the curve fitting procedure showed that the magnitude of a_L must be decreased under isotropic conditions and the magnitude of α must be increased.

The issue of whether the bromide concentrations from SE10 and NE10 should be interpreted as resident or flux-concentrations has been examined by fitting both of the solutions, (79) and (90), to the field data. As shown in Figure 24, it is seen that the resident-concentration solution yields better results when the aquifer anisotropy is neglected and the flux-concentration solution produces better results when the aquifer anisotropy is taken into account. Since the aquifer is anisotropic, the better fitting by the resident-concentration solution in Figure 24a is considered to be an artifact. This suggests that the solute concentrations contained in groundwater samples obtained from observation wells should be considered as flux-concentration. It is also interesting

to note, that regardless of whether the resident or flux-concentration solution is applied in fitting the field data from SE10, the longitudinal dispersivity is constant at 0.6 meters and there is no need to use α in aiding the curve fitting (i.e., no molecular diffusion is occurring) possibly due to the fact that the concentration plume had not yet reached the unsaturated zone.

The difference in using the resident and flux-concentration solutions, (79) and (90), in fitting the field data from NE10, however, is not significant. To obtain the best fit conditions as shown in Figure 25, the fitted parameter, α, is needed. It is seen that the longitudinal dispersivity is approximately constant (1.4 m versus 1.2 m) as estimated by the two solutions, (79) and (90). The α value, however, is approximately one order of magnitude greater for the flux-concentration solution than for the resident-concentration solution.

CONCLUSIONS

The following conclusions can be drawn from this study:

(1) The model results, through the curve fitting procedure, show that ignoring the anisotropy of an aquifer can lead to significant errors in the analysis of pumping well tracer test data. This research shows that the two fitting parameters (longitudinal dispersivity and one-dimensional diffusion) will be in error if the aquifer anisotropy is ignored. In particular, the magnitude of the longitudinal dispersivity will be artificially low if the aquifer anisotropy is ignored and the magnitude of the one-dimensional diffusion parameter will be artificially high if the aquifer anisotropy is ignored.

(2) When the longitudinal dispersivity is expressed in a non-tensor form under anisotropic

conditions it is found that the magnitude of this parameter does remain constant along a single radial direction. However, as the radial direction changes, so does the magnitude of the longitudinal dispersivity. An exact relationship between the magnitude of the longitudinal dispersivity and the radial direction could not be determined due to insufficient field data.

(3) The magnitude of the one-dimensional diffusion parameter mimics the trend of the longitudinal dispersivity. This suggests that the diffusion parameter also has a directional property but, again, an exact relationship between the magnitude of the diffusion parameter and the radial direction could not be determined due to insufficient field data.

(4) The flux-concentration solution produces a closer match to the observed solute concentration data. This result supports the conclusions drawn by other authors which suggests that solute concentrations obtained from large-scale measuring devices such as sampling wells or pan lysimeters represent flux-concentration rather than resident-concentration values.

REFERENCES

Abramowitz, M. and I. A. Stegun, 1970. Handbook of Mathematical Functions., Dover Publication, 1046 pp.

American Society for Testing Materials, 1963. Grain size analysis of soils, D422-63, pp. 203-214, In Book of ASTM Standards, Pt. 11, Philadelphia, Pennsylvania.

Bachmat, Y. and J. Bear, 1964. The general equations of hydrodynamic dispersion in homogeneous, isotropic porous media. J. Geophys. Res., 69(12), 2561-2567.

Bear, J. 1972. Dynamics of Fluids in Porous Media. Americam Isvier, New York.

Boggs, S. B., Jr., 1987. Principles of Sedimentology and Stratigraphy, pp. 106-122: Merril Publishing Co., Columbus, Ohio.

Bowman, R. S., 1984. Evaluation of some new tracers for soil water studies. Soil Sci. Soc. Am. J. 48:987-993.

Carslaw, H. S. and J. C. Jaeger, 1959. Conduction of Heat in Solids (2nd Ed.), Oxford University Press, 510 pp.

Chen, C.-S., 1985. Analytical and approximate solutions to radial dispersion from an injection well to a geological unit with simultaneous diffusion into adjacent strata. Water Resources Research., 21(8), 1069-1076.

Chen, C.-S., 1986. Solutions for radionuclide transport from an injection well into a single fracture in a porous formation. Water Resources Research., 22(4), 508-518.

Chen, C.-S., 1987. Analytical solutions for radial dispersion with Cauchy boundary at injection well. Water Resources Research., 23(7), 1217-1224.

Chen, C.-S., Christopher Holmes, Weidong Li, David Chace, Mike Fort, Jingfang He, and

Jinzhong Liu, 1993. Multidimensional field and theoretical investigation of solute transport from an injection well into a homogeneous and anisotropic aquifer. Technical Completion Report. USGS Report No.14-08-0001-G1744.

Chen, C.-S. and G. D. Woodside, 1988. Analytical solution for aquifer decontamination by pumping. Water Resources Research., 24(8), 1329-1338.

Fattah, Q. N. and J. A. Hoopes, 1985. Dispersion in anisotropic, homogeneous porous media. J. Hydraulic. Div. Am. Soc. Civ. Eng., 111(5), 810-827.

Fort, M., 1992. Three-dimensional hydraulic conductivity tensor determination in an unconsolidated alluvial aquifer. Unpublished thesis. New Mexico Institute of Mining and Technology.

Freeze, R. A. and J. A. Cherry, 1979. Groundwater. Prentice-Hall Inc., New Jersey. pp. 35-37.

Gelhar, L. W. and M. A. Collins, 1971. General analysis of longitudinal dispersion in nonuniform flow. Water Resources Research., 7(6), 1511-1521.

Gelhar, L. W. and C. L. Axness, 1979. Three-dimensional stochastic analysis of macro-dispersion in a stratified aquifer. Water Resources Research., 15(6), 1387-1397.

Guvanasen, V. and V. M. Guvanasen, 1987. An approximate semianalytical solution for tracer injection tests in a confined aquifer with a radially converging flow field and finite volume of tracer and chase fluid. Water Resources Research., 23(8), 1607-1619.

Güven, O., F. J. Molz, and J. G. Melville, 1985. Analysis and interpretation of single-well tracer tests in stratified aquifers. Water Resources Research., 21(5), 676-684.

Hitchman, S. P., 1988. A collection manifold for multilevel groundwater sampling devices.

Groundwater., 26(3), 348-349.

Hoopes, J. A. and D. R. F. Harleman, 1967a. Dispersion in radial flow from a recharge well. Journal of Geophysics Research., 72(14), 3595-3607.

Hoopes, J. A. and D. R. F. Harleman, 1967b. Wastewater recharge and dispersion in porous media. J. Hydraul. Div. Am. Soc. Civ. Eng., 93(HY5) 51-71.

Hsieh, P. A. and S. P. Neuman, 1985. Field determination of three-dimensional hydraulic conductivity tensor of anisotropic media, 1. theory. Water Resources Research., 21(11), 1655-1665.

Hseih, P. A., 1986. A new formula for the analytical solution of the radial dispersion problem. Water Resources Research., 22(11), 1597-1605.

Kreft, A. and A. Zuber, 1978. On the physical meaning of the dispersion equation and its solutions for different initial and boundary conditions. Chem. Eng. Sci., 33, 1471-1480.

Lide, D. R., 1991. CRC Handbook of Chemistry and Physics. pp. 6-8.

Maloszewski, P. and A. Zuber, 1982. Determining the turnover time of groundwater systems with the aid of environmental tracers. Journal of Hydrology., 57, 207-231.

Neuman, S. P., C. L. Winter, and C. M. Newman, 1987. Stochastic theory of field-scale Fickian dispersion in anisotropic porous media. Water Resources Research., 23(3), 453-466.

Novakowski, K. S., 1992. The analysis of tracer experiments conducted in divergent radial flow fields. Water Resources Research., 28(12), 3215-3225.

Ogata, A., 1958. Dispersion in porous media. Ph.D. dissertation. Northwestern University. Evanston, Illinois.

Parker, J. C. and M. The. van Genuchten, 1984. Flux-averaged and volume-averaged concentrations in continuum approaches to solute transport. Water Resources Research., 20(7), 866-872.

Pickens, J. F., J. A. Cherry, G. E. Grisak, W. F. Merrit, and B. A. Risto. 1978. A multilevel device for groundwater sampling and piezometric monitoring. Groundwater., 16(5), 322-327.

Raimondi, P. G., H. F. Gardner, and C. B. Petrick, 1959. Effect of pore structure and molecular diffusion on the mixing of miscible fluids flowing in porous media. paper presented at Symposium on Oil Recovery Methods, Soc. Pet. Tech., San Francisco, California.

Sauty, J. P., 1980. An analysis of hydrodispersive transfer in aquifers. Water Resources Research., 16(1), 145-158.

Scheidegger, A. E., 1961. General theory of dispersion in porous media. J. Geophys. Res., 66(10), 3273-3278.

Sposito, G., W. A. Jury, and V. K. Gupta. 1986. Fundamental problems in the stochastic convection-dispersion model of solute transport in aquifers and field soils. Water Resources Research., 22(1), 77-88.

Stephens, D. B. and R. Knowlton, Jr., 1986. Soil water movement and recharge through sand at a semiarid site in New Mexico. Water Resources Research., 22(6), 881-889.

Talbot, A., 1979. The accurate numerical inversion of Laplace transforms. J. Inst. Math. Appl., 23, 97-120.

Tang, D. H. and D. K. Babu, 1979. Analytical solution of a velocity dependent dispersion

problem. Water Resources Research., 15(6), 1471-1479.

U. S. Department of the Interior; Water and Power Resources Service. 1981. Ground Water Manual: A guide for the investigation, development, and management of ground-water resources. Wiley Interscience Publ. New York. p. 208.

Vukovic, M. and A. Soro, 1992. Determination of Hydraulic Conductivity of Porous Media from Grain-Size Composition: Water Resources Publications, Littleton, Colorado.

Yates, S. R., 1988. Three-dimensional radial dispersion in a variable velocity flow field. Water Resources Research., 24(7) 1083-1090.

Yih, C. S., 1965. Dynamics of Nonhomogeneous Fluids. The MacMillan Company, New York., pp. 211-213.

Zody, S. P., 1988. Seismic refraction investigation of the shallow subsurface of the lower Rio Salado, northwest of San Acacia, New Mexico. Unpublished thesis. New Mexico Institute of Mining and Technology.

APPENDIX

FORTRAN code of the two-dimensional radial dispersion model used to determine the longitudinal dispersivity value by matching the theoretical solution to the field data.

```
      program chace1
c**********************************************************************
c**********************************************************************
c
c  Program "Chace1" is a modification of the program "Talbot_Chia"
c  that was developed by Li-Wei Chiang while at New Mexico Tech.
c  The modifications are such that the radial dispersion model can
c  solve for dimensionless concentrations in an aquifer under slug
c  injection conditions as well as the continuous and pulse
c  injection conditions that the model was originally developed
c  to handle.
c
c**********************************************************************
c
c  The Talbot method is applied to Chen [1987, Equation (21), (28),
c  (30), and (32)] involving six different radial dispersion
c  problems.
c
c**********************************************************************
c
c  New Mexico Institute of Mining and Technology Sun system version
c
c**********************************************************************
c
c                     Definition of variables:
c
c  Q: Dimensional discharge rate (L**3/t).
c  thick: Dimensional aquifer thickness (L).
c  void: Porosity (dimensionless).
c  time: Dimensional time (t).
c  alpha: Dimensional dispersivity (L).
c  beta: Vertical diffusion term
c  r: Dimensional radial distance (L).
c  rw: Dimensional well bore radius (L).
c  trace: Dimensional injection duration of the tracer (t).
c  c: Dimensional concentration (M/L**3).
c  c0: Dimensional injection concentration (M/L**3).
c  fs: Input Laplace domain function.
c  finv: Approximate value of the Laplace transform at each point
c        t(i).
c  n: Number of terms in the series.
c  nt: Number of times.
c  t: Dimensionless times (it is an array).
c  tend: Dimensionless duration of the injection period
```

```
c       (set to 0 if not applicable).
c  nr: Number of increments of dimensionless radial distance.
c  z: Shifting parameter (usually set to 0).
c  nu: Scale parameter (usually set to 1).
c  tau: Scale parameter that can be chosen for any real positive
c       number (such as 11, 6, 5, ... etc.).
c  rho0: Dimensionless radial distance of the well bore.
c  rho: Dimensionless radial distance.
c  drho: Dimensionless radial distance increment.
c  case: Applies to six different radial dispersion problems when;
c       case=1 for resident concentration for continuous injection
c       case=2 for resident concentration for pulse injection
c       case=3 for flux concentration for continuous injection
c       case=4 for flux concentration for pulse injection
c       case=5 for resident concentration for slug injection
c       case=6 for flux concentration for slug injection
c
c**********************************************************************
c**********************************************************************


      implicit real*8(a-h,o-z)
      dimension cbar(100),c(100),time(100),t(100),dis(10)
      real*8 nu
      integer case
      double precision Q,thick,void,alpha,beta,r,rw,trace,c0,tend

      common /num1/ z,nu,tau,pi
      common /num2/ beta,rho,case
      common /num3/ rho0,tend

      open(unit=7,file='dtalbot_c.dat',status='old')
      open(unit=6,file='dtalbot_c.out')

      read(7,*) Q,thick,void,alpha,beta,r,rw,trace,c0,
     +          n,nt,nr,z,nu,tau,case
      do 7 i=1,nt
        read(7,*) time(i),c(i)
 7    continue

      write(6,10) Q,thick,void,alpha,beta,r,rw,trace,c0,n,nt,z,nu,tau
 10   format(3x,'Discharge rate (Q) in (m**3/hr) = ',f7.4,/
     +       3x,'Aquifer thickness (thick) in (m) = ',f6.3,/
     +       3x,'The porosity (void) = ',f5.3,/
```

```
     +       3x,'Dispersivity (alpha) in (m) = ',f7.4,/
     +       3x,'Diffusion term (beta) = ',f7.6,/
     +       3x,'Radial distance (r) in (m) = ',f6.3,/
     +       3x,'Well bore radius (rw) in (m) = ',f5.3,/
     +       3x,'Tracer injection duration (trace) in (hr) = ',f7.4,/
     +       3x,'Injection concentration (c0) in (mg/l) = ',f10.3,/
     +       3x,'Number of terms in the series (n) = ',i3,/
     +       3x,'Number of dimensionless times (nt) = ',i3,/
     +       3x,'Shifting parameter (z) = ',f5.2,/
     +       3x,'Scale parameter (nu) = ',f5.2,/
     +       3x,'Scale parameter (tau) = ',f7.4,//)

      write(6,13) case
 13   format(5x,'case = 1 => (res. & cont. inj. b.c.);',/,
     +       5x,'case = 2 => (res. & pulse inj. b.c.);',/,
     +       5x,'case = 3 => (flux & cont. inj. b.c.);',/,
     +       5x,'case = 4 => (flux & pulse inj. b.c.);',/,
     +       5x,'case = 5 => (res. & slug inj. b.c.);',/,
     +       5x,'case = 6 => (flux & slug inj. b.c.);',//,
     +       10x,'*******************************',/,
     +       10x,'* The case being used is ',i3,' *'/,
     +       10x,'*******************************',//)

c**************************************************************************
c
c                       Begin calculations
c
c**************************************************************************

      rho=r/alpha
      rho0=rw/alpha
      drho=rho-rho0
      rho=rho0
      pi=4.d0*datan(1.d0)
      tend=Q*trace/2.d0/pi/thick/void/alpha**2

      do 11 i=1,nt
        t(i)=Q*time(i)/2.d0/pi/thick/void/alpha**2
        cbar(i)=c(i)/c0
 11   continue

      do 700 kkk=1,nr
        rho=rho0+drho
        write(6,*) '              kkk = ',kkk
```

```
      write(6,15) rho
15     format(/5x,'Dimensionless distance (rho) = ',f9.2/)
      write(6,16)
16     format(5x,' Calculated ',5x,' Calculated ',5x,'    Input    '
     +,5x,'    Input    ',/5x,'Dimensionless',5x,'Dimensionless',5x,' Di
     +mensional ',5x,'Dimensionless',/5x,'     Time    ',5x,'Concentrati
     +on',5x,'     Time    ',5x,'Concentration',/5x,'**************',5x,'
     +**************',5x,'**************',5x,'**************',/)
      do 600 i=1,nt
        dis(i)=rho
        call talbot(finv,t,n,i)
        write(6,20) t(i),finv,time(i),cbar(i)
20       format(5x,f11.3,5x,f11.5,7x,f11.3,7x,f11.5)
600    continue
700  continue

     stop
     end


c*************************************************************************
c*************************************************************************
c
c                    Talbot subroutine
c
c*************************************************************************
c*************************************************************************

     subroutine talbot(ft,t,n,i)
     implicit real*8(a-h,o-z)
     dimension t(100)
     real*8 lambda,nu
     integer case
     complex*16 s(200),ds(200),zz,sum,b,b1,b2,fs,s9

     common /num1/ z,nu,tau,pi
     common /num2/ beta,rho,case
     common /num3/ rho0,tend

     pibyn=pi/n
     zz=dcmplx(z,z)
     lambda=tau/t(i)

     nmi=n-1
```

```
      do 700 k=1,nmi
        u=k
        theta=u*pibyn
        alpha=theta*dcos(theta)/dsin(theta)
        s(k)=dcmplx(alpha,nu*theta)
        ds(k)=dcmplx(nu,theta+alpha*(alpha-1)/theta)*0.5
700   continue

      psi=tau*pibyn*nu
      cp=2.d0*dcos(psi)
      sp=dsin(psi)
      b=zz
      b1=b

      do 600 ka=1,nmi
        k=n-ka
        v2=dexp(dmax1(tau*dreal(s(k)),-1.8d+02))
        b2=b1
        b1=b
        s9=lambda*s(k)
        b=cp*b1-b2+v2*ds(k)*fs(s9)
600   continue

      s9=lambda+zz
      sum=dexp(tau)*nu*fs(s9)*0.5+cp*b-2.d0*(b1-b*dcmplx(
     +    z,sp))
      ft=lambda*dreal(sum)/n
      return
      end


c*************************************************************************
c*************************************************************************
c
c                    Complex function fs(s9)
c
c*************************************************************************
c*************************************************************************

      complex*16 function fs(s9)
      implicit complex*16 (a-h,o-z)
      integer one,case
      real*8 rho,rho0,tend
      double precision beta
```

```
      common /num2/ beta,rho,case
      common /num3/ rho0,tend
      one=1

      s9=s9+cdsqrt(beta*s9)

      y0=(1.d0+4.d0*rho0*s9)/(4.d0*s9**(2.d0/3.d0))
      y=(1.d0+4.d0*rho*s9)/(4.d0*s9**(2.d0/3.d0))

      x1=ai(y,one)
      x2=ai(y0,one)
      x3=aip(y0,one)


      if(case.eq.1) then
         fs=dexp((rho-rho0)/2.d0)*(1.d0/s9)*(x1/(0.5d0*x2-
     +      s9**(1.d0/3.d0)*x3))
      elseif(case.eq.2) then
         fs=dexp((rho-rho0)/2.d0)*(x1/(0.5d0*x2-
     +      s9**(1.d0/3.d0)*x3))
      elseif(case.eq.3) then
         fs=dexp((rho-rho0)/2.d0)*(1.d0/s9)*(x1*0.5d0-aip(y,one)*
     +      (s9**(1.d0/3.d0)))/(0.5d0*x2-s9**(1.d0/3.d0)*x3)
      elseif(case.eq.4) then
         fs=dexp((rho-rho0)/2.d0)*(x1*0.5d0-aip(y,one)*
     +      (s9**(1.d0/3.d0)))/(0.5d0*x2-s9**(1.d0/3.d0)*x3)
      elseif(case.eq.5) then
         tends9=-tend*s9
         fs=(1.d0-cdexp(tends9))*dexp((rho-rho0)/2.d0)/s9*
     +      (x1/(0.5d0*x2-s9**(1.d0/3.d0)*x3))
      else
         tends9=-tend*s9
         fs=(1.d0-cdexp(tends9))*dexp((rho-rho0)/2.d0)/s9*
     +      (x1*0.5d0-aip(y,one)*(s9**(1.d0/3.d0)))/(0.5d0*x2-s9**
     +      (1.d0/3.d0)*x3)
      endif

      return
      end



      complex*16 function ai(z,iopt)
c*****************************************************************************
```

```
c***********************************************************************
c
c       This function subroutine computes the Airy function ai(z).
c
c***********************************************************************
c
c  For positive arguments, a scaling option is available.
c
c  If iopt = 1, the result is not scaled.
c  If iopt = 2, the result is the function value multiplied by
c               (z**0.25)*exp(u), where u = (2./3.)*(z**1.5).
c
c  For non-positive arguments, no scaling option is available.  If
c  (iopt) is set to 2, it is ignored and a warning is printed.
c
c***********************************************************************
c***********************************************************************

      implicit complex*16 (a-h,o-z)
      real*8 zabs,zreal,zimag,theta
      real*8 c1,c2,pi,coef1,coef2,coef3,coef4,coef5,coef6
      real*8 pidd,pid4,pirt2,twthrd

      data c1,c2,pi/.35502 80538 878d0,.25881 94037 928d0,
     +   3.14159 26535 90d0/
      data coef1,coef2,coef3,coef4,coef5,coef6/9.555526226877d-29,
     +   4.235605597020d-32,1.661021802753d-35,1.013578212294d-29,
     +   4.309431174718d-33,1.624974047782d-36/

      pidd=pi/1.1d0
      pid4=pi/4.d0
      pirt2=dsqrt(pi)*2.d0
      twthrd=2.d0/3.d0

      zabs=cdabs(z)
      zreal=dreal(z)
      zimag=dimag(z)
      theta=datan2(zimag,zreal)

      if(zabs.gt.4.8d0) goto 100

c***********************************************************************
c
c                Compute ai(z) for abs(z) < 4.8
```

```
c
c*********************************************************************

      p=z**3

      f=1.d0+p*( 1.666666666667d-01+p*( 5.555555555556d-03+
     +       p*( 7.716049382716d-05+p*( 5.845491956603d-07+
     +       p*( 2.783567598382d-09+p*( 9.096626138505d-12+
     +       p*( 2.165863366311d-14+p*( 3.623665518679d-17+
     +       p*( 5.589267120625d-20+p*( 6.424444966235d-23+
     +       p*( 6.083754702874d-26+p*( 4.828376748313d-29+
     +       p*( 3.258014000211d-32+p*( 1.891994192922d-35+
     +       p*(      1.0d-10*coef1+p*(      1.0d-10*coef2+
     +       p*(      1.0d-10* coef3))))))))))))))))
      g=z*(1.d0+p*( 8.333333333333d-02+p*( 1.984126984127d-03+
     +          p*( 2.204585537919d-05+p*( 1.413195857640d-07+
     +          p*( 5.888316072501d-10+p*( 1.721729846052d-12+
     +          p*( 3.726687978470d-15+p*( 6.211146630783d-18+
     +          p*( 8.215802421670d-21+p*( 8.834196152333d-24+
     +          p*( 7.873615109032d-27+p*( 5.911122454228d-30+
     +          p*( 3.789181060403d-33+p*( 2.098106899448d-36+
     +          p*(      1.0d-10*coef4+p*(      1.0d-10*coef5+
     +          p*(      1.0d-10*coef6))))))))))))))))

      ai=c1*f-c2*g
      if(iopt.eq.2) goto 30

      return

 30   u=twthrd*z**1.5d0
      ai=(z**0.25d0)*cdexp(u)*ai

      return

c*********************************************************************
c
c       Compute ai(z) for abs(z) > 4.8; check the argument first.
c
c*********************************************************************
 100  if(dabs(theta).lt.pi) goto 110
      goto 200

 110  u=twthrd*z**1.5d0
      p=1.d0/u
```

```
      a=1.d0+p*(-6.944444444444d-02+p*( 3.713348765432d-02+
     +       p*(-3.799305912780d-02+p*( 5.764919041267d-02+
     +       p*(-1.160990640255d-01+p*( 2.915913992307d-01+
     +       p*(-8.776669695100d-01+p*( 3.079453030173d+00+
     +       p*(-1.234157333235d+01+p*( 5.562278536591d+01+
     +       p*(-2.784650807776d+02+p*( 1.533169432013d+03+
     +       p*(-9.207206599726d+03))))))))))))

      if(iopt.eq.2) goto 130
      ai=a*cdexp(-u)/pirt2/(z**0.25d0)

      return

  130 ai=a/pirt2

      return

c*******************************************************************************
c
c             Compute ai(z) for abs(z) > 4.8 and theta = pi
c
c*******************************************************************************

  200 zn=-z
      un=twthrd*zn**1.5d0
      w=un+pid4
      p=1.d0/(un**2)

      a=1.d0+p*(-3.713348765432d-02+p*( 5.764919041267d-02+
     +       p*(-2.915913992307d-01+p*( 3.079453030171d+00+
     +       p*(-5.562278536591d+01+p*( 1.533169432013d+03+
     +       p*(-5.989251356587d+04+p*( 3.148257417867d+06)))))))
      b=(1.d0/un)*( 6.944444444444d-02+p*(-3.799305912780d-02+
     +          p*( 1.160990640255d-01+p*(-8.776669695100d-01+
     +          p*( 1.234157333235d+01+p*(-2.784650807776d+02+
     +          p*( 9.207206599726d+03+p*(-4.195248751165d+05)))))))

      ai=(cdsin(w)*a-cdcos(w)*b)/cdsqrt(pi*cdsqrt(zn))
      if(iopt.eq.2) write (30,900)

      return

  900 format('***Warning*** iopt=2 is ignored for a non-positive ',
```

```
     +        'argument of ai(z).')

      end


      complex*16 function aip(z,iopt)
c**********************************************************************
c**********************************************************************
c
c  This function subroutine computes aip(z), the first derivative of
c  the Airy function ai(z).
c
c**********************************************************************
c
c  For positive arguments, a scaling option is available.
c
c  If iopt = 1, the result is not scaled.
c  If iopt = 2, the result is the function value multiplied by
c              exp(u)/(z**0.25), where u = (2./3.)*(z**1.5).
c
c  For non-positive arguments, no scaling option is available.  If
c  (iopt) is set to 2, it is ignored and a warning is printed.
c
c**********************************************************************
c**********************************************************************

      implicit complex*16 (a-h,o-z)
      real*8 zabs,zreal,zimag,theta
      real*8 c1,c2,pi,coef1,coef2,coef3,coef4,coef5,coef6
      real*8 pid4,pirt2,twthrd

      data c1,c2,pi/.35502 80538 878d0,.25881 94037 928d0,
     +   3.14159 26535 90d0/
      data coef1,coef2,coef3,coef4,coef5,coef6/4.066181373139d-30,
     +   1.694242238808d-33,6.268006802841d-37,4.662459776551d-28,
     +   2.111621275612d-31,8.449865048466d-35/

      pid4=pi/4.d0
      pirt2=dsqrt(pi)*2.d0
      twthrd=2.d0/3.d0

      zabs=cdabs(z)
      zreal=dreal(z)
      zimag=dimag(z)
```

```
      theta=datan2(zimag,zreal)

      if(zabs.gt.4.8d0) goto 100

c*********************************************************************
c
c                Compute aip(z) for abs(z) < 4.8
c
c*********************************************************************

      p=z**3
      zzd2=z**2/2.d0

      f=zzd2*(1.d0+p*( 6.666666666667d-02+p*( 1.388888888889d-03+
     +            p*( 1.402918069585d-05+p*( 8.350702795147d-08+
     +            p*( 3.274785409862d-10+p*( 9.096626138505d-13+
     +            p*( 1.883359448966d-15+p*( 3.018204245137d-18+
     +            p*( 3.854666979741d-21+p*( 4.015278103897d-24+
     +            p*( 3.476431258785d-27+p*( 2.541250920165d-30+
     +            p*( 1.589275122054d-33+p*( 8.599973604190d-37+
     +            p*(      1.0d-10*coef1+p*(      1.0d-10*coef2+
     +            p*(      1.0d-10*coef3))))))))))))))))
      g=1.d0+p*( 3.333333333333d-01+p*( 1.388888888889d-02+
     +       p*( 2.204585537919d-04+p*( 1.837154614932d-06+
     +       p*( 9.421305717602d-09+p*( 3.271286707501d-11+
     +       p*( 8.198713552633d-14+p*( 1.552786657696d-16+
     +       p*( 2.300424678068d-19+p*( 2.738600807224d-22+
     +       p*( 2.677029137071d-25+p*( 2.187115308064d-28+
     +       p*( 1.515672424161d-31+p*( 9.021859667626d-35+
     +       p*(      1.0d-10*coef4+p*(      1.0d-10*coef5+
     +       p*(      1.0d-10*coef6))))))))))))))))

      aip=c1*f-c2*g
      if(iopt.eq.2) goto 30

      return

 30   u=twthrd*z**1.5d0
      aip=cdexp(u)*aip/(z**0.25d0)

      return

c*********************************************************************
c
```

```
c       Compute aip(z) for abs(z) > 4.8; check argument first.
c
c*****************************************************************

 100  if(dabs(theta).lt.pi) goto 110
      goto 200

 110  u=twthrd*z**1.5d0
      p=1.d0/u

      a=1.d0+p*( 9.722222222222d-02+p*(-4.388503086420d-02+
     +       p*( 4.246283078989d-02+p*(-6.266216349203d-02+
     +       p*( 1.241058960273d-01+p*(-3.082537649011d-01+
     +       p*( 9.204799924129d-01+p*(-3.210493584649d+00+
     +       p*( 1.280729308074d+01+p*(-5.750830351391d+01+
     +       p*( 2.870332371092d+02+p*(-1.576357303337d+03+
     +       p*( 9.446354823095d+03))))))))))))

      if(iopt.eq.2) goto 130
      aip=-a*cdexp(-u)*(z**0.25d0)/pirt2

      return

 130  aip=-a/pirt2

      return

c*****************************************************************
c
c          Compute aip(z) for abs(z) > 4.8 and theta = pi.
c
c*****************************************************************

 200  zn=-z
      un=twthrd*zn**1.5d0
      w=un+pid4
      p=1.d0/(un**2)

      a=1.d0+p*( 4.388503086420d-02+p*(-6.266216349203d-02+
     +       p*( 3.082537649011d-01+p*(-3.210493584649d+00+
     +       p*( 5.750830351391d+01+p*(-1.576357303337d+03+
     +       p*( 6.133570666385d+04+p*(-3.214536521401d+06)))))))
      b=(1.d0/un)*(-9.722222222222d-02+p*( 4.246283078989d-02+
     +          p*(-1.241058960273d-01+p*( 9.204799924129d-01+
```

```
     +          p*(-1.280729308074d+01+p*( 2.870332371092d+02+
     +          p*(-9.446354823095d+03+p*( 4.282924004000d+05)))))))

      aip=-(cdcos(w)*a+cdsin(w)*b)*cdsqrt(cdsqrt(zn)/pi)
      if(iopt.eq.2) write(30,900)

      return

  900 format('***Warning*** iopt=2 is ignored for a non-positive ',
     +       'argument of aip(z).')

      end
```